ESTIMATION AND EQUALIZATION OF COMMUNICATIONS CHANNELS USING WAVELET TRANSFORMS

by

CANUTE VAZ

A Dissertation submitted to the

Graduate School-New Brunswick

Rutgers, The State University of New Jersey

in partial fulfillment of the requirements

for the degree of

Doctor of Philosophy

Graduate Program in Electrical and Computer Engineering

written under the direction of

Professor David G. Daut

and approved by

_____

_____

_____

_____

_____

New Brunswick, New Jersey

January, 2010

ABSTRACT OF THE DISSERTATION

Estimation and Equalization of Communications Channels Using Wavelet Transforms

By CANUTE VAZ

Dissertation Director:
Professor David G. Daut

This dissertation features the development of signal processing strategies for the estimation of channel impulse responses and the equalization of the effects of channels on communications signals propagating through them using the Discrete Wavelet Transform (DWT). The two strategies are developed as part of a wavelet-based signal processing platform, which can be used to enable reconfigurable radio transceivers.

The approach taken is to recast standard discrete time-domain signal processing procedures into a DWT-based framework. To facilitate this, three equivalent techniques of DWT-based convolution that use both subband coding as well as polyphase filter implementations are devised.

A DWT-based deconvolution procedure is derived analytically and is applied to perform estimation of several time-invariant multipath communications channels. Conditions of slow and fast fading are considered, and faded test signals are corrupted by Additive White Gaussian Noise (AWGN) that results in ratios of bit-energy-to-noise-power-density, E_b/N_0, in the range of 0 to 30 dB. Monte Carlo simulations of the estimation of the

channel impulse responses yield Mean-Square Error (MSE) results with excellent agreement for coarse levels of DWT resolution when compared with standard discrete time-domain deconvolution.

Using DWT-based convolution the linear equalization techniques of Zero Forcing Equalization (ZFE) and Minimum Mean-Squared Error (MMSE) equalization, are formulated and implemented in the wavelet-domain. Monte Carlo simulations of the equalization of a fast fading channel with E_b/N_0 in the range 0 dB to 60 dB show that the performance of both linear equalizers in the time- and wavelet-domains is essentially identical.

Allied with the primary objective of the dissertation, both DWT-based channel estimation and equalization are included in communications systems. In Monte Carlo simulations of these systems, signals that are digitally modulated using Binary Amplitude Shift Keying (BASK), Binary Frequency Shift Keying (BFSK) and 16-Quadrature Amplitude Modulation (16-QAM) schemes are propagated through a fast fading channel. The faded signals are corrupted by AWGN resulting in E_b/N_0 in the range 0 dB to 20 dB. The performance of these hybrid time- and DWT-based communications systems is evaluated with Symbol Error Rate (SER) curves showing no decrease in performance when compared with discrete time-domain system methods.

Acknowledgement

My Family

Mom, dad, and Beryl, thank you for your support and your love, through these past years. I have tried to emulate your qualities of perseverence, tenacity, and integrity, and doing so has brought me this far.

Professor David Daut

I am fortunate to have had you as my research advisor. Thank you for the guidance you have given me, for the kindness you have shown, and for always having my best interest in mind.

Professor Sigrid McAfee

You have mentored me and educated me, especially during my formative years as a graduate student. I have come this far because of your support and encouragement. Thank you, Professor McAfee.

My Dissertation Committee

I am grateful, Professor Robert Chant, Professor Sophocles Orfanidis, Professor Peddapullaiah Sannuti, for serving as members of my dissertation committee and for your evaluation of my dissertation.

Vivian Ho

It has been my good fortune to have had you as a friend and a colleague Thank you for the strength you have given to me over the years. You have been instrumental in making this dissertation possible.

“

Limits of the Human Mind

Ruthlessly trenchant fellow, wordy pedagogue, meddlesome theorist, you seek the limits of your mind. They are at the end of your nose.

”

- Voltaire, *Dictionnaire Philosophique*, 1764

Table of Contents

List of Tables

List of Illustrations

Chapter 1

Introduction

Contemporary communications systems employ a wide variety of signal transmission, reception, and processing techniques [1]. Advanced methodologies for high-speed communications, such as various time [2], frequency [3,4], and spatial [5,6] multiplexing techniques, are being commonly used in such systems, and are rapidly maturing.

In order to guide the design of such systems a wide range of standards and protocols are in use, with new technologies being invented regularly. It has recently been recognized that a new paradigm is needed for the development of future communications systems. A focus on interoperability between standards is necessary for both commercial and military applications.

One such platform is that of reconfigurable radios [7-9]. Ideally, such systems are reconfigurable in the sense that signals can be transmitted at different carrier frequencies and different modulation schemes, and can then be reliably identified and appropriately demodulated in real-time by a receiver that acquires these.

It is postulated that the use of Wavelet Transforms (WTs) [10-12] can enable such reconfigurable radios. The development of a Wavelet Platform for reconfigurable radios

is the primary motivation of this dissertation because two of the vital signal processing elements required in such a system are channel estimation and channel equalization.

Therefore, the foci of this research study are two-fold:

1. To investigate the feasibility of estimating channel impulse responses using the WT.
2. To investigate the feasibility of equalizing channel effects on a propagating signal with the use of the WT.

1.1 Motivation: A Wavelet Platform for Communications Systems

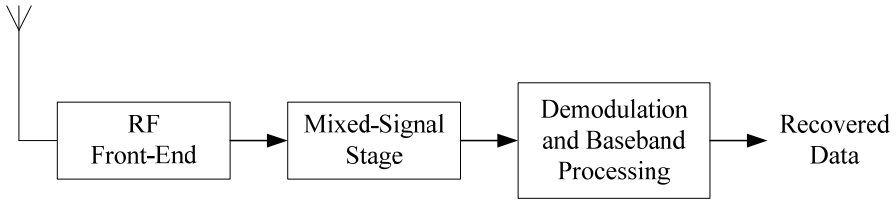

Fig. 1.1.1. Major system components of a communications receiver [13].

Communications receivers can be fundamentally reduced to consisting of three main stages, as seen in Fig. 1.1.1:

1. A Radio Frequency (RF) front-end;
2. A mixed-signal section;
3. Demodulation and baseband processing units.

The **RF front-end** is typically composed of analog electronic sub-systems such as mixers, Local Oscillators (LOs), Band-Pass Filters (BPFs), Variable Gain Amplifiers (VGAs), and antennae [14]. Apart from conditioning the analog signal, the RF front-end also downconverts a received passband signal to an Intermediate Frequency (IF) for ease of subsequent processing [15].

The **mixed-signal stage** of a receiver serves to digitize the downconverted signal output by the RF front-end. This stage is essential if the signal is to be digitally processed, but is omitted in the case of analog receivers [14].

The **demodulator** recovers the baseband data that were transmitted [16]. Any decoding operations that must be performed on the recovered data are handled by a **baseband processor** [4].

Radio transmitters also use a similar signal processing strategy as the receiver described, except in reverse. In transmitters, baseband data are first encoded as needed and are then used to modulate a carrier signal at an intermediate frequency. Such a modulated signal is then upconverted to the RF passband and transmitted.

The topological duality of radio transmitters and receivers is illustrated in Fig. 1.1.2.

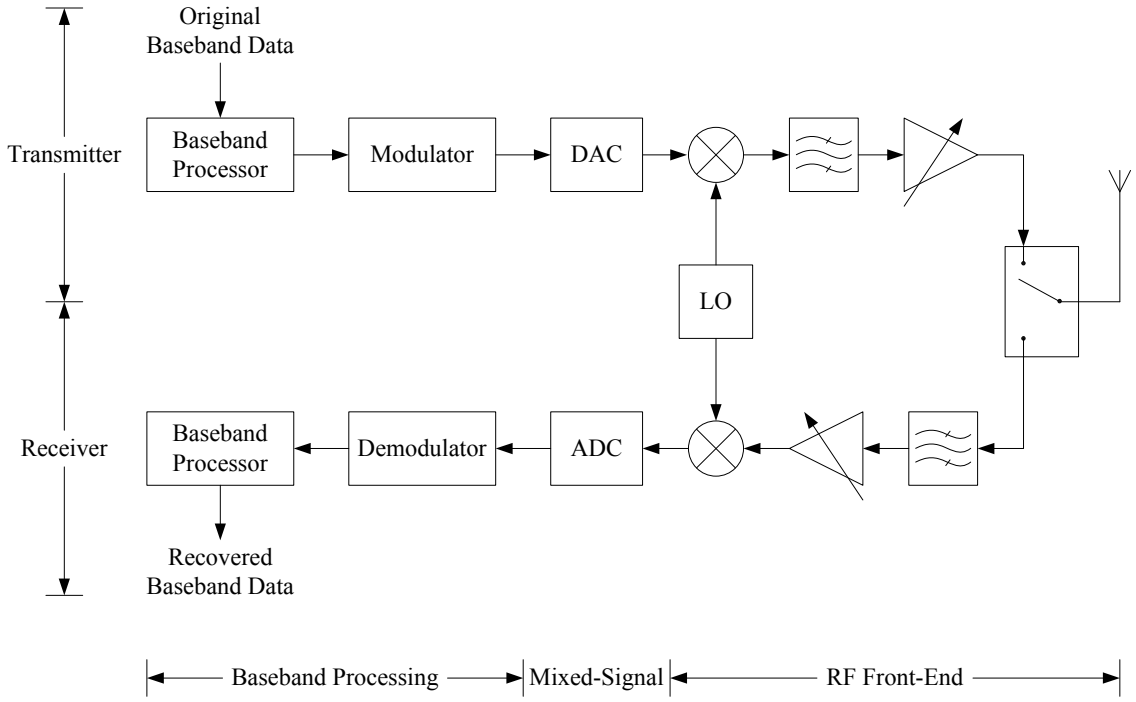

Fig. 1.1.2. Typical essential sub-systems in a radio transceiver [13].

Recent efforts in the research and development of wireless communications systems have been focused on techniques such as Orthogonal Frequency Division Multiplexing (OFDM) [17-19], Multiple-Input Multiple-Output (MIMO) systems [20-22], and hybrid OFDM-MIMO techniques as well [23-26].

One limitation of these advanced techniques, however, is the same as of basic systems: the lack of interoperability between radios designed to implement different communications standards. A major hindrance to the interoperability between systems using different standards is that often each standard requires the use of different modulation schemes [27-33]. A trivial solution to this problem is to simply construct receivers with banks of demodulators specific to several modulation schemes of interest.

A more elegant solution would be to construct a receiver that has the ability to automatically identify the modulation scheme used in a received signal and then automatically demodulate the signal as well. In the literature, the process of automatically identifying modulation schemes is formally called Automatic Modulation Recognition (AMR) [34].

The wavelet transform is one mathematical theory that can be used to develop such a receiver. In fact, the concepts of wavelet-based AMR and demodulation have already been recently invented [35,36]. Studies have shown that these new systems perform with exceptional robustness even when signals are corrupted by a large amount of additive noise [36].

In a general sense, wavelets are rapidly decaying oscillatory functions that can be used as basis functions to represent signals. They are especially useful in representing practical signals, which are usually not monochromatic.

With the use of the Fourier transform, a time-domain signal can be expressed in terms of a sinusoidal set of basis functions in the spectral domain. In this process, however, the temporal detail of the signal is obscured. The Short-Time Fourier Transform (STFT) [37], on the other hand, does allow for temporal details of a signal to be preserved as it makes use of windowed basis functions. The window functions, however, cannot be varied in size. Therefore, the STFT is subject to the problem of finite resolution: a narrow, highly-localized time-domain window provides poorly localized spectral-domain

resolution, and conversely a poorly-localized time-domain window of fixed size provides highly localized spectral resolution. This drawback of fixed window sizes is especially problematic in the analysis of digitally modulated communications signals.

In the case of wavelet transforms, the window functions, i.e., the wavelets, can be temporally translated and can be dilated in time as well. This latter feature allows for the variation of the width of wavelet windows to a specific desired resolution. Comparing translated and scaled (dilated) wavelets with the original signal yields cross-correlation coefficients such that each correlation contains the frequency information of the original signal while automatically preserving the temporal information of the signal.

It is this powerful feature of wavelets that is used in the wavelet transform-based automatic modulation recognition and demodulation techniques, which form the core of the Wavelet Platform for reconfigurable radios.

A system-level illustration of the Wavelet Platform in a communications system is provided in Fig. 1.1.3. As seen in Fig. 1.1.3, the Wavelet Platform is composed of five major signal processing operations:

1. De-noising
2. Channel Estimation
3. Channel Equalization
4. Automatic Modulation Recognition
5. Demodulation.

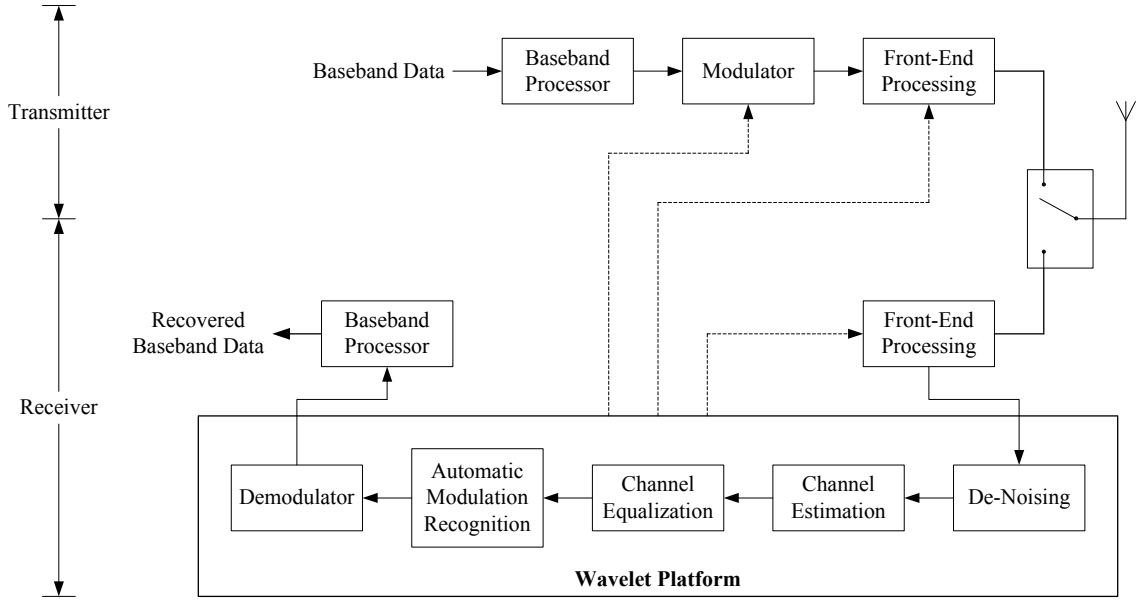

Fig. 1.1.3. System-level view of a reconfigurable radio transceiver built on the Wavelet Platform [38].

In Fig. 1.1.3, the Wavelet Platform is shown as a part of a reconfigurable radio receiver, which is in turn a part of a reconfigurable radio transceiver. The dashed lines indicate that the Wavelet Platform can provide appropriate information to sub-systems in both the transmitter and receiver so that operating parameters such as the modulation scheme, carrier frequency, filter frequency response characteristics, etc., may be altered if needed. Such feedback of relevant information enables reconfigurability of the transceiver while it is operating.

The signal processing strategies of channel estimation and channel equalization are essential components of any practical communications system [3,16]. They are,

therefore, integral components of the Wavelet Platform as well. The core components of the Wavelet Platform, however, are the wavelet transform-based AMR and automatic demodulation sub-systems. Also, one well-developed application of wavelet transforms is the de-noising of signals [39-41]. For this reason it is also included in the Wavelet Platform [42].

In brief, the intention of developing wavelet-based methodologies for channel estimation and channel equalization is to augment the processes of wavelet-based AMR and automatic signal demodulation.

Viewed independently, an investigation into determining whether wavelet-based channel estimation and equalization is feasible, and, if so, practicable, directly serves to advance the state of the art of communications receiver technology.

1.2 Objectives of the Research

There are six primary objectives of this research study:

1. To determine whether it is possible to estimate the time-domain impulse response of an unknown channel using a wavelet transform approach.
2. If possible, to develop and verify a method for wavelet transform-based channel estimation.
3. To determine whether it is possible to equalize the fading effects of channels on signal using a wavelet transform-based approach.

4. If possible, to develop and verify a method for wavelet transform-based channel equalization.
5. Utilize the wavelet transform-based channel estimation and equalization methodologies in communication systems, and evaluate the performance of the new systems.
6. Compare the performance of the wavelet transform-based signal processing methodologies and the new communications systems with corresponding discrete time-domain methodologies and systems.

All of the wavelet transform-based methodologies that are developed in this dissertation use the Discrete Wavelet Transform (DWT) [10-12]. In particular, the filter bank approach of DWT, which is implemented using the well-established signal processing methodology called Multiresolution Analysis (MRA) [43,44], is to be used.

Channel Estimation

Channel estimation is to be carried out with the use of pilot signals, which are used to sound the channel prior to the transmission of the actual message signal. In the corresponding case of time-domain signals, such an estimation can be computed by the deconvolution of an uncorrupted transmitted signal from the corrupted received signal.

Therefore, in this investigative effort, the desired DWT-based channel estimation procedure is to be a DWT-based deconvolution procedure.

An analytical formulation of DWT-based deconvolution is to be developed, and is to be validated using computer simulations. The simulations are to be Monte Carlo experiments so as to provide statistically significant results. Test channel models that are used in the communications literature are to be used.

Channel Equalization

Two types of channel equalization are to be considered. The first is Minimum Mean-Squared Error (MMSE) equalization, and the second is Zero-Forcing Equalization (ZFE). A common approach for DWT-based equalization is to be developed, and then implemented with both MMSE equalization and ZFE.

DWT-based equalization is to be described analytically, and verified using Monte Carlo computer simulation experiments. For the purposes of validation, a channel with a Gaussian Power Delay Profile (PDP) is to be used in conjunction with the digital modulation schemes Binary Amplitude Shift Keying (BASK), Binary Frequency Shift Keying (BFSK), and 16-symbol Quadrature Amplitude Modulation (16-QAM).

DWT-based Convolution

Both DWT-based estimation and equalization require the development of the technique of DWT-based convolution. The procedures are to be developed and described analytically.

Application in Communication Systems

The efficacy of the DWT-based channel estimation and channel equalization procedures is to be tested in communication systems. Specifically, three systems are to be used, each consisting of a transmitter and receiver pair that implement BASK, BFSK and 16-QAM. Performance of these new systems is to be evaluated by computing Symbol Error Rates (SERs).

Noise Processes

Test signals in all Monte Carlo simulations are to be corrupted by Additive White Gaussian Noise (AWGN) .

Experiments and Controls

For all of these studies there exist well-defined counterparts in the time-domain, specifically in the discrete time-domain. Thus, the veracity of results for each DWT-based research topic described in this section can directly be compared to the results in the time-domain for each corresponding topic.

The control experiments and the corresponding DWT-based research topics in this study are provided in Table 1.2.1.

Table 1.2.1 Experiments and corresponding controls

	Experiment	Control
1.	DWT-based channel estimation	Discrete time-domain-based channel estimation
2.	DWT-based MMSE equalization	Discrete time-domain-based MMSE equalization
3.	DWT-based ZFE	Discrete time-domain-based ZFE
4.	Communication systems with DWT-based signal processing components	Communication systems with standard discrete time-domain-based signal processing components

1.3 Organization of the Dissertation

As has been described in Section 1.2, this dissertation has multiple research topics at its core. The four topics are identified as follows.

1. Enabling research: DWT-based convolution
2. Development: DWT-based channel estimation
3. Development: DWT-based channel equalization
4. Application: Communication systems with WT-based sub-systems

The development of DWT-based convolution is necessary for the other three topics. DWT-based estimation and DWT-based equalization are independent topics when viewed as signal processing strategies. They are both, however, used in conjunction with each other in communications systems.

Therefore, each of these topics is addressed in separate chapters. Each of these chapters is replete with specific objectives, hypotheses, theoretical formulations, and experimental validations.

Following this first, introductory, section, the theoretical aspects of several prerequisite communications concepts are provided in Chapter 2. The specific concepts include communication signal, channel, and system models and the standard theories of MMSE equalization and ZFE. A comprehensive survey of the literature relevant to the topics researched in this study is presented in Chapter 3. The theory of WTs is formally introduced in Chapter 4, with emphasis being on MRA and the DWT.

Procedures for DWT-based convolution are provided in Chapter 5. Specifically, four equivalent methods are analytically derived and explained with the aid of illustrations. DWT-based deconvolution is described in Chapter 6. The procedure is validated via simulation experiments involving several channel models, and the results are discussed. In Chapter 7 a technique for DWT-based channel equalization is presented, using which DWT-based MMSE equalization and DWT-based ZFE are implemented in simulation experiments.

Chapter 8 contains three communications systems that use DWT-based channel equalizers and channel estimators, as needed. The performance of the systems is evaluated, and results compared with their standard, discrete time-domain, counterparts.

The dissertation is concluded in Chapter 9 with a summary of the research that has been presented, an exposition of the limitations of the topics, and a list of suggested future work that could be carried out as extensions of this dissertation.

Chapter 2

Theoretical Preliminaries

The formal definitions of signals, as used in this dissertation and in the general context of communications, are presented in Section 2.1. Commonly-used terms, such as baseband signals, low-pass equivalent signals, passband and band-pass signals, etc., are explained. The standard discrete-time channel model is presented in detail in Section 2.2. The concepts that are used in the model are used throughout this work, either in conjunction with other concepts of communications channels or independently.

The concept of linear equalization of signal is described in Section 2.3. Analytical formulations of the two specific types of equalization that are used in this dissertation, i.e., MMSE equalization and ZFE, are also provided in the section.

In Section 2.4 the concepts of multipath channels and the consequential undesirable phenomenon of Intersymbol Interference (ISI) are introduced. The fading effects of multipath channels on signals are discussed in Section 2.5.

2.1 Signal Definitions

Consider a real-valued time-domain signal, $s(t)$, that is to be transmitted, and has spectral content located about the frequency, f_c, which denotes the carrier frequency of the signal. The frequency spectrum of $s(t)$, i.e., $S(f)$, is shown in Fig. 2.1.1.

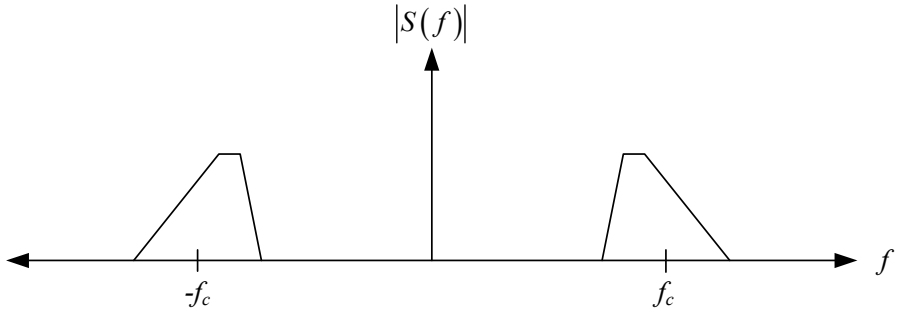

Fig. 2.1.1. Frequency spectrum of a band-pass signal.

A signal of this type is called a **band-pass signal** since it can be filtered by a band-pass filter prior to transmission and still retain most (if not all) of its spectral content. The band-pass filter serves to limit the spectral content of the signal to a specific bandwidth about a specific center frequency. In general, the bandwidth of the signal to be transmitted is smaller than its center frequency, f_c. A band-pass signal is also sometimes referred to as a **passband signal**, and the two terms may be used interchangeably.

A band-pass signal can be generally expressed as [3]

$$s(t) = \mathrm{Re}\left\{ s_l(t) e^{j2\pi f_c t} \right\} \tag{2.1.1}$$

where $s_l(t)$ is called the **low-pass equivalent** of $s(t)$, the band-pass signal. In particular, $s_l(t)$ can be conveniently described in polar form as

$$s_l(t) = a(t)e^{j\theta(t)} \tag{2.1.2}$$

where $a(t)$ is called the envelope of $s(t)$, $\theta(t)$ the phase of $s(t)$, and, therefore, $s_l(t)$ itself is called the complex envelope of $s(t)$.

The expression for $s(t)$ in (2.1.1) can be simplified using Euler's formula to explicitly show the cosine function comprising the band-pass signal

$$s(t) = \mathrm{Re}\left\{a(t)e^{j\theta(t)}e^{j2\pi f_c t}\right\}$$

$$\Rightarrow s(t) = \mathrm{Re}\left\{a(t)e^{j\left[2\pi f_c t+\theta(t)\right]}\right\}$$

$$\Rightarrow s(t) = a(t)\cos\left(2\pi f_c t + \theta(t)\right). \tag{2.1.3}$$

An alternative expression for the band-pass signal is also available by expressing the low-pass equivalent signal in (2.1.2) in Cartesian form, i.e.,

$$s_l(t) = s_l^{\mathrm{I}}(t) + s_l^{Q}(t). \tag{2.1.4}$$

Substituting (2.1.4) into (2.1.1), allows for the band-pass signal to expressed as

$$s(t) = \mathrm{Re}\left\{\left[s_l^{\mathrm{I}}(t) + js_l^{Q}(t)\right]e^{j2\pi f_c t}\right\}$$

$$\Rightarrow s(t) = s_l^{\mathrm{I}}(t)\cos\left(2\pi f_c t\right) - s_l^{Q}(t)\sin\left(2\pi f_c t\right). \tag{2.1.5}$$

The cosine term in (2.1.5) is commonly referred to as the **In-phase (I)** carrier component of the band-pass signal, and the sine term is referred to as the **Quadrature (Q)** component, as it is $\pi/2$ radians out-of-phase with respect to the I carrier component. From the definition of a band-pass signal in (2.1.5) $s_l^{\mathrm{I}}(t)$ and $s_l^{\mathrm{Q}}(t)$ can be thought of as multiplying function that modulate the amplitude of the I and Q carrier components, respectively [3].

2.2 Standard Channel Model

In the remainder of this dissertation, only low-pass equivalent signals are considered instead of band-pass signals for the sake of convenience, without any loss of generality [3]. Consider a discrete information-bearing sequence of symbols, represented by $\{I_n\}$, and a pulse that is generated by a low-pass filter having an impulse response $g(t)$. The pulse is assumed to have a band-limited frequency spectrum, $G(f)$, such that $|G(f)| = 0 \ \forall \ |f| > W$, where W is the bandwidth of $G(f)$. The transmitted signal can, therefore, be described in terms of $\{I_n\}$ and $g(t)$ as

$$s(t) = \sum_{n=0}^{\infty} I(n)\, g(t - nT), \tag{2.2.1}$$

where T is the duration of the $g(t)$.

The signal, $s(t)$, is transmitted through a channel, the impulse response of which is denoted by $c(t)$. A functional block diagram depicting the signal propagation path from transmitter to receiver, along with the fundamental sub-systems in typical communications transmitters and receivers, is shown in Fig. 2.2.1.

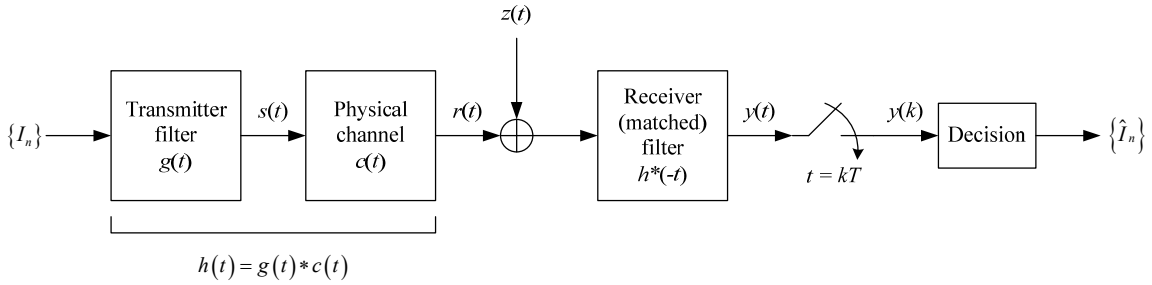

Fig. 2.2.1. Block diagram of signal transmission and reception.

The convolution operations performed by the low-pass transmitter filter and the channel can be combined into one impulse response function, $h(t)$, as

$$h(t) = \int_{-\infty}^{\infty} g(\tau)c(t-\tau)d\tau . \tag{2.2.2}$$

Hence, the low-pass signal that is acquired by a radio receiver can be represented by

$$r(t) = \sum_{n=0}^{\infty} I(n)h(t-nT) + z(t), \tag{2.2.3}$$

where $z(t)$ is used to denote noise that may be added to the signal during propagation through the channel.

Upon reception, the signal is filtered by a matched filter, i.e., a filter with an impulse response that is matched to the combined impulse responses of the transmit filter and the

channel, $h(t)$. Specifically, the impulse response of such a matched filter at the receiver is $h^*(-t)$.

At a higher level of abstraction, an impulse response function $x(t)$ can be defined as the response of the matched filter, $h^*(-t)$, to an excitation $h(t)$, i.e.,

$$x(t) = \int_{-\infty}^{\infty} h^*(t)\, h(t+nT)\, dt\,. \tag{2.2.4}$$

This definition is depicted in Fig. 2.2.2.

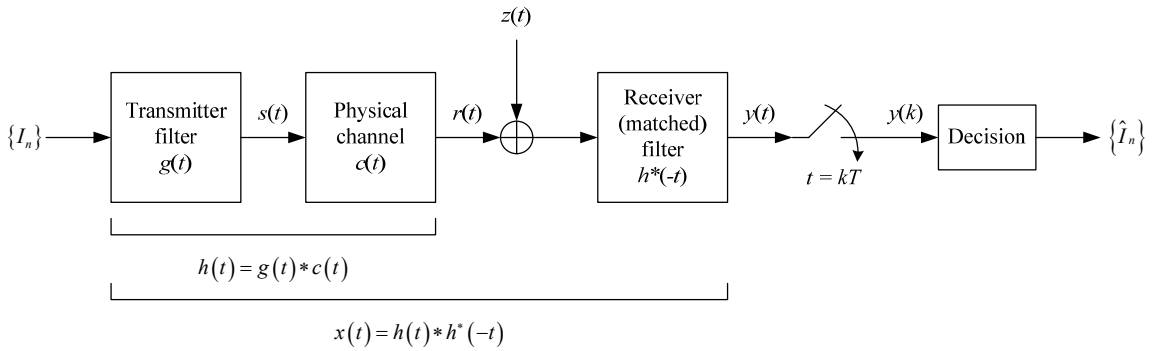

Fig. 2.2.2. Block diagram of systems and channel, with $x(t)$ shown.

The output of the matched filter, $y(t)$, can now be described as

$$y(t) = \sum_{n=0}^{\infty} I(n)\, x(t-nT) + v(t) \tag{2.2.5}$$

where $v(t)$ is the response of the matched filter to the noise $z(t)$, i.e.,

$$v(t) = \int_{-\infty}^{\infty} z(\tau)\, h^*(t-\tau)\, d\tau\,. \tag{2.2.6}$$

Following matched filtering, the signal $y(t)$ is sampled at a rate of $1/T$ samples/s, i.e., at $t = kT$ for $k = 0,1,\ldots$. The output of the sampler can be described analytically as

$$y(kT) = \sum_{n=0}^{\infty} I(n)\, x(kT - nT) + v(kT)$$

$$\Rightarrow y(k) = \sum_{n=0}^{\infty} I(n)\, x(k-n) + v(k). \tag{2.2.7}$$

Note that the delay due to propagation of the signal through the channel is omitted in this formulation.

Equation (2.2.7) can be also be expressed as

$$y(k) = x(0)\, I(k) + \sum_{\substack{n=0 \\ n \neq k}}^{\infty} I(n)\, x(k-n) + v(k). \tag{2.2.8}$$

Setting $x(0) = 1$ for convenience, causes the output of the sampler to be expressed as

$$y(k) = I(k) + \sum_{\substack{n=0 \\ n \neq k}}^{\infty} I(n)\, x(k-n) + v(k). \tag{2.2.9}$$

In the expression of the sampled matched filtered version of the received signal, i.e., in (2.2.9), $I(k)$ is the information symbol at the k^{th} sampling instant that is to be recovered, the summation $\sum_{\substack{n=0 \\ n \neq k}}^{\infty} I(n)\, x(k-n)$ represents the interference of all of the other symbols with the k^{th} symbol, i.e., the ISI, and $v(k)$ is the filtered additive noise at the k^{th} sampling instant.

2.3 Linear Equalization

As seen in (2.2.4), $x(t)$ denotes the combined impulse response of the transmitter filter, the physical channel, and the receiver (matched) filter, i.e.,

$$x(n) = \int_{-\infty}^{\infty} h^*(t)\,h(t+nT)\,dt\,.$$

Let $X(z)$ be the double-sided z-transform of $\{x_k\}$, i.e.,

$$X(z) = \sum_{k=-L}^{L} x(k)\,z^{-k}\,, \tag{2.3.1}$$

where the approximation is made that the k^{th} symbol output by the matched filter is affected by ISI due to the L symbols that precede it and the L symbols follow it.

The channel, expressed as a z-domain summation in (2.3.1), is depicted as a tapped-delay line filter having $2L + 1$ tap weights and $2L$ delays in Fig. 2.3.1. Each delay corresponds to the time interval T, which is the baseband symbol rate, and is represented by z^{-1} in the z-domain. The input to the channel is the original symbol sequence at the transmitter, $\{I_k\}$, the noise that is added to the sampled signal after matched filtering is $\{\nu_k\}$, and the resulting output, from which estimates of the symbols must be recovered, is $\{y_k\}$.

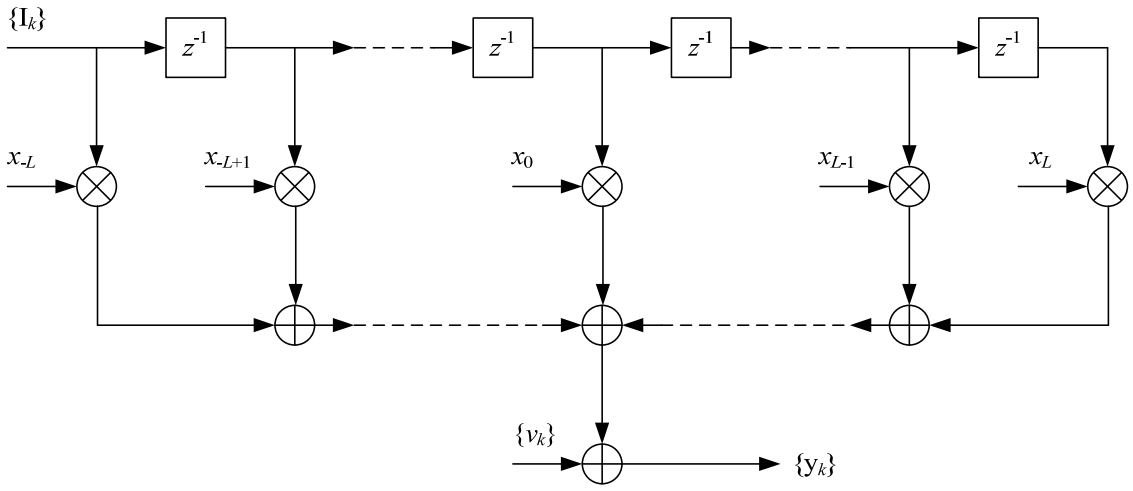

Fig. 2.3.1. A tapped-delay line model of a communications channel.

The output of the discrete-time channel model seen in Fig. 2.3.1. is

$$y(k) = I(k) + \sum_{\substack{n=0 \\ n \neq k}}^{\infty} I(n)\, x(k-n) + v(k). \tag{2.3.2}$$

In order to mitigate the effects of the channel, the discrete-time sequence $\{y_k\}$ is input to an equalizer. The function of the equalizer is to reduce the superposition of the second (summation) term in (2.2.8) on $I(k)$. By supplying the decision mechanism with such an equalized signal an estimate of the original baseband symbol sequence, $\{\hat{I}_n\}$, can be obtained.

An updated block diagram of the typical communications system containing an equalizer is provided in Fig. 2.3.2. The illustration also shows the transfer functions of several of

the systems in the z-domain, as well as some time-domain representations. Of particular interest is transfer function of the equalizer, $B(z) = 1/X(z)$.

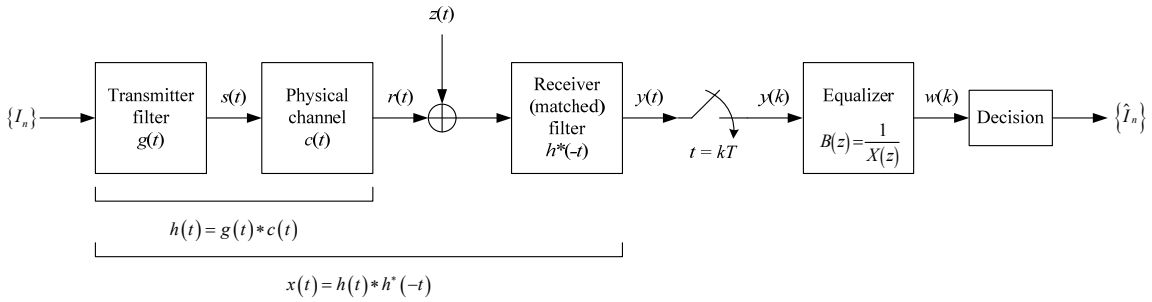

Fig. 2.3.2. Communications system and channel block diagram, including equalization.

Fig. 2.3.3. is an illustration of a typical channel equalizer that is implemented as a tapped-delay line with tap coefficients $\{b_k\}$. The output of the equalizer is the discrete-time sequence $\{w_k\}$, which is denoted by $W(z)$ in the z-domain.

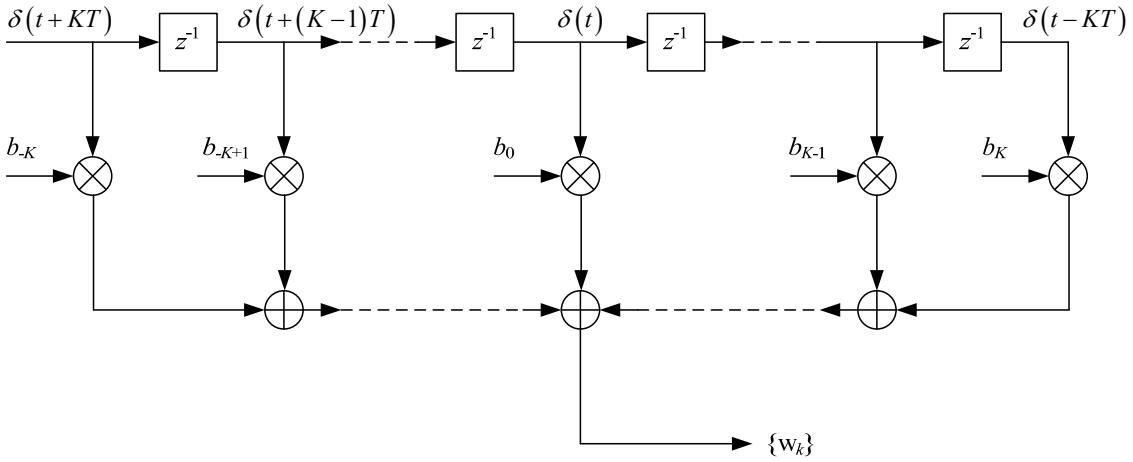

Fig. 2.3.3. A channel equalizer implemented as a tapped-delay line filter.

As shown in Fig. 2.3.3, let the equalizer have $2K + 1$ tap weights and $2K$ taps. Therefore, the transfer function of the filter can be expressed as

$$B(z) = \sum_{m=-K}^{K} b(m) z^{-m} . \tag{2.3.3}$$

Assume that the input to the equalizer is, generally, a discrete-time function $y(k)$, which has the z-transform

$$Y(z) = \sum_{k=-\infty}^{\infty} y(k) z^{-k} . \tag{2.3.4}$$

The output of the equalizer having the transfer function $B(z)$ and an input $Y(z)$, as shown in Fig. 2.3.3, is, therefore,

$$W(z) = Y(z) B(z)$$

$$\Rightarrow W(z) = \left(\sum_{k=-\infty}^{\infty} y(k) z^{-k} \right) \left(\sum_{m=-K}^{K} b(k) z^{-m} \right)$$

$$\Rightarrow W(z) = \sum_{k=-\infty}^{\infty} \sum_{m=-K}^{K} b(m) y(k) z^{-(k+m)} . \tag{2.3.5}$$

Let $l = k + m$ so that (2.3.5) can be rewritten as

$$W(z) = \sum_{k=-\infty}^{\infty} \sum_{m=-K}^{K} b(m) y(l-m) z^{-l} . \tag{2.3.6}$$

Defining the output of the equalizer as the convolution

$$w(l) = \sum_{m=-K}^{K} b(m) y(l-m) \tag{2.3.7}$$

enables the z-transform of the output of the equalizer, in (2.3.5) to be expressed as

$$W(z)=\sum_{l=-\infty}^{\infty} w(l)z^{-l}. \tag{2.3.8}$$

2.3.1 Zero-Forcing Equalization

Consider the scenario where an arbitrary signal $V(z)$ is originally transmitted through the channel $X(z)$ instead of a baseband symbol sequence $\{I_n\}$. Following Fig. 2.3.2, in the absence of noise, the input to the equalizer is

$$Y(z)=V(z)X(z) \tag{2.3.9}$$

and, therefore, the output of the equalizer is

$$W(z)=V(z)X(z)B(z). \tag{2.3.10}$$

This allows the transfer function of the equalized system to be described as

$$H(z)=\frac{W(z)}{V(z)}=X(z)B(z). \tag{2.3.11}$$

From (2.3.11) it is clear that in order for the equalized signal to be equal to the signal that is originally transmitted, the condition

$$H(z)=1$$

$$\Rightarrow B(z)=\frac{1}{X(z)} \tag{2.3.12}$$

must be satisfied. This condition implies that in order to reverse any channel effects the received signal must be operated on by a filter having a transfer function that is the reciprocal of the transfer function of the channel.

In the discrete time-domain the impulse response of this equalized system can be expressed as the convolution

$$h(k) = x(k) * b(k)$$

$$\Rightarrow h(k) = \sum_{m=-K}^{K} b(m)\, x(k-m). \tag{2.3.13}$$

In order to have a perfectly equalized signal that is free of ISI, according to (2.3.12),

$$h(k) = \begin{cases} 1, & k = 0 \\ 0, & k \neq 0 \end{cases}. \tag{2.3.14}$$

By the imposition of this condition in (2.3.14), the contributions of ISI components at all discrete instants of time to the k^{th} signal sample are forced to be equal to zero by the equalizer. For this reason the equalizer satisfying the condition in (2.3.14) is called a Zero-Forcing Equalizer.

Practically, however, the condition in (2.3.12), and its time-domain equivalent in (2.3.14), cannot be enforced since they would require filters with an infinite number of taps. Therefore, ZFEs with finite numbers of taps, such as $2L + 1$ must be designed. To this end, (2.3.14) is approximated as

$$\hat{h}(k) = \begin{cases} 1, & k = 0 \\ 0, & k = \pm 1, \pm 2, \ldots, \pm K \end{cases} \tag{2.3.15}$$

so that when $K \to \infty$, $\hat{h}_k \to h_k$.

By expressing the convolution between the input signal and the equalizer in (2.3.13) in Toeplitz matrix form, and applying the approximate condition for equalization in (2.3.15), the tap weights of the equalizer can be found by solving the matrix equation

$$\begin{bmatrix} x_0 & \cdots & x_{-K+1} & x_{-K} & x_{-K-1} & \cdots & x_{-2K} \\ \vdots & \ddots & \vdots & \vdots & \vdots & \ddots & \vdots \\ x_{K-1} & \cdots & x_0 & x_{-1} & x_{-2} & \cdots & x_{-K-1} \\ x_K & \cdots & x_1 & x_0 & x_{-1} & \cdots & x_{-K} \\ x_{K+1} & \cdots & x_2 & x_1 & x_0 & \cdots & x_{-K+1} \\ \vdots & \ddots & \vdots & \vdots & \vdots & \ddots & \vdots \\ x_{2K} & \cdots & x_{K+1} & x_K & x_{K-1} & \cdots & x_0 \end{bmatrix} \begin{bmatrix} b_{-K} \\ \vdots \\ b_{-1} \\ b_0 \\ b_1 \\ \vdots \\ b_K \end{bmatrix} = \begin{bmatrix} 0 \\ \vdots \\ 0 \\ 1 \\ 0 \\ \vdots \\ 0 \end{bmatrix}. \tag{2.3.16}$$

2.3.2 Minimum Mean-Squared Error Equalization

In order to implement MMSE equalization, a pilot signal, $d(t)$, is transmitted prior to the transmission of the message signal, $s(t)$. This additional signal is used to gauge the effects of the channel on the signal so that the coefficients of the MMSE equalizer can be determined.

Let **y** and **d** be the inputs to a tapped-delay line equalizer. The vector **y** denotes the received signal that is to be equalized with respect to the pilot signal **d**. It is assumed that both **y** and **d** are Wide-Sense Stationary (WSS) and the autocorrelation functions of both signals are known. The tap weights of the equalizer are given by the vector **b**, which is of length $2K+1$.

The output of the equalizer is denoted by $w(n)$, and is defined by the convolution

$$w(n) \triangleq \sum_{i=-K}^{K} b(i)\, y(n-i). \tag{2.3.17}$$

Let the error between any n^{th} element of the output sequence $\{y_n\}$ and the corresponding n^{th} element of the pilot vector **d**, i.e., of the sequence $\{d_n\}$ be defined as

$$e(n) = d(n) - y(n). \tag{2.3.18}$$

Note that **d** and **w** are generally not of equal lengths, as is required in (2.3.18). Therefore, either the longer of the two vectors must be truncated to become the same length as the other, or the shorter vector must be padded with zeros at the beginning and end so as to become the same length as the longer vector.

An intuitive way to interpret (2.3.18) is to think of $e(n)$ as the *instantaneous error* between $d(n)$ and $w(n)$. In order to construct a filter to equalize all elements of **w**, however, a more general measure of the error between **d** and **w** is needed. Such a metric must take into consideration both **d** and **w** in their entirety, and not just any n^{th} element of **w** and the corresponding element of **d**. In fact, the average value of each such n^{th} error could be used as a statistical metric. Such an approach is especially powerful since both **d** and **y** can be generally considered to be random processes.

One such average error metric is the Mean Squared Error (MSE) criterion. The MSE between the two random processes can also be interpreted in a more intuitive fashion as being the average error between the records **d** and **w** when taken in their entirety, and not

element-wise. Such an interpretation is analogous to the concept of the average power of an (electromagnetic) signal, which is averaged over the entire time duration of the signal. On the other hand, the instantaneous error, $e(n)$, is akin to the instantaneous power of a signal, which is evaluated only at a particular instant of time, i.e., at one sample or slice of time.

Hence, the MSE between **d** and **w** is therefore defined as the objective function, *J*, in terms of $e(n)$ as

$$J = E\left\{\left|e(n)\right|^2\right\}$$

$$\Rightarrow J = E\left\{\left|d(n) - w(n)\right|^2\right\}, \tag{2.3.19}$$

where $E\{\cdot\}$ is the expectation value operator.

In the case where **d** and **w** are real, (2.3.18) becomes

$$J = E\left\{\left(d(n) - y(n)\right)^2\right\}$$

$$\Rightarrow J = E\left\{d^2(n)\right\} - E\left\{2d(n)y(n)\right\} + E\left\{y^2(n)\right\}. \tag{2.3.20}$$

Substituting (2.3.17) in (2.3.20) results in the expanded expression

$$J = E\left\{d^2(n)\right\} - 2E\left\{d(n)\sum_{i=-K}^{K} b(i)x(n-i)\right\} + E\left\{\left(\sum_{i=-K}^{K} b(i)x(n-i)\right)^2\right\}. \tag{2.3.21}$$

The MSE between **d** and **w** must now be minimized. More precisely, the gradient of objective function of the MSE, i.e., *J*, is to be minimized with respect to the tap weights of the equalizer, each $b(i)$. This condition is expressed as

$$\frac{\partial}{\partial b(i)} J = 0 \qquad \text{for } i = -K, -K+1 \ldots, 0, \ldots, K-1, K . \tag{2.3.22}$$

Enforcing (2.3.22) on (2.3.23) results in

$$-\sum_{i=-K}^{K} E\{d(n)x(n-i)\} + \sum_{i=-K}^{K}\sum_{j=-K}^{K} b(j) E\{x(n-j)x(n-i)\} = 0 . \tag{2.3.23}$$

Recognizing that the autocorrelation function of **y** is

$$R_{yy}(i,j) = E\{y(n-i)y(n-j)\} \tag{2.3.24}$$

and the cross-correlation function of **d** and **y** is

$$R_{dy}(j) = E\{d(n)y(n-j)\}, \tag{2.3.25}$$

(2.3.23) can be recast as

$$\sum_{i=-K}^{K}\sum_{j=-K}^{K} b(j) R_{yy}(i,j) = \sum_{i=-K}^{K} R_{dy}(i) \tag{2.3.26}$$

$$\Rightarrow \sum_{j=-K}^{K} b(j) R_{yy}(i,j) = R_{dy}(i) \text{ for } i = -K, -K+1 \ldots, 0, \ldots, K-1, K . \tag{2.3.27}$$

This equation can be expressed concisely in matrix form as

$$\mathbf{R}_{yy}\mathbf{b}^{\mathrm{T}} = \mathbf{R}_{dy}^{\mathrm{T}} \tag{2.3.27}$$

where $\mathbf{R}_{yy}$ is the autocorrelation matrix of the input signal **y**, and is defined as

$$\mathbf{R}_{yy}=\begin{bmatrix} R_{yy}(-K,-K) & R_{yy}(-K+1,-K) & \cdots & R_{yy}(0,-K) & \cdots & R_{yy}(K-1,-K) & R_{yy}(K,-K) \\ R_{y}(-K,-K+1) & R_{yy}(-K+1,-K+1) & \cdots & R_{yy}(0,-K+1) & \cdots & R_{yy}(K-1,-K+1) & R_{yy}(K,-K+1) \\ \vdots & \vdots & \ddots & \vdots & \ddots & \vdots & \vdots \\ R_{yy}(-K,0) & R_{yy}(-K+1,0) & \cdots & R_{yy}(0,0) & \cdots & R_{yy}(K-1,0) & R_{yy}(K,0) \\ \vdots & \vdots & \ddots & \vdots & \ddots & \vdots & \vdots \\ R_{yy}(-K,K-1) & R_{yy}(-K+1,K-1) & \cdots & R_{yy}(0,K-1) & \cdots & R_{yy}(K-1,K-1) & R_{yy}(K,K-1) \\ R_{yy}(-K,K) & R_{yy}(-K+1,K) & \cdots & R_{yy}(0,K) & \cdots & R_{yy}(K-1,K) & R_{yy}(K,K) \end{bmatrix},$$

the equalizer tap weight vector **b** is of the form

$$\mathbf{b}=\begin{bmatrix} b_{-K} & b_{-K+1} & \cdots & b_0 & \cdots & b_{K-1} & b_K \end{bmatrix}$$

and the cross-correlation vector of **d** and **x** is

$$\mathbf{R}_{dy}=\begin{bmatrix} R_{dy}(-K) & R_{dy}(-K+1) & \cdots & R_{dy}(0) & \cdots & R_{dy}(K-1) & R_{dy}(K) \end{bmatrix}.$$

Hence, the desired equalizer tap weights can be found by solving the inverse problem

$$\mathbf{b}^{\mathrm{T}}=\mathbf{R}_{yy}^{-1}\mathbf{R}_{dy}^{\mathrm{T}}, \tag{2.3.29}$$

which results from (2.3.27).

When the random process $\{y_n\}$ is WSS, the condition on the autocorrelation function of **y** that

$$R_{yy}(t_1,t_2)=R_{yy}(t_1+\tau,t_2+\tau)\,\forall\,\tau\in\mathbb{R} \tag{2.3.30}$$

must hold. This condition implies that

$$R_{yy}(i,j)=R_{yy}(i+k,j+k). \tag{2.3.31}$$

Also note that,

$$R_{yy}(i,j)=R_{yy}(j,i). \tag{2.3.32}$$

Although most generally $\mathbf{R}_{yy}$ is a symmetric matrix, it is seen from (2.3.31) and (2.3.32) that with the assumptions that have been made, viz., $\{y_n\}$ is WSS, $\mathbf{R}_{yy}$ is in fact a

Hermitian Toeplitz matrix. Therefore, when $\mathbf{R}_{yy}$ is non-singular, (2.3.29) can be efficiently solved by using a suitable procedure for computing the inverse $\mathbf{R}_{yy}$.

2.4 Multipath Channels

Signals that propagate through wireless channels are subject to a myriad of propagation effects such as harmonic distortion, dispersion and reflections from objects that the signals may be inadvertently incident upon. The signal acquired by the antenna of a receiver is, therefore, a distorted version of the transmitted signal. Typically, however, the received signal is a superposition of several such time-delayed distorted signals. This detrimental phenomenon that channels subject on propagating signals is called **fading**, and the channels that cause such effects are called **fading channels**.

Fading channels which cause multiple time-delayed copies of a transmitted signal, i.e., provide multiple propagation paths for a transmitted signal, are called **multipath channels**.

As mentioned previously, ISI is an important effect that fading channels have on transmitted signals. This is particularly significant when the information-bearing baseband signal is a digital pulse. The corresponding digitally modulated band-pass signal that is transmitted then has spectral components occupying a wide bandwidth. If the physical and electrical characteristics of the channel cause it to be dispersive, the signal is detrimentally affected. Such a faded signal effectively represents baseband

digital pulses that have been spread out temporally and interfere either constructively or destructively with adjacent pulses. This phenomenon is called ISI.

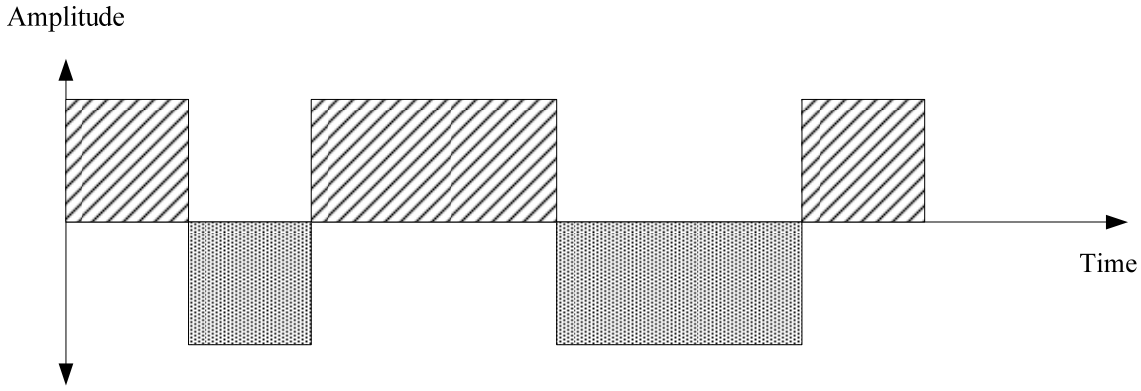

Fig. 2.4.1. Baseband bit sequence represented by a transmitted band-pass signal.

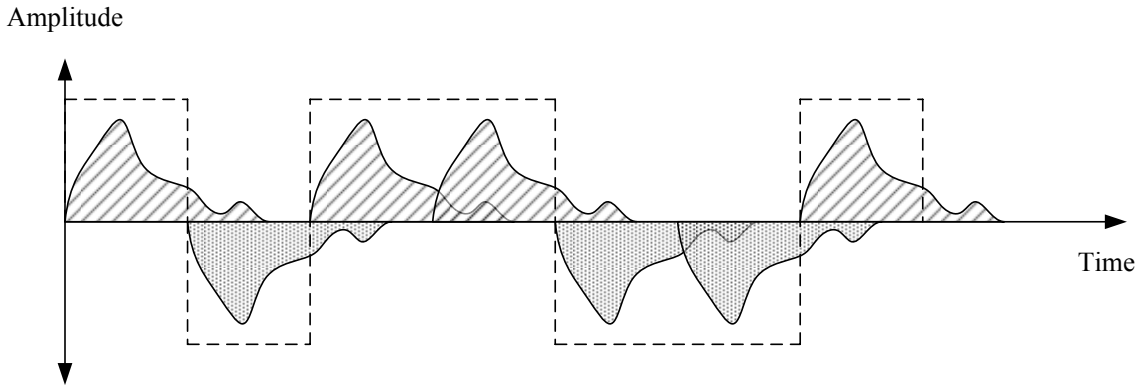

Fig. 2.4.2. Baseband bit sequence represented by a transmitted band-pass signal that has been affected by ISI.

Figure 2.4.1 is an illustration of a baseband digital pulse train that represents the bit sequence {1 0 1 1 0 0 1}. Figure. 2.4.2 is an illustration of the same baseband signal except after the effect of ISI. Note that the rendering of ISI in Fig. 2.4.2 only shows the overlaps, i.e., the smearing, of the pulses, and not the actual resultant signal. The actual

signal will be a continuous time-domain signal that contains superpositions of any of the pulse overlaps.

In order to minimize ISI signals are typically filtered prior to transmission through a bandlimited channel so that the signal bandwidth is restricted, thereby preemptively reducing the effect of ISI.

2.4.1 Mathematical Definitions

Consider the band-pass transmitted signal, as defined in (2.1.1),

$$s(t) = \mathrm{Re}\left\{ s_l(t) e^{j2\pi f_c t} \right\}. \tag{2.4.1.1}$$

Let the channel, $c(t)$, consist of multiple propagation paths with each path being defined by a propagation delay and an attenuation factor. Let $\alpha_n(t)$ be the attenuation factor for the n^{th} path and $\tau_n(t)$ be the propagation delay for the n^{th} path. Therefore, the received signal can be generally described as

$$r(t) = \sum_n \alpha_n(t) s\left[t - \tau_n(t) \right]. \tag{2.4.1.2}$$

Substituting (2.4.1.1) in (2.4.1.2) in order to express the received signal in terms of the transmitted signal components gives

$$r(t) = \sum_n \alpha_n(t) \mathrm{Re}\left\{ s_l\left[t - \tau_n(t) \right] e^{j2\pi f_c \left[t - \tau_n(t) \right]} \right\}$$

$$\Rightarrow r(t) = \mathrm{Re}\left\{ \left(\sum_n \alpha_n(t) e^{-j2\pi f_c \tau_n(t)} s_l\left[t - \tau_n(t) \right] \right) e^{j2\pi f_c t} \right\}. \tag{2.4.1.3}$$

From the convolution operation implicit in (2.4.1.3), the low-pass equivalent received signal can be identified as

$$r_l(t) = \sum_n \alpha_n(t) s_l\left[t - \tau_n(t)\right] e^{j2\pi f_c \tau_n(t)}. \tag{2.4.1.4}$$

Hence, the low-pass equivalent multipath channel impulse response can be inferred from (2.4.1.4) to be

$$c(\tau;t) = \sum_n \alpha_n(t) e^{j2\pi f_c \tau_n(t)} \delta\left[t - \tau_n(t)\right]. \tag{2.4.1.5}$$

Of course, multipath channels can also be defined in continuous-time as well. In this scenario, the received signal can be expressed generally in terms of the transmitted signal, $s(t)$, and the attenuation factor, $\alpha(t)$, as

$$r(t) = \int_{-\infty}^{\infty} \alpha(\tau;t) s(t-\tau)\, d\tau. \tag{2.4.1.6}$$

Substituting the expression for the transmitted signal in (2.4.1.1) into (2.4.1.6) gives

$$r(t) = \int_{-\infty}^{\infty} \alpha(\tau;t) \operatorname{Re}\left\{ s_l(t-\tau) e^{j2\pi f_c (t-\tau)} \right\} d\tau$$

$$\Rightarrow r(t) = \operatorname{Re}\left\{ \left[\int_{-\infty}^{\infty} \alpha(\tau;t) e^{-j2\pi f_c \tau} s_l(t-\tau)\, d\tau \right] e^{j2\pi f_c t} \right\}. \tag{2.4.1.7}$$

Again, identifying the convolution operation implicit in (2.4.1.7), the impulse response of a multipath channel in the continuous-time case is recognized to be

$$c(\tau;t) = \alpha(\tau;t) e^{-j2\pi f_c t}. \tag{2.4.1.8}$$

2.4.2 Interpretation of Definitions

Let a sinusoid, i.e., an unmodulated carrier, be transmitted through the multipath channel defined in (2.4.1.4). In this case, $s_l(t) = 1 \ \forall \ t$. Therefore, the received signal is

$$r_l(t) = \sum_n \alpha_n(t) e^{-j2\pi f_c \tau_n(t)}$$

$$\Rightarrow r_l(t) = \sum_n \alpha_n(t) e^{-j\theta_n(t)} \tag{2.4.2.1}$$

where $\theta_n(t) = 2\pi f_c \tau_n(t)$.

It is seen in (2.4.2.1) that when $\tau_n(t)$ changes by a factor of $1/f_c$ the phase of the n^{th} received sinusoid changes by 2π. Since typical contemporary communications systems transmit signals with frequencies in the MHz and GHz ranges, this observation implies that even small changes in the physical structure of the channel can effect significant changes in the phase of a signal.

A reasonable assumption is that changes in the propagation delays, $\{\tau_n(t)\}$s, that are associated with the various paths are independent of the changes of the delays of other paths, and change randomly. This assumption allows for the received signal, $r_l(t)$, to be modeled as a random process. In particular, when the channel is composed of a large number of paths the central limit theorem can be applied, and $r_l(t)$ can be modeled as a complex-valued Gaussian random process. This implies that the impulse response of the channel itself, $c(\tau;t)$, can also be modeled as a complex-valued Gaussian process [3].

Of particular significance are the two general cases that arise depending on whether or not a multipath channel contains a Line-of-Sight (LoS) propagation path. When an LoS path exists, the channel impulse response, $c(\tau;t)$, can be modeled as a zero-mean complex-valued Gaussian process and its envelope, i.e., $|c(\tau;t)|$, is Rayleigh distributed, in the variable *t*. Such a channel is called a **Rayleigh fading channel**. As wireless channels are usually passive, i.e., do not provide any signal gain, the power of the received LoS component of the received signal is the largest when compared with the other components [3].

On the other hand, a wireless channel that does not contain LoS path, but is only composed of other fixed and moving scatterers, cannot be modeled as a complex-valued Gaussian process having zero-mean. The complex envelope of such a channel can be modeled by using a Rice distribution. Such a channel is called a **Rician fading channel** [3].

In both Rayleigh and Rician fading channels the phase of the channel impulse response is uniformly distributed over the interval $(0, 2\pi]$.

2.5 Fading Effects of Multipath Channels

In order to explore the fading effects of multipath channels two assumptions are made. The first assumption is that the impulse response of a multipath channel, i.e., $c(\tau;t)$, is Wide-Sense Stationary. In general, a random process, $x(t)$, is WSS iff

1. Its mean is constant, i.e.,

$$\mathrm{E}\{x(t)\} = \mathrm{E}\{x(t+\tau)\} \quad \forall \quad t \in \mathbb{R}.$$

2. Its autocorrelation function, $R_x(t_1,t_2)$, depends only on the difference between the time instants t_1 and t_2, i.e.,

$$R_x(t_1,t_2) = R_x(t_1+\tau,t_2+\tau) = R_x(t_1-t_2,0) \quad \forall \quad t \in \mathbb{R}.$$

Again, the operator $\mathrm{E}\{\cdot\}$ denotes the expected value, i.e., the mean, of the argument.

In keeping with this assumption of WSS, the autocorrelation function of the channel impulse response is defined as [3]

$$\phi_c(\tau_1,\tau_2;\Delta t) = \frac{1}{2}\mathrm{E}\{c^*(\tau_1;t)c(\tau_2;t+\Delta t)\}, \tag{2.5.1}$$

where Δt is the time that elapses between two observations of $\phi_c(\tau_1,\tau_2)$.

The second assumption is that the attenuation and phase deviation associated with one path in the multipath channel are uncorrelated with the attenuation and phase deviation of any other path in the channel. The type of multipath propagation that occurs according to this assumption is called **Uncorrelated Scattering** (US).

Therefore, the autocorrelation function of the channel impulse response in (2.5.1) can be modified for the case of a WSS-US channel to be

$$\phi_c(\tau_1;\Delta t)\delta(\tau_1-\tau_2)=\frac{1}{2}\mathrm{E}\left\{c^*(\tau_1;t)c(\tau_2;t+\Delta t)\right\}. \tag{2.5.2}$$

If the autocorrelation function of the channel impulse response is evaluated for $\Delta t=0$ it becomes simply $\phi_c(\tau)$, which is the average power output by the channel when excited by an impulse. Since this average output power is a function of the delay time associated with the channel, the function $\phi_c(\tau)$ is called the **Power Delay Profile** (PDP) of the channel.

Additionally, the general time-variant transfer function of the channel can be expressed in the Fourier-domain as

$$C(f;t)=\int_{-\infty}^{\infty}c(\tau;t)e^{-j2\pi f\tau}d\tau. \tag{2.5.3}$$

Since the channel is assumed to be WSS-US, the transfer function of the channel in (2.5.3) is

$$\phi_c(f_1,f_2;\Delta t)=\frac{1}{2}E\left\{C^*(f_1;t)C(f_2;t+\Delta t)\right\}. \tag{2.5.4}$$

Substituting (2.53) into (2.5.4) results in the frequency-domain expression

$$\phi_c(f_1,f_2;\Delta t)=\frac{1}{2}\int_{-\infty}^{\infty}\int_{-\infty}^{\infty}E\left\{c^*(t_1;t)c(\tau_2;t+\Delta t)\right\}e^{j2\pi(f_1\tau_1-f_2\tau_2)}d\tau_1 d\tau_2$$

$$\Rightarrow\phi_c(f_1,f_2;\Delta t)=\int_{-\infty}^{\infty}\int_{-\infty}^{\infty}\phi_c(\tau_1;\Delta t)\delta(\tau_1-\tau_2)e^{j2\pi(f_1\tau_1-f_2\tau_2)}d\tau_1 d\tau_2$$

$$\Rightarrow \phi_c\left(f_1, f_2; \Delta t\right) = \int_{-\infty}^{\infty} \phi_c\left(\tau_1; \Delta t\right) e^{j2\pi(f_1 - f_2)\tau_1} d\tau_1$$

$$\Rightarrow \phi_c\left(f_1, f_2; \Delta t\right) = \int_{-\infty}^{\infty} \phi_c\left(\tau_1; \Delta t\right) e^{-j2\pi\Delta f \tau_1} d\tau_1 \equiv \phi_c\left(\Delta f; \Delta t\right) \tag{2.5.5}$$

where $\Delta f = f_2 - f_1$.

It is seen in (2.5.5) that $\phi_c\left(\Delta f; \Delta t\right)$ is simply the Fourier transform of the channel PDP, $\phi_c\left(\tau\right)$. In addition, this equation for $\phi_c\left(\Delta f; \Delta t\right)$ explicitly shows the US property of the channel since the autocorrelation function of the channel transfer function only depends on the difference between the frequencies f_2 and f_1. The function $\phi_c\left(\Delta f; \Delta t\right)$ is called the **spaced-frequency, spaced-time correlation function of the channel** [3].

The function $\phi_c\left(\Delta f; \Delta t\right)$ can be interpreted in two ways. The first is by letting the difference in the observation times of the function, i.e., Δt, be 0. In this case the function becomes $\phi_c\left(\Delta f; 0\right)$, and is the **spaced-frequency correlation function of the channel** [3]. Conversely, in the second interpretation the difference in the fundamental frequencies corresponding to the different path delays, i.e., f_1 and f_2 to τ_1 and τ_2, respectively, is zero. In other words, $\Delta f = 0$. In this case the function $\phi_c\left(\Delta f; \Delta t\right)$ is reduced to $\phi_c\left(0; \Delta t\right)$, which is called the **spaced-time correlation function** [3].

Beginning with the first case, i.e., of the spaced-frequency correlation function of the channel, let $\Delta t = 0$. Therefore, for brevity, let $\phi_c\left(\Delta f; 0\right) = \phi_c\left(\Delta f\right)$ and $\phi_c\left(\tau; 0\right) = \phi_c\left(\tau\right)$.

Evaluating $\phi_c(\Delta f;\Delta t)$ in (2.5.5) for $\Delta t = 0$ gives the relationship between the autocorrelation functions of the channel impulse response in the time- and frequency-domains to be

$$\phi_c(\Delta f) = \int_{-\infty}^{\infty} \phi_c(\tau) e^{-j2\pi\Delta f\tau} d\tau \,. \tag{2.5.6}$$

The illustrations in Fig. 2.5.1 are provided as a visual aid to understanding the concepts of the PDP and the spaced-frequency correlation function of a channel.

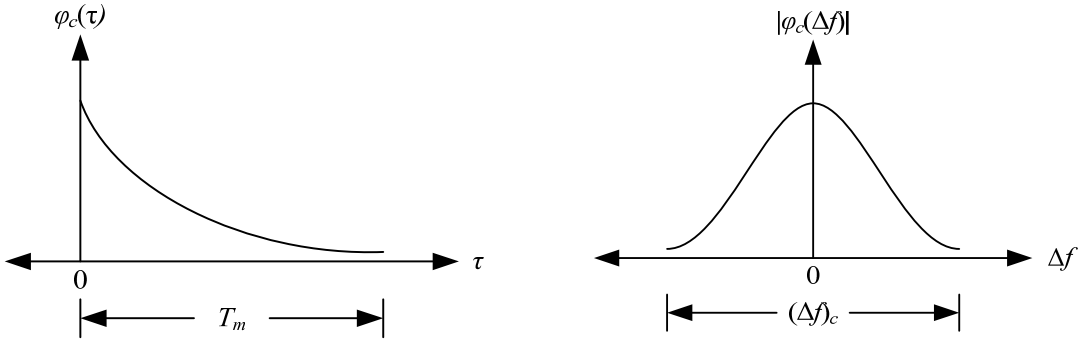

(a) Power delay profile. (b) Spaced-frequency correlation function.

Fig. 2.5.1. Illustrations of a general spaced-frequency correlation function and the power delay profile of a multipath channel [3].

In Fig. 2.5.1(b), the quantity $(\Delta f)_c$ denotes the **coherence bandwidth** of the channel. If the bandwidth of a transmitted signal is less than the channel coherence bandwidth then the channel is frequency non-selective, and is called a **flat fading channel**. On the other hand, if the signal bandwidth is greater than $(\Delta f)_C$, then the frequency content of the

signal that lies outside $(\Delta f)_C$ will be faded. In this case the channel is said to be a **frequency selective channel**.

Analogously, in the time-domain, corresponding to $(\Delta f)_C$ is the quantity T_m, which is shown in Fig. 2.5.1(a). T_m is called the **multipath spread of the channel**. It denotes the range of the time delay, τ, over which the PDP of the channel is non-zero. In the case when a digitally modulated signal is transmitted, if the period of the baseband symbol, T_S, is shorter than the duration of T_m. then the channel is a **flat fading channel**. If, however, the symbol period is longer than the duration of T_m, then the channel is **frequency selective**.

T_m is also called the **coherence time** of the channel. It has an inverse relationship to the coherence bandwidth, which can be approximately expressed as [3, 45]

$$(\Delta f)_C \approx \frac{1}{T_m}. \tag{2.5.7}$$

The second interpretation of, $\phi_c(\Delta f;\Delta t)$, the spaced-frequency, spaced-time correlation function of the channel, is the spaced-time correlation function, which is denoted by $\phi_c(0;\Delta t)$. In this case, only temporal variations of the channel are considered and, so, Δf is set to 0. The variations of the channel impulse response, and consequently the channel correlation function, are ascribed to Doppler effects associated with motion of the transmitter, the receiver or the multipath scatterers of the channel.

Let the Fourier transform of $\phi_c(\Delta f;\Delta t)$ with respect to Δt be denoted by $S_C(\Delta f;\lambda)$, i.e.,

$$S_C(\Delta f;\lambda)=\int_{-\infty}^{\infty}\phi_C(\Delta f;\Delta t)e^{-j2\pi\lambda\Delta t}d\Delta t\,, \tag{2.5.8}$$

where λ is the Doppler frequency.

Now let $\Delta f=0$ and let $S_C(0;\lambda)\equiv S_C(\lambda)$ for brevity, so that (2.5.8) becomes

$$S_C(\lambda)=\int_{-\infty}^{\infty}\phi_C(0;\Delta t)e^{-j2\pi\lambda\Delta t}d\Delta t\,, \tag{2.5.9}$$

where $S_C(\lambda)$ is called the **Doppler power spectrum of the channel**.

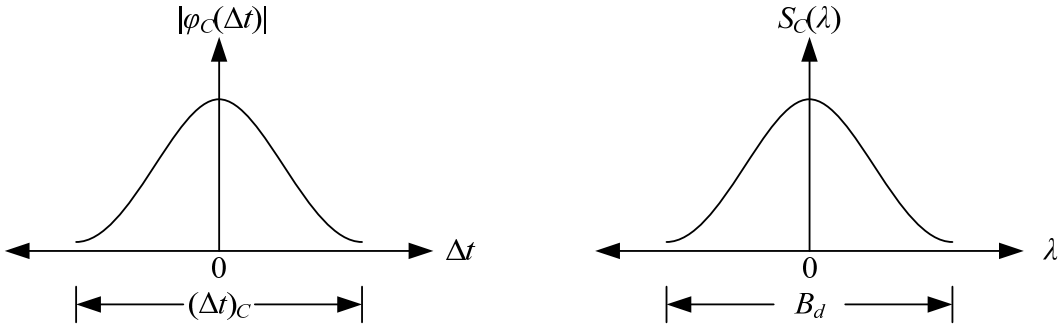

(a) Spaced-time correlation function. (b) Doppler power spectrum.

Fig. 2.5.2. Illustrations of a general Doppler power spectrum and the spaced-time correlation function of a multipath channel with Doppler effects [3].

As seen in Fig. 2.5.2 (b), the range of frequencies over which the Doppler power spectrum, $S_C(\lambda)$, is non-zero is called the **Doppler spread** of the channel, and is denoted by B_d. Correspondingly, as seen in Fig. 2.5.2(a), the **channel coherence time** is

denoted by $(\Delta t)_C$, which is essentially the duration of time between observations of the channel impulse response during which the channel impulse response is non-zero.

In the case when the channel coherence time is shorter than the symbol period of the transmitted signal, i.e., $(\Delta t)_C < T_S$, **fast fading** occurs. This condition implies that the impulse response of the channel can change during the duration of a baseband symbol. Conversely, when the channel coherence time is longer than the symbol period, i.e., $(\Delta t)_C > T_S$, the fading of the signal occurs slowly in the sense that the channel impulse response does not change during the duration of a baseband symbol. This condition is called **slow fading**.

When observed in the Fourier-domain, since the Doppler spread of the channel is inversely related to the channel coherence time, i.e.,

$$B_d \approx \frac{1}{(\Delta t)_C},$$

a small Doppler spread is indicative of a fast fading channel, and a large Doppler spread of a slow fading channel.

The Fourier transform pairs that have been presented for the cases of fading based on multipath delay spread and Doppler spread are provided in a concise format in Table 2.5.1. Furthermore, the concepts of channel fading that have been presented in this section are summarized in Tables 2.5.2 and 2.5.3.

Table 2.5.1. Fourier transform pairs for the two types of fading considered.

Fading based on	Time-Domain	Frequency-Domain
Multipath Time Delay Spread	$\phi_C(\tau) \underset{F^{-1}\{\cdot\}}{\overset{F\{\cdot\}}{\rightleftharpoons}} \phi_C(\Delta f)$	
Doppler Spread	$\phi_C(\Delta t) \underset{F^{-1}\{\cdot\}}{\overset{F\{\cdot\}}{\rightleftharpoons}} S_C(\lambda)$	

Table 2.5.2. Summary of channel fading based on multipath time delay spread.

	Flat Fading	Frequency-Selective Fading
Time -Domain	Multipath delay spread is smaller than symbol period, i.e., $T_m < T_S$.	Multipath delay spread is longer than symbol period, i.e., $T_m > T_S$.
Frequency -Domain	Signal bandwidth is smaller than the channel coherence bandwidth, i.e., $W < (\Delta f)_C$.	Signal bandwidth is greater than the channel coherence bandwidth, i.e., $W > (\Delta f)_C$.

Table 2.5.3. Summary of channel fading based on Doppler spread.

	Fast Fading	Slow Fading
Time -Domain	Channel coherence time is shorter than the symbol period, i.e., $(\Delta t)_C < T_S$.	Channel coherence time is longer than the symbol period, i.e., $(\Delta t)_C > T_S$.
Frequency -Domain	Doppler spread of the channel, B_d, is large.	Doppler spread of the channel, B_d, is small.

Chapter 3

Literature Survey

The two focal points of the research presented in this dissertation are the development of wavelet-based channel estimation and equalization procedures. The approach that is taken to accomplish these tasks involves establishing intuitive and analytically robust techniques for DWT-based convolution. The techniques are developed in this dissertation. A survey of the published literature on all of these three topics is presented in this chapter.

The first topic that is developed in this dissertation is DWT-based convolution. Prior publications on this topic by the mathematics and engineering communities are identified, discussed and critiqued in Section 3.1. The new research on DWT-based convolution is presented in Chapter 5.

Literature on the topic of DWT-based channel estimation is discussed in Section 3.2. The technique of DWT-based deconvolution and its application to channel estimation, both of which are highlights of this dissertation, are described in Chapter 6.

The third topic that is developed in this dissertation is DWT-based channel equalization. Existing literature on this topic is discussed in Section 3.3. Channel equalization that is developed using DWT-based convolution procedures developed in this dissertation is described in Chapter 7.

It must be noted here that several publications containing varied implementations of DWT-based channel estimation and equalization have been found after extensive searches, and the most relevant literature is presented in this chapter. Despite detailed searches, however, no publications regarding the implementation of such strategies in communications systems, which is the ultimate objective of this dissertation, have been found.

3.1 Discrete Wavelet Transform-Based Convolution

Since the early development of the theory of wavelet transforms, there have been major research efforts to represent mathematical operators using orthonormal bases of compactly supported wavelets [46-52]. The representation of differential operators has been of particular interest in such studies.

Expressing operators using wavelets can lead to easily solvable systems of equations. One example is the case of systems of differential equations. Expressing differential operators using wavelet bases, and thus transforming the equations using the wavelet transform, leads to systems of algebraic equations that may then be solved in a much simpler manner. This procedure has been successfully applied in the area of transmission lines research for the solutions of couple multiconductor transmission line equations using wavelet representations of operators [53-57].

With such applications being a motivating factor, it has been shown, in rigorous mathematical detail, that the differential operator d^n/dx^n can be represented using wavelets in the non-standard form [49]. In the same work the convolution operator is also represented using wavelet bases in the non-standard form.

While the advantage of such a formulation is that numerical solutions of various systems of equations may be rendered more tractable, there exists an inherent drawback. The formulation is not developed in the typical sense of MRA and the DWT, i.e., with a filter bank approach. Due to this fact the expression of operators using wavelet bases in the non-standard form does not lend itself to direct use in signal processing systems that primarily use filter banks.

Recognizing this shortcoming, a study on the implementation of operators via filter banks has been published [52]. In this particular filter bank approach, operators are expressed as filters. Specifically, the mathematical theory developed involves combining operators with prefect reconstruction filters so that the resulting filters have the simultaneous effect of convolution and wavelet analysis (decomposition).

The primary focus of the abovementioned research is to combine one of two functions to be convolved with one of the two DWT analysis filters. This new filter is then used as a replacement for the original filter. The second convolving function is then analyzed using this new filter and the other analysis filter that is intact. Synthesizing the resulting

wavelet coefficients using the original high-pass and low-pass synthesis filters then provides the desired convolution result.

While this method is ideal for the purposes of this dissertation, the inherent intricacies that are involved in computing the necessary filters do not lend it to be a readily practicable solution for many engineering problems.

An alternative approach to solving the problem of wavelet-based convolution is found in the field of digital signal processing, specifically in the area of multirate filter banks [58]. Specifically, the theory of convolution is implemented with the use of orthonormal filter banks. In keeping with the concepts of multirate filter banks, a theory for the use of such filter banks with unequal decimation in subbands is developed [59,60].

In the abovementioned set of research works a multidimensional subband convolution theorem is developed within the general framework of orthonormal and biorthonormal filter banks [61]. Since the DWT is expressly implementable as such filter banks, an immediate consequence was the special case of the wavelet convolution theorem [61]. The specific method for DWT-based convolution was derived graphically.

This particular method is the genesis of the DWT-based convolution procedures developed in this dissertation. Furthermore, analytical derivations are accompanied by graphical illustrations of the steps as described in Chapter 5.

It should also be mentioned, for the sake of completeness, that there have been other research efforts in developing wavelet-based convolution. Among these are a publication on convolution using the Undecimated DWT (UDWT) [62] and one describing a convolution theorem for the Continuous Wavelet Transform (CWT) [63].

3.2 Discrete Wavelet Transform-Based Channel Estimation

Wavelets have been used to the blind identification of system impulse responses, and by extension to Finite Impulse Response (FIR) channels [64-66]. These studies use wavelet basis function for the expansion of system and channel models. Second-order statistics of the expansion coefficients are used in order to estimate the system and channel model coefficients.

In the general procedure followed in these studies, first a time-varying channel model is considered, with known input and output functions. The unknown channel impulse is then expanded with the use of wavelet basis functions. A linear Least Squares (LS) approach is then used to recover correlation information of the expansion coefficients. A subspace method is then applied to the correlation matrix of the coefficients to recover the desired expansion coefficients. The unknown system or channel impulse responses are then estimated [66].

In another study that uses a similar approach multiplicative channel fading is modeled as an autoregressive process [67]. Filter banks are used to precode symbols transmitted

through the channel, and second-order statistics of the output data are computed. From these data the correlation information of the channel are obtained. A Kalman filter is then used to track time variations of the channel, and transmitted symbols are recovered by block processing.

The second important set of studies on wavelet-based channel estimation is based on the abovementioned techniques [68-70]. In these, again, the model coefficients of an unknown time-varying channel are decomposed using orthonormal wavelets. The applications of these studies, however, are specific for use in the design of macrocell wireless communications systems.

Specifically, a multipath channel is represented in a reduced-order dimensional space by matching the scattering function of the channel to its decomposition. With the assumption of a multi-user multipath channel model, the second-order statistics of the time variations of the channel are obtained. Using such a wavelet-based representation of the channel, generalized likelihood detection statistics for TDMA [68] and DS/CDMA [69] signals are devised.

Although the theories developed in these studies [64-70] are analytically well-developed, they do not use the method that is desired in this dissertation, i.e., channel estimation using a wavelet-based convolution procedure, or more appropriately using wavelet-based deconvolution.

In addition to the two main research efforts previously discussed there have also been a few other studies on the use of wavelets for channel estimation. One recent work extends the concepts of expanding unknown time-varying channels using wavelet basis functions, and estimating the unknown coefficients with the use of an LS approach [71]. A parametric study using several different wavelets was also included in the study.

Another recent research work makes use of pilot symbols for use in a Maximum Likelihood (ML) channel estimation procedure [72]. The estimation is based on an LS algorithm. The connection to wavelets in this case is oblique, however, since this estimation is an applied to the case of Ultra Wideband (UWB) signals that are based on a wavelet packet modulation scheme. As such, this study is not useful for the purposes of this dissertation.

A study in which OFDM UWB channels are estimated using wavelets is also available in the literature [73]. In this particular study, a multiband OFDM channel is modeled over 3 subbands, which are expressed in the wavelet-domain. By choosing a Bernoulli-Gaussian *a priori* distribution for the wavelet coefficients of the channel, a Maximum *A Posteriori* (MAP) estimator yields a thresholding procedure in an Expectation Maximization (EM) algorithm. Due to the esoteric nature of the methodologies used in this study they are not amenable for use in the context of this dissertation.

Other interesting publications in the area of wavelet-based channel estimation include a study on using the wavelet packet transform for the identification of underwater acoustic

channels [74], and a study on application of blind channel identification in seismic signal processing [75]. The latter work uses statistical methods to accomplish the desired deconvolution operation in that application.

3.3 Discrete Wavelet Transform-Based Channel Equalization

In the literature on wavelet-based methods of channel equalization it is found that almost all methods exclusively use one particular formulation. This formulation involves the expansion of a signal that has been faded by a channel using wavelet bases [76-83]. The wavelet coefficients are then equalized based on a mean-square error minimization criterion. The equalized wavelet coefficients are then synthesized into an equivalent, equalized, time-domain signal using an inverse wavelet transform procedure. It must be noted that this common, general, procedure is used in order to accomplish adaptive equalization of signals propagated through channels with time-varying impulse responses.

For the purposes of this dissertation the general methodology outlined above is not useful because it does not provide a common framework using which different linear equalization strategies can be implemented in the wavelet-domain. Such a framework is developed in this dissertation with the use of wavelet-based convolution.

One of the earlier works on this subject made use of a general topology of a transform-domain Least Mean Squares (LMS) adaptive filter [84], and adapted it for use with

wavelets. The topology calls for the transformation of a signal using orthogonal basis functions. The coefficients of such an expansion are then equalized using an LMS algorithm. The basis functions used in this particular case were the Haar and Daubechies4 wavelets.

A second set of studies continues with this approach, but extends it to include the non-linear procedure called Decision Feedback Equalization (DFE) [77,78]. In these studies 16-QAM test signals are analyzed with a Daubechies4 wavelet. The results of wavelet-based DFE and LMS equalization are compared with standard time-domain-based DFE and LMS equalization and appear to be in good agreement. The main drawback of both of these studies is that details of the analytical formulations and implementations are not provided clearly, as is needed for replication of the methods.

Two more research studies that implement very similar procedures are also found in the literature [79,80]. A sixth such study attempts to extend the generality of the approach in inserting filters at each subband of an MRA scheme [80]. A seventh publication also inserts adjustable FIR filters within each subband of a wavelet-analyzed signal, and then uses an LMS algorithm to update the filter tap coefficients [81].

These latter two studies [80,81], do follow the same general ideology of this dissertation, but with two major differences

1. There are no rigorous analytical justifications of the techniques.
2. Dyadic decimation in analysis filter banks is neglected.

The research developed in this dissertation addresses both of these issues by providing a thorough system-theoretic analytical framework for DWT-based channel equalization and also use equalizers in conjunction with the necessary dyadic decimators.

In addition to the main publications on wavelet-based equalization previously described, there are also a few others that use wavelets, but in methods dissimilar to the ideology of wavelet-based equalization in this dissertation. Among these are a study on using wavelet-packet based LMS equalization strategy [83], and the use of wavelet-based channel estimation techniques for adaptive equalization [85,86]. Other research works make use of wavelet neural networks for channel equalization but are not pertinent in the context of this dissertation [87-91].

Chapter 4

Wavelet Transforms

The wavelet transform can be viewed as a mapping of a time-domain signal to a joint time-scale representation. It makes use of window functions that called wavelets. With the use of windows of wide width, low-frequency components of a signal can be analyzed, and with narrow windows high-frequency spectral components can be analyzed [44].

The Continuous Wavelet Transform (CWT) is expressed in integral form as being the cross-correlation between a wavelet and the signal of interest. The DWT, however, is typically obtained via the filter theory approach called Multiresolution Analysis (MRA).

Section 4.1 provides a brief outline of the CWT to illustrate the genesis of wavelet transforms and the subsequent development of the DWT. The filter theory of MRA implemented by the technique of subband coding is described in detail in Section 4.2. The Perfect Reconstruction (PR) criterion for the generation of Quadrature Mirror Filters (QMFs) that are needed for signal analysis and synthesis are derived, as are two examples of PR QMFs.

In Section 4.3 wavelets are applied to the theory of subband coding, and the premise of using a filter theoretic approach is analytically justified. Section 4.4 contains the formal definitions of the DWT.

Before proceeding further, it has to be noted that Sections 4.2, 4.3 and 4.4 closely follow the presentation in a review article on the DWT that was published in the October 1998 issue of the IEEE Antennas and Propagation Magazine [92].

4.1 Continuous Wavelet Transform

Consider a continuous-time, square-integrable, function, $f(t)$, and a set of basis functions, $\psi^*_{a,b}(t)$, which are the wavelets. The CWT of $f(t)$ is a decomposition of $f(t)$ into $\psi^*_{a,b}(t)$, i.e.,

$$W_f(a,b) = \int f(t)\psi^*_{a,b}(t)\,dt\,. \tag{4.1.1}$$

In (4.1.1), the symbol $*$ denotes complex conjugation, *a* is the dilation parameter, *b* is the translation parameter, and the scaled-and-translated wavelets, $\psi_{a,b}(t)$, are generated from a single wavelet, i.e., as

$$\psi_{a,b}(t) = \frac{1}{\sqrt{a}}\psi\left(\frac{t-b}{a}\right). \tag{4.1.2}$$

It is seen from (4.1.2) that when $a>1$ the wavelets are dilated and when $a<1$ the wavelets are contracted. Hence, regardless of the dilation, and also translation, wavelets retain their functional form, i.e., time-domain shape.

Wavelets are also subjected to energy normalization of the form

$$\int \left|\psi_{a,b}(t)\right|^2 dt = \int \left|\psi(t)\right|^2 dt = 1\,, \tag{4.1.3}$$

which results in the normalization constant of $1/\sqrt{a}$ that appears in (4.1.2).

The design of wavelets must generally satisfy the fundamental properties that are listed below [44].

A. Admissibility

The Fourier transform of a wavelet must have a zero component at zero frequency. This condition of admissibility is described mathematically as

$$c_\psi = \int_{-\infty}^{\infty} \frac{|\psi(\omega)|^2}{|\omega|} d\omega < \infty \tag{4.1.4}$$

where $\psi(\omega)$ is the Fourier transform of the wavelet, $\psi(t)$, and c_ψ is called the admissibility constant. This condition also allows for the definition of the inverse wavelet transform. By implementing this condition wavelets are required to be square integrable functions.

B. Regularity

Since wavelets can be scaled temporally, the inverse relationship between scale and bandwidth can be detrimental in practical applications because scaling to a fine resolution (i.e., high localization in time) leads to very large bandwidths. The regularity condition is, therefore, imposed so that the wavelet transform coefficients decrease quickly in magnitude as the scaling increases, i.e., becomes finer.

This condition can be interpreted to mean that a wavelet can be localized in the frequency-domain by causing it to vanish rapidly in the time-domain. A measure of the regularity of a wavelet can be determined from the condition

$$M_p = \int t^p \psi(t)\, dt = 0 \qquad \forall\, p = 0,1,2,\ldots,n\,, \tag{4.1.5}$$

where M_p is the p^{th} moment of the wavelet, $\psi(t)$, then the wavelet is said to be of order *n*. Note that from the admissibility condition $M_0 = 0$.

The regularity condition in (4.1.5) may be expressed equivalently in the Fourier-domain. In this case, the derivatives of the Fourier transform of a wavelet of order *n*, must be equal to zero, i.e.,

$$\psi^{(p)}(\omega)\Big|_{\omega=0} = 0 \qquad \forall\, p = 0,1,2,\ldots,n\,. \tag{4.1.6}$$

C. Linear Transformations

Wavelets must also satisfy the linear transformation properties of superposition, translation, and rescaling. Specifically,

i.) Linear Superposition: $$W_{f_1+f_2}(a,b) = W_{f_1}(a,b) + W_{f_2}(a,b) \tag{4.1.7}$$

ii.) Translation: $$W_{f(t-t_0)}(a,b) = W_{f(t)}(a,b-t_0) \tag{4.1.8}$$

iii.) Rescaling: $$W_{m^{1/2}f(mt)}(a,b) = W_{f(t)}(ma,mb)\,. \tag{4.1.9}$$

An example of a wavelet function is the Morlet wavelet. It is a complex sinusoid that is modulated by a Gaussian function according to

$$\psi(t) = e^{j\omega_0 t} e^{-t^2/2}\,. \tag{4.10}$$

The Fourier transform of the real part of the Morlet wavelet is

$$\psi(\omega) = \sqrt{\frac{\pi}{2}} \left\{ e^{-\frac{(\omega-\omega_0)^2}{2}} + e^{-\frac{(\omega+\omega_0)^2}{2}} \right\}. \tag{4.1.11}$$

As seen in Figs. 4.1.1 and 4.1.2, the Morlet wavelet readily decays in the time-domain and is band-limited in the frequency-domain. This particular wavelet does not, however, satisfy the admissibility condition since $\psi(\omega)\big|_{\omega=0} \neq 0 \Rightarrow c_\psi = \infty$.

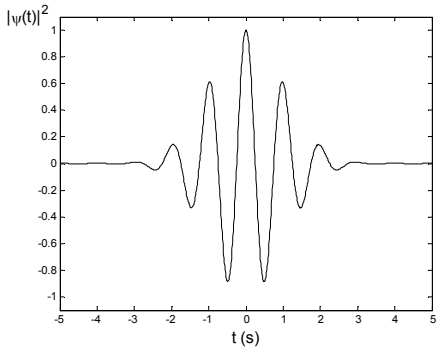

Fig. 4.1.1. The Morlet wavelet in the time-domain.

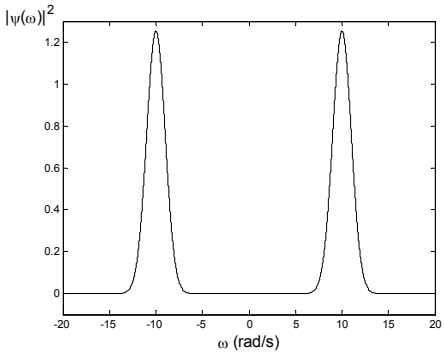

Fig. 4.1.2. The Morlet wavelet in the frequency-domain.

The Morlet wavelet is, however, still practicable in the case of a large value of ω_0, due to which $\psi(0) \to 0$. For example, if $\omega_0 = 5$ rad/s, then

$$\psi(0) = \sqrt{2\pi} e^{-25/2} \approx 10^{-5},$$

which may be considered negligibly small in numerical computations. In Fig. 4.1.2 $\omega_0 = 10$ rad/s.

4.2 Multiresolution Analysis Using Subband Coding

Multiresolution analysis is a technique that allows for the analysis of signals in multiple frequency bands. The analysis and synthesis of signals into wavelet bases can be carried out using MRA. The specific approach of MRA that is most commonly used for DWT is called subband coding. In subband coding the frequency spectrum of a signal is divided into several independent subbands. Each resulting subband may then be operated upon as desired.

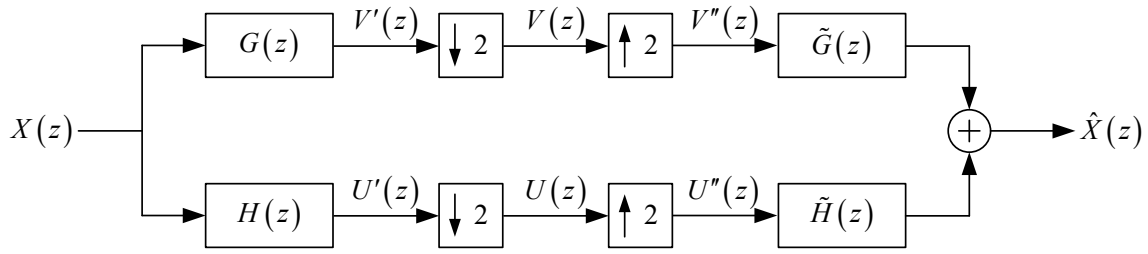

Fig. 4.2.1. Two-channel subband coding analysis and synthesis.

The system block diagram shown in Fig. 4.2.1 is that of a one-level MRA. The input signal is demultiplexed into two parallel streams, one of which is analyzed by a low-pass filter and the other by a high-pass filter.

Consider a discrete-time input signal, $x(n)$, that has the z-transform

$$X(z) = \sum_n x(n) z^{-n} \tag{4.2.1}$$

where

$$z = e^{j\omega} . \tag{4.2.2}$$

Let $x(n)$ have a bandwidth, BW_x, of π rad/s. The precursor continuous time signal from which $x(n)$ is obtained is sampled at the Nyquist rate of $\omega_s = 2\pi$ rad/s.

In Fig. 4.2.1 the relevant quantities are defined as:

$G(z)$ is the analysis high-pass filter to which $x(n)$ is input, and has a bandwidth of $\pi/2 \le \omega \le \pi$,

$H(z)$ is the analysis low-pass filter to which $x(n)$ is also input, and has a bandwidth of $0 \le \omega \le \pi/2$,

$\tilde{G}(z)$ is the synthesis high-pass filter, and

$\tilde{H}(z)$ is the synthesis low-pass filter.

Now, the intermediate signals obtained after filtering $X(z)$ with the analysis filters are

$$V'(z) = X(z)G(z) \text{ and} \tag{4.2.3}$$

$$U'(z) = X(z)H(z). \tag{4.2.4}$$

Following the signal path, $V'(z)$ and $U'(z)$ are decimated, i.e., downsampled, by a factor of 2. The decimated signals can be expressed as

$$V(z) = \frac{1}{2}\left[V'\left(z^{1/2}\right) + V'\left(-z^{1/2}\right)\right] \text{ and} \tag{4.2.5}$$

$$U(z) = \frac{1}{2}\left[U'\left(z^{1/2}\right) + U'\left(-z^{1/2}\right)\right]. \tag{4.2.6}$$

Next, these signals are upsampled by a factor of 2, which results in two more intermediate signals, i.e.,

$$V''(z) = V\left(z^2\right) \text{ and} \tag{4.2.7}$$

$$U''(z) = U\left(z^2\right). \tag{4.2.8}$$

Substituting (4.2.3) in (4.2.5) and (4.2.4) in (4.2.6) results in

$$V''(z) = \frac{1}{2}\left[V'(z) + V'(-z)\right] \text{ and} \tag{4.2.9}$$

$$U''(z) = \frac{1}{2}\left[U'(z) + U'(-z)\right]. \tag{4.2.10}$$

Hence, the output of the filter bank can be written as

$$\hat{X}(z) = V''(z)\tilde{G}(z) + U''(z)\tilde{H}(z). \tag{4.2.11}$$

Substituting (4.2.9) and (4.2.10) in (4.2.11) gives

$$\hat{X}(z) = \frac{1}{2}\left[V'(z) + V'(-z)\right]\tilde{G}(z) + \frac{1}{2}\left[U'(z) + U'(-z)\right]\tilde{H}(z). \tag{4.2.12}$$

The synthesized output, $\hat{X}(z)$, can now be expressed in terms of the original signal, $X(z)$, by substituting (4.2.3) and (4.2.4) into (4.2.12) yields

$$\begin{aligned}\hat{X}(z) &= \frac{1}{2}\left[X(z)G(z)+X(-z)G(-z)\right]\tilde{G}(z)+ \\ &\quad \frac{1}{2}\left[X(z)H(z)+X(-z)H(-z)\right]\tilde{H}(z) \\ \Rightarrow \hat{X}(z) &= \frac{1}{2}\left[G(z)\tilde{G}(z)+H(z)\tilde{H}(z)\right]X(z)+ \\ &\quad \frac{1}{2}\left[G(-z)\tilde{G}(z)+H(-z)\tilde{H}(z)\right]X(-z).\end{aligned} \tag{4.2.13}$$

The estimated signal, $\hat{X}(z)$, in (4.2.13) contains both the original transmitted signal (the first term) and an alias of the signal (the second term).

In order to remove the aliasing, the second term of (4.2.13) must be equal to zero, i.e.,

$$G(-z)\tilde{G}(z)+H(-z)\tilde{H}(z)=0. \tag{4.2.14}$$

For (4.2.14) to be realizable, consider $H(z)$ to be a Finite Impulse Response (FIR) filter of order $N+1$, where N is always an odd number.

The anti-aliasing condition in (4.2.14) can be satisfied by choosing

$$\tilde{G}(z)=-H(z) \text{ and} \tag{4.2.15a}$$

$$G(z)=\tilde{H}(z). \tag{4.2.15b}$$

Upon imposition of the anti-aliasing condition, the output of the filter bank, $\hat{X}(z)$, in (4.2.13) becomes

$$\hat{X}(z)=\frac{1}{2}\left[G(z)\tilde{G}(z)+H(z)\tilde{H}(z)\right]X(z). \tag{4.2.16}$$

Now, consider the definitions that

$$\tilde{H}(z)\triangleq z^{-N}H\left(z^{-1}\right) \tag{4.2.17a}$$

$$\Rightarrow \tilde{h}(n)\triangleq h(N-n) \tag{4.2.17b}$$

and

$$\tilde{G}(z)\triangleq z^{-N}G\left(z^{-1}\right) \tag{4.2.18a}$$

$$\Rightarrow \tilde{g}(n)\triangleq g(N-n). \tag{4.2.18b}$$

By combining (4.2.15b) and (4.2.17a), $G(z)$ can be expressed in terms of $H\left(z^{-1}\right)$ as

$$G(z)=\tilde{H}(-z)=(-z)^{-N}H\left((-z)^{-1}\right)$$

$$\Rightarrow G(z)=-z^{-N}H\left(-z^{-1}\right) \tag{4.2.19}$$

since N is always odd.

By substituting (4.2.15a), (4.2.17a) and (4.2.19) into (4.2.16), $\tilde{X}(z)$ can now be expressed only in terms of $H(z)$ as

$$\tilde{X}(z)=\frac{1}{2}\left[-z^{-N}H\left(-z^{-1}\right)\left(-H(-z)\right)+H(z)z^{-N}H\left(z^{-1}\right)\right]X(z)$$

$$\Rightarrow \tilde{X}(z)=\frac{1}{2}\left[H(-z)H\left(-z^{-1}\right)+H(z)H\left(z^{-1}\right)\right]z^{-N}X(z). \tag{4.2.20}$$

Equation (4.2.20) implies that if the filter $H(z)$ is designed in such a way that

$$H(-z)H\left(-z^{-1}\right)+H(z)H\left(z^{-1}\right)=2, \tag{4.2.21}$$

then the synthesized estimate of $X(z)$, i.e., $\tilde{X}(z)$, will be exactly equal to $X(z)$, albeit with a delay of N samples.

Substituting the mapping

$$z = e^{j\omega}, \tag{4.2.22}$$

into (4.2.21) gives, after some manipulation,

$$\left|H\left(e^{j\omega}\right)\right|^2 + \left|H\left(e^{j(\omega+\pi)}\right)\right|^2 = 2. \tag{4.2.23}$$

Equation (4.2.23), and equivalently (4.2.21), is called the **Perfect Reconstruction** (PR) criterion. $H(z)$ and $G(z)$ are called **Quadrature Mirror Filters** (QMFs).

From the preceding derivation it is seen that if the filter $H(z)$ is known, then the other three filters can be readily derived so as to form a perfect reconstruction filter bank. Specifically, if $H(z)$ is known, then (to summarize)

$$G(z) = -z^{-N} H\left(-z^{-1}\right), \tag{4.2.19}$$

$$\tilde{H}(z) = z^{-N} H\left(z^{-1}\right), \tag{4.2.17a}$$

and

$$\tilde{G}(z) = -H(-z). \tag{4.2.15a}$$

Example: Consider the case where $N = 3$. In this case $H(z)$ can be expressed as

$$H(z) = h(0) + h(1)z^{-1} + h(2)z^{-2} + h(3)z^{-3}. \tag{4.2.24}$$

Using (4.2.19), the analysis high-pass filter, $G(z)$, for this case, can be expressed as

$$G(z) = h(3) - h(2)z^{-1} + h(1)z^{-2} - h(0)z^{-3}. \tag{4.2.25}$$

Similarly, using (4.2.17) the synthesis low-pass filter becomes

$$\tilde{H}(z) = h(3) + h(2)z^{-1} + h(1)z^{-2} + h(0)z^{-3}, \tag{4.2.26}$$

and using (4.2.15) the synthesis high-pass filter can be expressed as

$$\tilde{G}(z) = -h(0) + h(1)z^{-1} - h(2)z^{-2} + h(3)z^{-3}. \tag{4.2.27}$$

The coefficients of $H(z)$ must now be solved for. The first step in this process is to revisit the PR condition in (4.2.21) and to then substitute (4.2.24) into it. This procedure gives

$$\begin{aligned} &\left(h(0) - h(1)z^{-1} + h(2)z^{-2} - h(3)z^{-3}\right)\left(h(0) - h(1)z + h(2)z^{2} - h(3)z^{3}\right) + \\ &\left(h(0) + h(1)z^{-1} + h(2)z^{-2} + h(3)z^{-3}\right)\left(h(0) + h(1)z + h(2)z^{2} - h(3)z^{3}\right) = 2 \end{aligned}$$

$$\begin{aligned} \Rightarrow &\left[h(0)h(2) + h(1)h(3)\right]z^{-2} + \left[h^{2}(0) + h^{2}(1) + h^{2}(2) + h^{2}(3)\right] \\ &\qquad + \left[h(0)h(2) + h(1)h(3)\right]z^{2} = 1. \end{aligned} \tag{4.2.28}$$

Equating the coefficients of both sides of (4.2.28) gives the relationships

$$h^{2}(0) + h^{2}(1) + h^{2}(2) + h^{2}(3) = 1 \text{ and} \tag{4.2.29}$$

$$h(0)h(2) + h(1)h(3) = 0. \tag{4.2.30}$$

The two equations (4.2.29) and (4.2.30) can be used to solve for the four unknowns. Next, assume that the frequency responses of $H(z)$ and $G(z)$ are as shown in Fig.

4.2.2. Note that Fig. 4.2.2a is an illustration of typical, i.e., practical, QMFs while the ideal cases are shown in Fig. 4.2.2b.

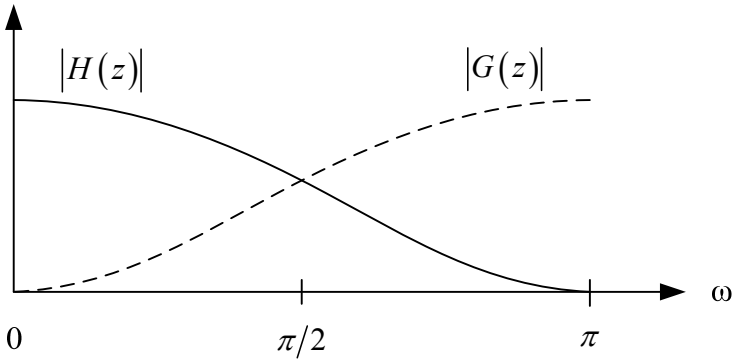

Fig. 4.2.2a. Typical frequency response of the QMFs.

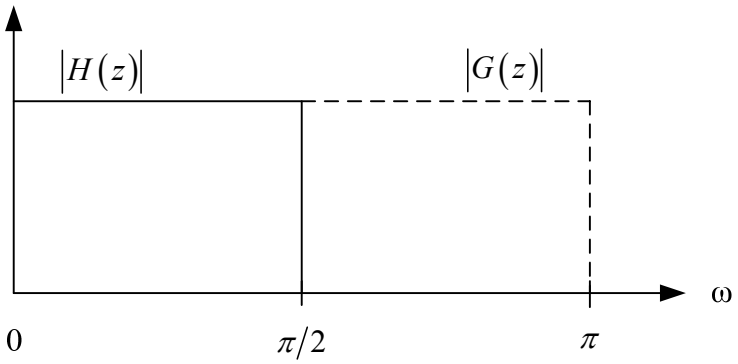

Fig. 4.2.2b. Ideal frequency response of the QMFs.

Now, due to the fact that $G(z)$ is an HPF, at $\omega = 0$

$$G(z)\big|_{\omega=0} = 0 .$$

This property can be reflected in $H(z)$ by using it in (4.2.19), which gives

$$-z^{-N} H\left(-z^{-1}\right)\big|_{\omega=0} = 0$$

$$\Rightarrow H(-1) = 0 \tag{4.2.31}$$

$$\Rightarrow h(0) - h(1) + h(2) - h(3) = 0\,. \tag{4.2.32}$$

Furthermore, the PR condition can also be evaluated at $\omega = 0$, which results in

$$\left|H(1)\right|^2 + \left|H(-1)\right|^2 = 2\,. \tag{4.2.33}$$

Substituting (4.2.31) into (4.2.33) yields

$$\left|H(1)\right|^2 = \sqrt{2}$$

$$\Rightarrow H(1) = \sqrt{2} \tag{4.2.34}$$

$$\Rightarrow h(0) + h(1) + h(2) + h(3) = \sqrt{2}\,. \tag{4.2.35}$$

Adding (4.2.32) and (4.2.35) gives

$$h(0) + h(2) = \frac{1}{\sqrt{2}}\,, \tag{4.2.36}$$

and subtracting (4.2.32) from (4.2.35) gives

$$h(1) + h(3) = \frac{1}{\sqrt{2}}\,. \tag{4.2.37}$$

Equations (4.2.36) and (4.2.37) are two more equations that can be used to solve for the four unknown coefficients of $H(z)$. It should be noted, however, that (4.2.29), (4.2.30) and (4.2.35) are linearly dependent. Therefore, a one more, independent, equation is still required.

One method of obtaining such an equation was developed by Daubechies [11]. In this method it is required that all derivatives of $H(z)$, up to order *p*, be equal to zero at $\omega = 0$. This results in $H(z)$ being smooth. Equivalently, the p^{th} derivative of $\tilde{G}(z)$ can be set equal to zero, i.e.,

$$\tilde{G}^{(p)}(1) = 0. \tag{4.2.38}$$

Since,

$$\tilde{G}(z) = -h(0) + h(1)z^{-1} - h(2)z^{-2} + h(3)z^{-3}, \tag{4.2.39}$$

$$\Rightarrow \tilde{G}^{(1)}(z)\Big|_{z=1} = -h(1) + 2h(2) - 3h(3),$$

using (4.2.36) yields

$$-h(1) + 2h(2) - 3h(3) = 0. \tag{4.2.40}$$

Now, let $h(3)$ be the first variable to be solved for. Therefore, from (4.2.37),

$$h(3) = \frac{1}{\sqrt{2}} - h(3), \tag{4.2.41}$$

and using (4.2.40) and (4.2.41)

$$h(2) = \frac{1}{2}\left[h(1) + 3h(3)\right]$$

$$\Rightarrow h(2) = \frac{1}{2\sqrt{2}} + h(3). \tag{4.2.42}$$

Substituting (4.2.42) in (4.2.36) gives

$$h(0)=\frac{1}{2\sqrt{2}}-h(3). \tag{4.2.43}$$

Substituting the expressions for $h(0)$, $h(1)$, and $h(2)$, (4.2.43), (4.2.41) and (4.2.42) respectively, into (4.2.29) gives

$$h^2(0)+h^2(1)+h^2(2)+h^2(3)=1$$

$$\Rightarrow\left(\frac{1}{2\sqrt{2}}-h(3)\right)^2+\left(\frac{1}{\sqrt{2}}-h(3)\right)^2+\left(\frac{1}{2\sqrt{2}}+h(3)\right)^2+h^2(3)=1. \tag{4.2.44}$$

Solving the quadratic equation in (4.2.44) results in two unique solutions, both of which are valid and may be used. In this example only one solution is selected:

$$h(3)=\frac{1-\sqrt{3}}{4\sqrt{2}}=-0.1294. \tag{4.2.45}$$

Substituting (4.2.45) into (4.2.43) to obtain $h(0)$ results in

$$h(0)=\frac{1+\sqrt{3}}{4\sqrt{2}}=0.4830, \tag{4.2.46}$$

substituting (4.2.45) into (4.2.41) to solve for $h(1)$ gives

$$h(1)=\frac{3+\sqrt{3}}{4\sqrt{2}}=0.8365, \tag{4.2.47}$$

and finally substituting (4.2.45) into (4.2.42) gives

$$h(2)=\frac{3-\sqrt{3}}{4\sqrt{2}}=0.2241. \tag{4.2.48}$$

Hence, the desired fourth-order FIR filter, $H(z)$, has been derived to be

$$H(z) = 0.4830 + 0.8365z^{-1} + 0.2241z^{-2} - 0.1294z^{-3}. \quad (4.2.49)$$

Immediately, using (4.2.25), (4.2.26) and (4.2.27), the other three filters are found to be

$$G(z) = -0.1294 - 0.2241z^{-1} + 0.8365z^{-2} - 0.4830z^{-3}, \quad (4.2.50)$$

$$\tilde{H}(z) = -0.1294 + 0.2241z^{-1} + 0.8365z^{-2} + 0.4830z^{-3} \quad (4.2.51)$$

and

$$\tilde{G}(z) = -0.4830 + 0.8365z^{-1} - 0.2241z^{-2} - 0.1294z^{-3}. \quad (4.2.52)$$

The QMFs, $H(z)$ and $G(z)$, that have just been derived are associated with the Daubechies2 wavelet and scaling function. In fact, when implementing the DWT using the Daubechies2 wavelet it is exactly these filters (4.2.49)-(4.2.52) that are used in the filter banks. This relationship is elaborated on in Sections 4.3 and 4.4.

4.3 Combining Wavelets and Subband Coding

Having explored the technique of MRA and its implementation using subband coding, the concepts of these filter theories and the theory of wavelets must be established.

It should be noted that wavelets cannot be expressed as discrete time functions but only as continuous time functions. In addition, the dilation equation, which is the most important relationship in MRA, can only be solved with continuous time functions. For these reasons the theory that is presented from this point onwards makes use of

continuous time signals and functions. These may be sampled at a suitable rate as needed in order to produce discrete time signal sequences that are needed.

Consider the signal, $x(t)$, which, as previously defined, has a bandwidth from 0 to π. Also consider a new function $\phi(t)$. Assume that translating $\phi(t)$ by integer values of m results in functions $\phi(t-m)$ that form a Riesz basis for the space in which $x(t)$ is defined. The compact notation

$$\phi_m(t) = \phi(t-m) \tag{4.3.1}$$

is used to describe such shifts for the sake of brevity.

Let dilated versions of $\phi(t)$ be represented by combinations of the shifted versions of $\phi(t)$ that are weighted by some coefficients $\{\tilde{h}(m)\}$ as

$$\phi(t/2) = \sqrt{2}\sum_{m=0}^{N} \tilde{h}(m)\phi(t-m)$$

$$\Rightarrow \phi(t) = \sqrt{2}\sum_{m=0}^{N} \tilde{h}(m)\phi(2t-m), \tag{4.3.2}$$

which is known as the **dilation equation**, or the **two-scale relation**, or the **two-scale difference equation**. This equation describes how the function $\phi(t)$ can be expressed as a weighted sum of dilations and translations of $\phi(t)$ itself.

Equivalently, since the weighting coefficients can be expressed as

$$\tilde{h}(n) = h(N-m), \tag{4.3.3}$$

(4.3.2) can be rewritten as

$$\phi(t) = \sqrt{2}\sum_{m=0}^{N} h(N-m)\,\phi(2t-m)\,. \tag{4.3.4}$$

The function $\phi(t)$, which solves the dilation equation for a particular sequence of $\tilde{h}(m)$, or $h(m)$, is called the **scaling function**, or the **father wavelet**.

Now, all functions $\phi(t-m)$ are required to be normalized, i.e.,

$$\int \phi(t-m)\,dt = 1\,. \tag{4.3.5}$$

Substituting (4.3.2) in (4.3.5), and using a suitable change in variables, results in

$$\sqrt{2}\sum_{m=0}^{N} \tilde{h}(m) \int \frac{\phi(2t-2k-m)}{2}\, d(2t) = 1$$

$$\Rightarrow \frac{\sqrt{2}}{2}\sum_{m=0}^{N} \tilde{h}(m) = 1$$

$$\Rightarrow \sum_{m=0}^{N} \tilde{h}(m) = \sqrt{2}\,. \tag{4.3.6}$$

Note that the condition in (4.3.6) is the same as the condition established in (4.2.34), which was a consequence of the PR condition found in the theory of subband coding.

The wavelets can now be correspondingly defined as

$$\psi(t) = \sqrt{2}\sum_{m=0}^{N} \tilde{g}(m)\,\phi(2t-m)\,. \tag{4.3.7}$$

Since $\tilde{g}(m)$ can be written in terms of $h(m)$ as

$$\tilde{g}(m) = -(-1)^m \tilde{h}(N-m), \tag{4.3.8}$$

equation (4.3.7) can be rewritten as

$$\psi(t) = \sqrt{2}\sum_{m=0}^{N} -(-1)^m \tilde{h}(N-m)\phi(2t-m), \tag{4.3.9}$$

where the function $\psi(t)$ is called the **mother wavelet**.

Hence, if the filter coefficients $\{\tilde{h}(m)\}$ are known, the scaling function, $\phi(t)$, can be found by iteratively solving the dilation equation in (4.3.4). In order to do so, first $\phi(t)$ is assumed to be a Heaviside function, which is filtered using $\{\tilde{h}(m)\}$. The outputs of this operation are then also filtered using the coefficients $\{\tilde{h}(m)\}$, and this process of filtering is repeated until the desired convergence is reached. Once $\phi(t)$ is obtained, $\psi(t)$ is then solved for by using either (4.3.7) or (4.3.9).

Example: The Haar Wavelet

For the case of $N=1$, the filter coefficients $\{\tilde{h}(m)\}$ according to (4.3.6) or equivalently by using the perfect reconstruction formulation in Section 4.2 on subband coding, i.e., according to (4.3.32),

$$\tilde{h}(0) = \frac{1}{\sqrt{2}} \text{ and} \tag{4.3.10a}$$

$$\tilde{h}(1)=\frac{1}{\sqrt{2}}. \tag{4.3.10b}$$

Using these values the dilation equation in (4.3.4) becomes

$$\phi(t)=\phi(2t)+\phi(2t-1). \tag{4.3.11}$$

One solution to (4.3.11) is the scaling function

$$\phi(t)=\begin{cases}1, & 0\le t<1\\ 0, & \text{otherwise.}\end{cases} \tag{4.3.12}$$

The mother wavelet that is generated by using this scaling function is

$$\psi(t)=\begin{cases}-1, & 0\le t<1/2\\ 1, & 1/2\le t<1\\ 0, & \text{otherwise.}\end{cases} \tag{4.3.13}$$

The function $\psi(t)$ in (4.3.13) is known as the Haar wavelet, and $\phi(t)$ in (4.3.12) is the corresponding scaling function. The Haar wavelet and scaling function are graphically illustrated in Figs. 4.3.1a and b.

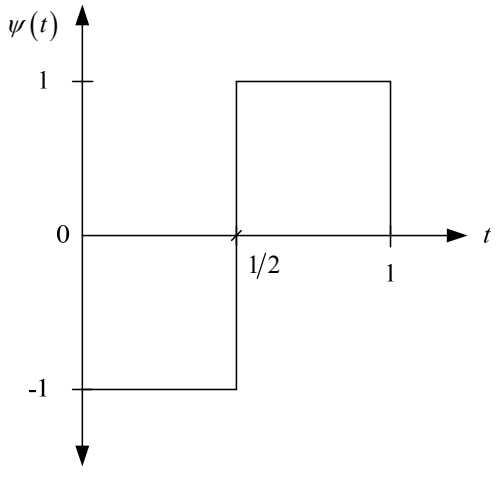

Fig. 4.3.1a. The Haar wavelet.

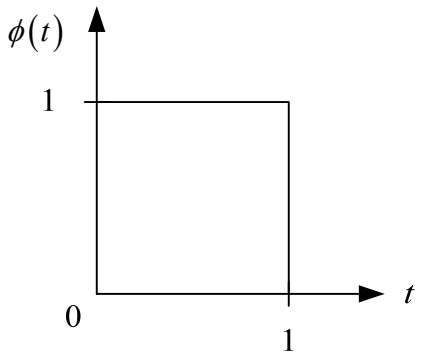

Fig. 4.3.1b. The Haar scaling function.

Before moving on to the formal definition of the framework of the DWT it must be noted that the scaling function is, in general, orthogonal to translated versions of itself, i.e.,

$$\int_{-\infty}^{\infty} \phi(t)\phi(t-m)\,dt = 0\,. \tag{4.3.14}$$

The mother wavelet and translations of itself are also orthogonal, i.e.,

$$\int_{-\infty}^{\infty} \psi(t)\psi(t-m)\,dt = 0\,. \tag{4.3.15}$$

4.4 Discrete Wavelet Transform

The original function, $x(t)$, may be expressed in terms of wavelets in an infinite summation as

$$x(t) = \sum_{n=-\infty}^{\infty}\sum_{k=-\infty}^{\infty} d_{k,n}\psi_{k,n}(t) \tag{4.4.1}$$

where

$$\psi_{k,n}(t) = 2^{-n/2}\psi\left(2^{-n}t - k\right). \tag{4.4.2}$$

Note that the functions used in (4.4.1) and (4.4.2) are defined in continuous time, and the variable n is the dilation parameter and k is the translation parameter.

The wavelets, $\psi_{k,n}(t)$, are orthonormal (with the multiplier $2^{-n/2}$ being a normalization factor), i.e.,

$$\int \psi_{j,k}(t)\psi_{n,i}(t)\,dt = \delta_{j,n}\delta_{k,i}\,, \tag{4.4.3}$$

where $\delta_{j,n}$ and $\delta_{k,i}$ are Kronecker delta functions. Hence, the coefficients in (4.4.1), $d_{k,n}$, can be defined as the inner product of the signal and the wavelet, i.e.,

$$d_{k,n} = \int x(t)\psi_{n,k}(t)dt$$

$$\Rightarrow d_{k,n} = \langle x, \psi_{n,k} \rangle, \tag{4.4.4}$$

and are called the **detail coefficients** in the DWT.

As with the mother wavelet in (4.4.2), the scaling function can be described compactly as

$$\phi_{i,j}(t) = 2^{-i/2}\phi\left(2^{-i}t - j\right). \tag{4.4.5}$$

The scaling function is orthogonal to its own translations, i.e.,

$$\int \phi_{j,k}(t)\phi_{j,n}(t)dt = \delta_{k,n}, \tag{4.4.6}$$

and wavelets and scaling functions are orthogonal to each other for any dilation or translation that is

$$\int \phi_{j,k}(t)\psi_{i,n}(t)dt = 0 \quad \forall i \le j. \tag{4.4.7}$$

The **approximation coefficients** of the DWT can now be defined as the inner product of the signal and the scaling function, i.e.,

$$c_{k,n} = \int x(t)\phi_{k,n}(t)dt$$

$$\Rightarrow c_{k,n} = \langle x, \phi_{n,k} \rangle. \tag{4.4.8}$$

The detail coefficients, $d_{k,n}$, can now be obtained recursively by using the approximation coefficients, $c_{k,n}$. From (4.4.3), (4.4.6) and (4.4.7) it can be inferred that the set

$$\left\{\phi(t-k);\psi(t-k)\right\}_{k=-\infty}^{\infty} \tag{4.4.9}$$

is an orthonormal set that represents a basis. From the dilation equation in Section 4.3, i.e., (4.3.4), and from (4.3.7),

$$\left\{\sqrt{2}\phi(2t-k)\right\}_{k=-\infty}^{\infty} \tag{4.4.10}$$

also form an orthonormal set for the same space. These definitions are for the scale $n=0$, as defined by (4.4.2).

Therefore, any function, $p(t)$, can be expanded as

$$p(t)=\sum_k a^0(k)\sqrt{2}\phi(2t-k) \tag{4.4.11a}$$

$$\Rightarrow p(t)=\sum_k\left[a^1(k)\phi(t-k)+b^1(k)\psi(t-k)\right]. \tag{4.4.11b}$$

In (4.4.11a), $a^0(k)$ are the coefficients used to represent $p(t)$ with $\phi(2t-k)$. In general terms, $a^j(k)$ and $b^j(k)$ are the coefficients used to weight the scaling function and the mother wavelet, respectively, at the scale *j*.

Again, using the dilation equation for the scaling function, (4.3.4),

$$\phi(t-n)=\sqrt{2}\sum_k \tilde{h}(k)\phi(2t-2n-k), \tag{4.4.12}$$

and, similarly, by using (4.3.7) the mother wavelet can be expressed as

$$\psi(t-n)=\sqrt{2}\sum_k \tilde{g}(k)\phi(2t-2n-k). \tag{4.4.13}$$

Now, $a^1(n)$, the coefficients used to represent $p(t)$ with $\phi(t-n)$, can be expressed as

$$a^1(n) = \int_{-\infty}^{\infty} p(t)\phi(t-n)\,dt$$

$$\Rightarrow a^1(n) = \int_{-\infty}^{\infty} p(t)\sum_k \tilde{h}(t)\sqrt{2}\phi(2t-2n-k)dt$$

$$\Rightarrow a^1(n) = \sum_k \tilde{h}(k)a^0(2n+k)$$

$$\Rightarrow a^1(n) = \sum_k a^0(k)\tilde{h}(k-2n). \tag{4.4.14}$$

Similarly,

$$b^1(n) = \sum_k a^0(k)\tilde{g}(k-2n). \tag{4.4.15}$$

A bijective mapping can now be formed between $a^1(n)$ and $b^1(n)$ in (4.4.14) and (4.4.15) and the approximation and detail coefficients, $c_{k,j}$ and $d_{k,j}$, respectively, i.e.,

$$c_{k,j} \leftrightarrow a^j(k) \text{ and} \tag{4.4.16a}$$

$$d_{k,j} \leftrightarrow b^j(k). \tag{4.4.16b}$$

Hence, (4.4.14) and (4.4.15) can be generalized in order to express the approximation and detail coefficients recursively as

$$c_{k,j+1} = \sum_n c_{n,j}\tilde{h}(n-2k) \tag{4.4.17a}$$

$$\Rightarrow c_{k,j+1} = \sum_n c_{n,j}h(N+2k-n) \quad \forall\, j \geq 0 \tag{4.4.17b}$$

and

$$d_{k,j+1} = \sum_n c_{n,j}\tilde{g}(n-2k) \tag{4.4.18a}$$

$$\Rightarrow d_{k,j+1} = \sum_n c_{n,j} g\left(N + 2k - n\right) \quad \forall\, j \geq 0\,. \tag{4.4.18b}$$

This set of equations, (4.4.17) and (4.4.18), provide the method by which the DWT of function may be performed. The most striking aspect of these recursion relations is that there is no need for the scaling function or the mother wavelet to be explicitly known in order for the DWT to be practicable. All that is required are the PR filters, $\{h(n)\}$, $\{g(n)\}$, $\{\tilde{h}(n)\}$ and $\{\tilde{g}(n)\}$.

A caveat of the DWT is that $x(t)$ was expressed as an infinite sum of $\psi(t)$ basis functions in (4.4.1) as

$$x(t) = \sum_{n=-\infty}^{\infty} \sum_{k=-\infty}^{\infty} d_{k,n} \psi_{k,n}(t)\,.$$

From a practical standpoint, however, $x(t)$ must be expressed as a finite sum instead. This condition can be enforced by making use of the scaling function so that $x(t)$ may now be expressed as

$$x(t) = \sum_{n=0}^{M} \sum_k d_{k,n} \psi_{n,k}(t) + \sum_k c_{k,M} \phi_{M,k}(t)\,. \tag{4.4.19}$$

Notice in (4.4.19) that $x(t)$ is expressed predominantly in terms of the detail coefficients corresponding to translations of the mother wavelet, i.e., the HPFs, except at the final, or finest, scale of resolution, *M*. At the level of resolution $n = M$, the signal is expressed in terms of both detail and approximation coefficients.

In order to complete this presentation on wavelet transforms it is necessary to address the issue of synthesizing, i.e., reconstructing, $x(t)$ from the detail and approximation coefficients in (4.4.19). Therefore, again consider a function $p(t)$ expressed as

$$p(t)=\sum_{k}\left[a^{1}(k)\sqrt{2}\sum_{n}\tilde{h}(n)\phi(2t-2k-n)+b^{1}(k)\sqrt{2}\sum_{n}\tilde{g}(n)\phi(2t-2k-n)\right]$$

$$\Rightarrow p(t)=\sqrt{2}\sum_{k}\left[a^{1}(k)\sum_{n}\tilde{h}(n-2k)\phi(2t-n)+b^{1}(k)\sum_{n}\tilde{g}(n-2k)\phi(2t-n)\right]. \quad (4.4.20)$$

Equating (4.4.20) to $p(t)$ in (4.4.11a) establishes the relationship

$$a^{0}(k)=\sum_{n}\left[a^{1}(n)\tilde{h}(k-2n)+b^{1}(n)\tilde{g}(k-2n)\right]. \quad (4.4.21)$$

$$\Rightarrow a^{0}(k)=\sum_{n}\left[a^{1}(n)h(N+2n-k)+b^{1}(n)g(N+2n-k)\right]. \quad (4.4.22)$$

Now if this IDWT process is started at the mth scale, or level, or resolution with the coefficients $c_{k,m}$ and $d_{k,m}$, then the approximation coefficients of the next higher, i.e., coarser, scale can be found using

$$c_{k,m-1}=\sum_{n}\left[c_{n,m}\tilde{h}(k-2n)+d_{n,m}\tilde{g}(k-2n)\right]. \quad (4.4.23)$$

If this process is continued recursively, the values of $c_{k,-1}$ comprise the synthesized estimate of $x(t)$.

Chapter 5

Convolution Using the Discrete Wavelet Transform

Convolution is one of the most widely used operations in the analysis and manipulation of electrical signals. The operation is well-defined in commonly used domains such as the time-, Fourier-, Laplace-, and z-domains. It has not, however, been adequately defined for use in conjunction with the DWT.

Definition of convolution in the context of wavelet transforms allows for signal processing strategies using the DWT to be devised. Two of these strategies are channel estimation and channel equalization. Studies of the feasibility and efficacy of both of these strategies comprise Chapters 6, 7 and 8 of this dissertation.

The development of DWT-based channel estimation and equalization is, however, hinged on the ability to convolve finite-length discrete-time signal sequences within the framework of the DWT.

A method of enabling convolution while using the DWT has been developed in the literature in the context of the implementation of subband coding with the use of multirate filters. This method was titled the Wavelet Convolution Theorem [61]. The underlying concept of the approach is the “merging” or “moving” a filter that is placed at the output of a DWT filter bank from that position outside the filter bank to a position in

the synthesis part of the DWT filter bank. This procedure is termed the Backward Merge Approach in this dissertation.

In this chapter, the Backward Merge Approach has been extended by using polyphase filters, which provides an equivalent mechanism for DWT-based convolution. In addition, the concept has been used to merge filters initially placed at the input of a DWT filter bank to positions in the analysis section of the filter bank. This procedure is termed the Forward Merge Approach, and has also been extended for use with polyphase filters.

Before exploring the four methodologies for DWT-based convolution, the multirate signal processing concepts of the noble identities and polyphase filtering are described in Section 5.1. The Backward Merge Approach, upon which this work is based, is explained in Section 5.2, and is implemented with polyphase filters in Section 5.3. The Forward Merge Approach is developed in Section 5.4, and it is implemented with polyphase filters as described in Section 5.5.

A central component of the DWT that has been described in Chapter 4 is the use dyadic decimation and interpolation within the filter banks. The filter banks used in the theory subband coding described in Chapter 4 are specific cases of maximally-decimated uniform filter banks [58,94]. An M-channel maximally-decimated filter bank is shown in Fig. 5.1.1.

In Fig. 5.1.1 the filters $H_m(z)$ are the analysis filters and $F_m(z)$ are the synthesis filters. The input signal $x(n)$ is split into *M* streams, which are input to the analysis filters. The analysis filters output *M* subband signals that are decimated by a factor *M*, i.e., $x_m(n)$. These decimated signals can then be upsampled by a factor of *M* and then synthesized into $\hat{x}(n)$ by the synthesis filters, $F_m(z)$.

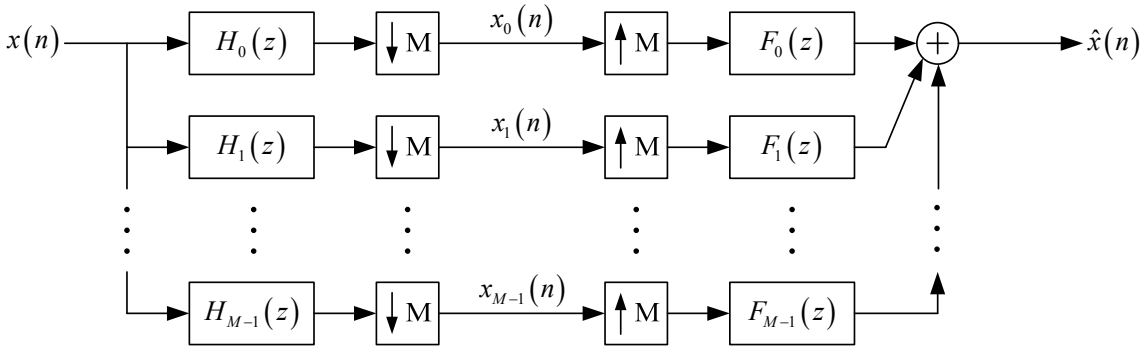

Fig. 5.1.1. *M*-channel maximally-decimated uniform filter bank.

5.1 Noble Identities and Polyphase Filtering

Consider the operation of filtering followed by decimation as shown in Fig. 5.1.2.

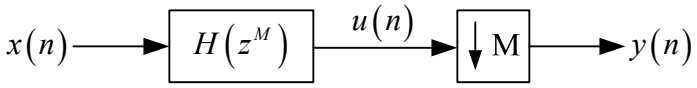

Fig. 5.1.2. Filtering followed by decimation.

After filtering by $H(z^M)$, the input signal becomes

$$U(z) = X(z)H(z^M), \tag{5.1.1}$$

while the output can be expressed as [58]

$$Y(z) = \frac{1}{M}\sum_{k=0}^{M-1} U\left(z^{1/M} e^{-j2\pi k/M}\right). \tag{5.1.2}$$

Therefore, the output of the process can be written in terms of the input as

$$Y(z) = H(z)\frac{1}{M}\left[X\left(z^{1/M}\right)H(z) + X\left(-z^{1/M}\right)H(z)\right]$$

$$\Rightarrow Y(z) = \frac{1}{M}\left[X\left(z^{1/M}\right) + X\left(-z^{1/M}\right)\right]H(z), \tag{5.1.3}$$

which implies that the input signal can first be decimated by a factor of M and then filtered, instead of being filtered first and then decimated.

This relationship is known as the **first noble identity**. and is illustrated in Fig. 5.1.3.

Fig. 5.1.3. The first noble identity.

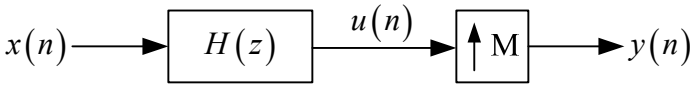

Fig. 5.1.4. Filtering followed by upsampling.

Next, consider the case where a signal is first filtered and then upsampled, as shown in Fig. 5.1.4. In this case

$$U(z) = X(z)H(z) \tag{5.1.4}$$

and

$$Y(z) = U(z^M). \tag{5.1.5}$$

$$\Rightarrow Y(z) = X(z^M)H(z^M), \tag{5.1.6}$$

which implies that the input signal, $x(n)$, may be filtered and then upsampled instead of being upsampled first and then filtered. This relationship is called the **second noble identity**, and is illustrated in Fig. 5.1.5.

Fig. 5.1.5. The second noble identity.

While the two noble identities are very useful in manipulating filtering sequences, there is one major drawback. In the event that a signal is input to a filter having a transfer function $H(z)$ and the output of the filter is to be decimated by a factor *M*, according to the first noble identity the order of operations can be swapped as long as the new filter has a transfer function that is $H(z^{1/M})$. Such a filter, however, cannot be readily generated from $H(z)$.

A similar situation also occurs with the second noble identity. In the case where a signal is upsampled by a factor of M and is then filtered by $H(z)$, the second noble identity indicates that the order of operations can be swapped with the use of a new filter $H\left(z^{1/M}\right)$. Once again, this is not a feasible solution.

Unfortunately it is exactly these two scenarios that occur in the M-channel maximally-decimated uniform filter bank in Fig. 5.1.1, and in the DWT. A solution that allows for the swapping of positions as described above is found with the use of polyphase filters.

Consider the transfer function of a filter that is defined as

$$H(z)=\sum_{n=-\infty}^{\infty} h(n)z^{-n}, \tag{5.1.7}$$

which can be expanded and grouped as

$$\begin{aligned} H(z)=&\left[\ldots+h(-4)z^{4}+h(-2)z^{2}+h(0)+h(2)z^{2}+h(4)z^{-4}\ldots\right]+\\ &z^{-1}\left[\ldots+h(-3)z^{4}+h(-1)z^{2}+h(1)+h(3)z^{2}+\ldots\right]. \end{aligned} \tag{5.1.8}$$

Let the two sets of grouped terms in (5.2.8) be denoted by

$$E_0(z)=\sum_{n=-\infty}^{\infty} h(2n)z^{-n} \tag{5.1.9a}$$

and

$$E_1(z)=\sum_{n=-\infty}^{\infty} h(2n+1)z^{-n}. \tag{5.1.9b}$$

Therefore, the filter $H(z)$ can now be expressed as

$$H(z) = E_0(z^2) + z^{-1}E_1(z^2). \tag{5.1.10}$$

In discrete time notation, the two sub-sequences that $h(n)$ has been split into are

$$e_0(n) = h(2n) \tag{5.1.11a}$$

and

$$e_1(n) = h(2n+1). \tag{5.1.11b}$$

Such a representation is called the two-component polyphase decomposition of $H(z)$. Furthermore, the new filters, $E_0(z)$ and $E_1(z)$, are called the polyphase components of $H(z)$.

This formulation can be immediately extended to represent $H(z)$ as an *M*-component polyphase decomposition, i.e.,

$$H(z) = \sum_{k=0}^{M-1} z^{-k} E_k(z^M). \tag{5.1.12}$$

Here also, the filters $E_k(z)$ are the polyphase components of $H(z)$ and are expressed in discrete time as

$$e_k(n) = h(nM + k) \qquad \forall\, 0 \le k \le M-1. \tag{5.1.13}$$

An important cautionary note about the polyphase decomposition of a filter is that the polyphase components, $E_k(z)$, depend on the number of subsequences into which $H(z)$ is to be decomposed, i.e., on *M*. For example, the two polyphase components, $E_0(z)$ and $E_1(z)$ generated for the case when $M = 2$ will generally not be equal to the

polyphase components $E_0(z)$ and $E_1(z)$ when $M=3$. (In the latter case a third filter $E_2(z)$ will also be generated.)

Polyphase Implementation of Decimation Filters

Polyphase decomposition can now be applied to the case of a decimation filter. Consider the case where a signal $x(n)$ is to be filtered by $H(z)$ and then decimated by a factor of 3. This scenario is shown in Fig. 5.1.6.

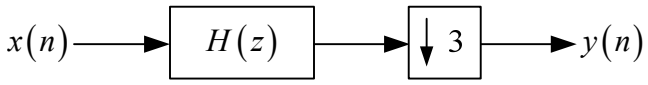

Fig. 5.1.6. Decimation filter ($M=3$).

By using (5.1.12), $H(z)$ can be decomposed into the 3-component polyphase form

$$H(z)=E_0(z^3)+z^{-1}E_1(z^3)+z^{-2}E_2(z^3). \tag{5.1.14}$$

Based on (5.1.14), the decimation filter can be redrawn to the form shown in Fig. 5.1.7.

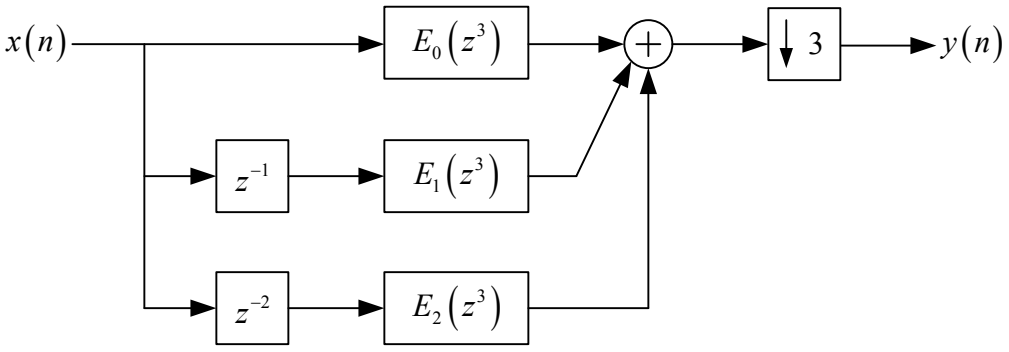

Fig. 5.1.7. Decimation filter showing polyphase decomposition.

It should be noted here that the operation of decimation is commutative. Specifically, for two functions $X_1(z)$ and $X_2(z)$, the following relationship holds

$$\left[X_1(z)+X_2(z)\right]_{\downarrow M}=\left[X_1(z)\right]_{\downarrow M}+\left[X_2(z)\right]_{\downarrow M}. \tag{5.1.15}$$

The decimation filter in Fig. 5.1.7 can now be modified with the use of (5.1.15). The decimator is, therefore, moved inside the summation operator, as seen in Fig. 5.1.8.

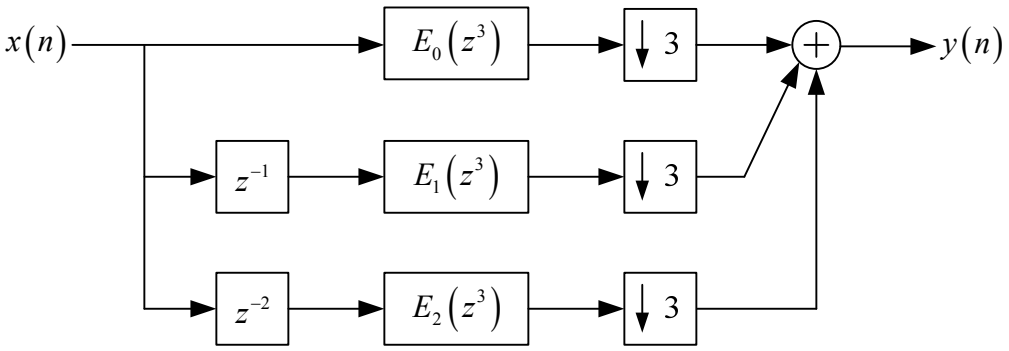

Fig. 5.1.8. Decimation filter in an intermediate step of derivation.

At this stage, the first noble identity can be invoked and the orders of the filters and decimators in each sub-channel can be interchanged. This, finally, leads to the polyphase implementation of the decimation filter, which is shown in Fig. 5.1.9. The polyphase components used in Fig. 5.1.9 can be easily derived from $h(n)$ by using (5.1.13), i.e.,

$$e_0(n)=h(3M), \tag{5.1.16a}$$

$$e_1(n)=h(3M+1), \text{ and} \tag{5.1.16b}$$

$$e_2(n)=h(3M+2). \tag{5.1.16c}$$

By following this procedure, the polyphase implementation of any *M*-fold decimation filter can be derived.

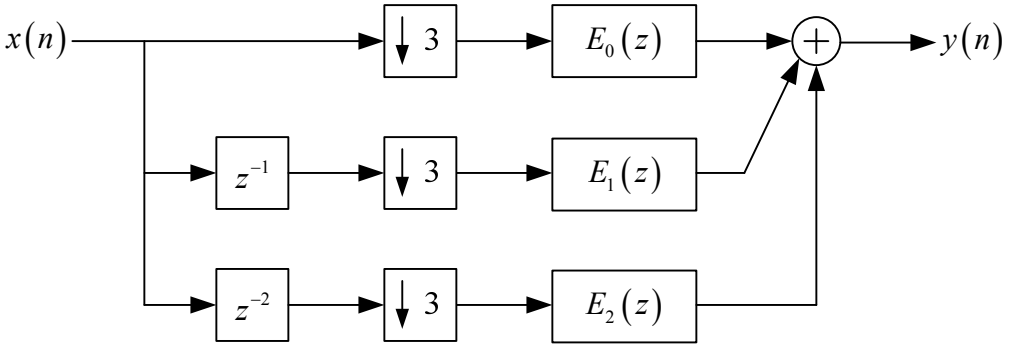

Fig. 5.1.9. Polyphase implementation of the decimation filter ($M = 3$).

The polyphase implementation of an *M*-fold decimation filter is more computationally efficient by a factor of *M*. In order to establish this improvement, let the length of the sequence $\{x(n)\}$ be *N*, and the length of the filter $H(z)$ be *L*. Discrete time-domain convolution between $x(n)$ and $h(n)$ requires *NL* multiplications. This is the case in a decimation filter, such as the example shown in Fig. 5.1.6. The polyphase implementation of the filter, as shown in Fig. 5.1.9, however, requires only $NL/3$ multiplications. In general, *M*-component polyphase implementations of decimation filters have an order of complexity given by $O(NL/M)$.

Polyphase Implementation of Interpolation Filters

The polyphase implementation of interpolation filters can be obtained in a manner similar to the decimation filters. Consider a signal $x(n)$ that is to be interpolated by a factor of M and then filtered by $H(z)$ as shown in Fig. 5.1.10.

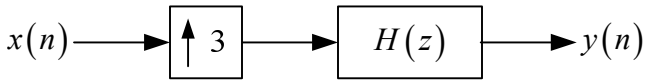

Fig. 5.1.10. Interpolation filter ($M = 3$).

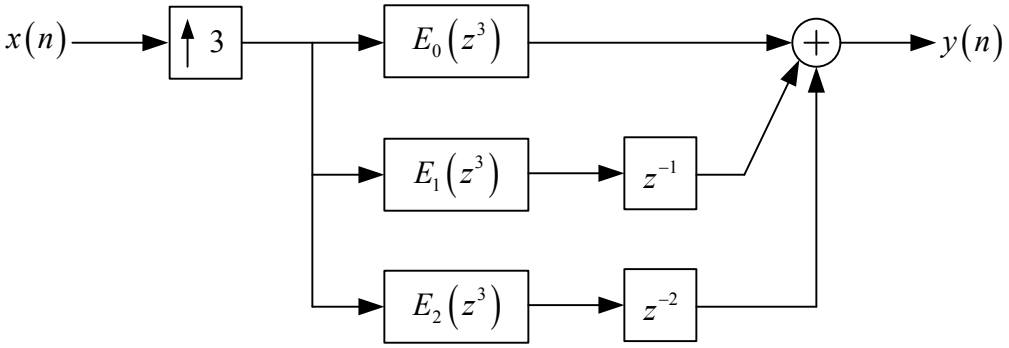

Fig. 5.1.11. Interpolation filter showing polyphase decomposition.

As in the case of the decimation filter, using (5.1.14), $h(z)$ can be decomposed into the 3-component polyphase form. The resulting interpolation filter is shown in Fig. 5.1.11, and an equivalent form of this interpolation filter is shown in Fig. 5.1.12. It should be noted that in Figs. 5.1.11 and 5.1.12 the delays, z^{-1} and z^{-2}, are placed after the polyphase components $E_1(z^3)$ and $E_1(z^3)$, respectively, instead of before as was done previously (Figs. 5.1.7 - 5.1.9 for the decimation filters).

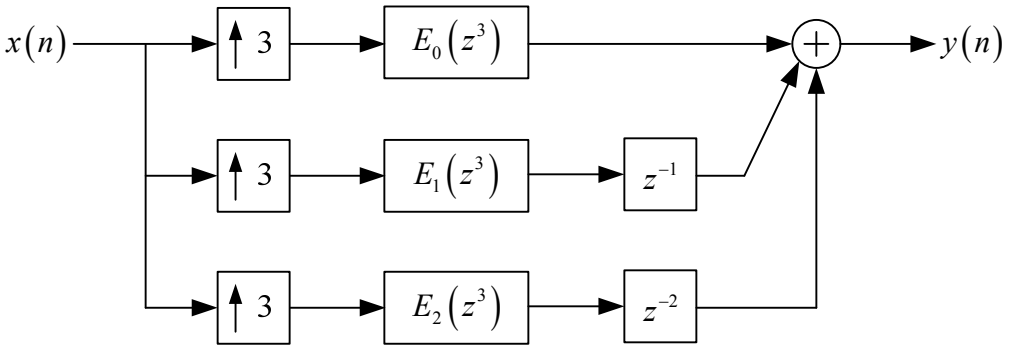

Fig. 5.1.12. Interpolation filter in an intermediate step of derivation.

The second noble identity can be applied to the interpolation filter shown in Fig. 5.1.13. The result is the polyphase implementation of the interpolation filter for the case when $M = 3$. The coefficients of the polyphase components are the same as in (5.1.16). Again, by following this procedure the polyphase implementation of *M*-fold interpolation filters can be realized.

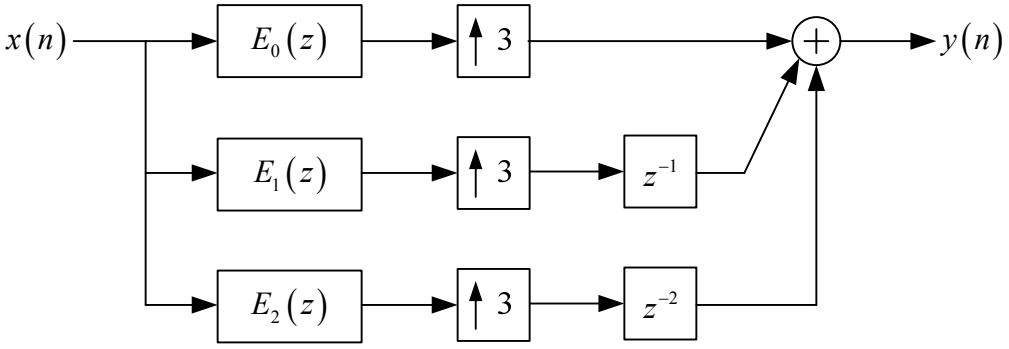

Fig. 5.1.13. Polyphase implementation of the interpolation filter ($M = 3$).

The polyphase implementation of an *M*-fold interpolation filter is also more computationally efficient than a standard *M*-fold interpolation filter by a factor of *M*.

Again, let the length of $\{x(n)\}$ be N, and the length of the $H(z)$ be L. The 3-fold interpolation filter shown in Fig. 5.1.10, requires $3NL$ multiplications, whereas the polyphase implementation of the same filter, shown in Fig. 5.1.13, requires only NL multiplications. In general, polyphase implementations of M-fold interpolation filters have an order of complexity given by $O(NL)$.

The concepts of the polyphase implementation of decimation and interpolation filters can be applied to a maximally-decimated uniform filter bank with two subbands. The choice of two subbands is because the DWT is implemented with a PR filter bank having two subbands. The resulting filter, which is composed of polyphase implementations of decimation and interpolation filters is shown in Fig. 5.1.14.

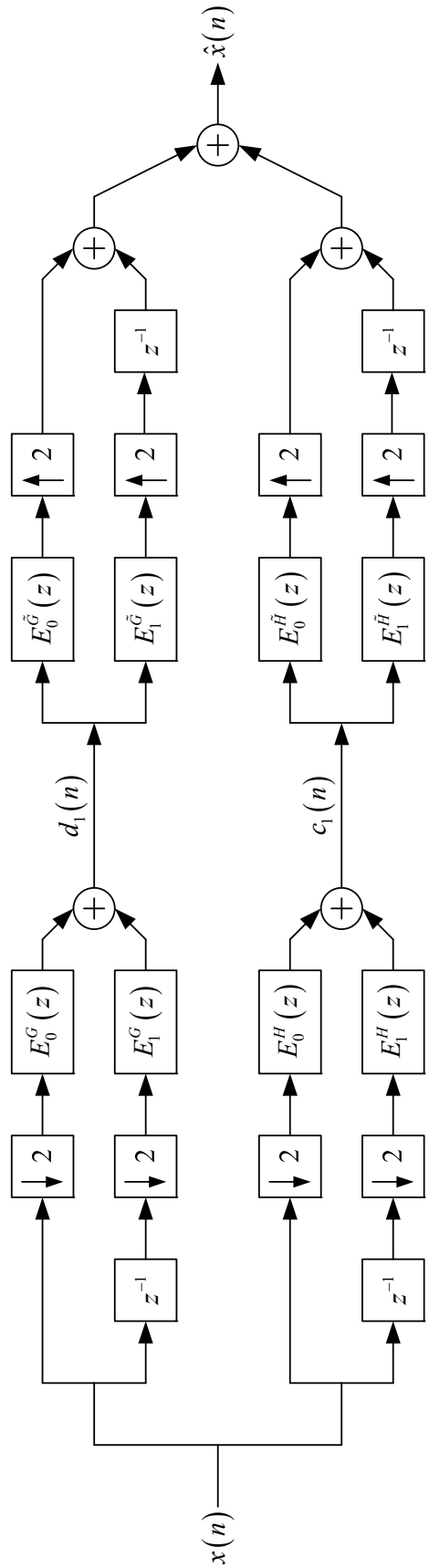

Fig. 5.1.14. Polyphase implementations applied to a maximally-decimated uniform filter bank having 2 subbands.

5.2 The Backward Merge Approach

One method for DWT subband convolution has previously been established in a research study available in the literature [61]. The method was labeled the Wavelet Convolution Theorem by the authors of the study. This method is used as a start-point for the development of the topics in this dissertation. The approach taken in the Wavelet Convolution Theorem is called the Backward Merge Approach in this dissertation, and has inspired three new variations of DWT-based convolution. These three new variations are described in the remaining sections of this chapter.

Wavelet Convolution Theorem

Consider the case where a pair of DWT and IDWT exist so that the PR condition is satisfied. A function $x(t)$ can be expanded using wavelet bases as

$$x(t) = \sum_k \sum_n x_{DWT}(k,n) f_k\left(t - na^k T\right) \tag{5.2.1}$$

where

$$x_{DWT}(k,n) = \int_{-\infty}^{\infty} x(t) h_k\left(na^k T - t\right) dt\,. \tag{5.2.2}$$

The convolution of two signals $x(t)$ and $y(t)$ can therefore be computed as

$$x(t) * y(t) \triangleq \int_{-\infty}^{\infty} x(\tau) y(t-\tau) d\tau$$

$$\Rightarrow x(t) * y(t) = \sum_k x_{DWT}(k,n) y_k\left(t - na^k T\right) \tag{5.2.3}$$

where $y_k(t)$ is the output of the filter $f_k(t)$ and $y(t)$ is the input to the filter.

This theorem is arrived at graphically in three steps. Note that in Figs. 5.2.1 - 5.2.3 only one channel of the filter bank is shown but the convolution procedure is to be applied at every channel of the filter bank.

Step 1 As seen in Fig. 5.2.1, $x(t)$ is analyzed and then synthesized by a DWT and IDWT filter bank, the output of which is $x(t)$ again. This output is then input to a filter $Y(j\Omega)$, which is the Fourier transform of $y(t)$. The result of this operation is $x(t) * y(t)$.

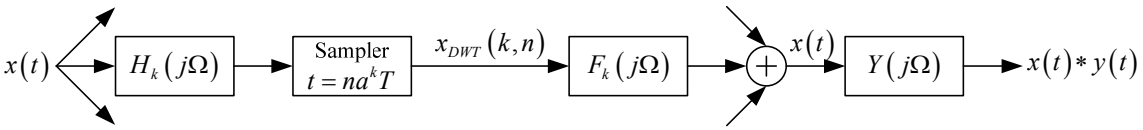

Fig. 5.2.1. Step 1 of the Wavelet Convolution Theorem.

Step 2 Using the distributive property of (Fourier-domain) multiplication, the filter $Y(j\Omega)$ is moved inside the filter bank.

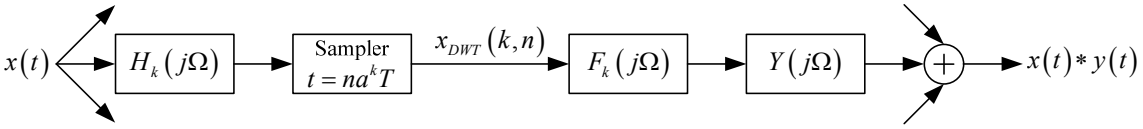

Fig. 5.2.2. Step 2 of the Wavelet Convolution Theorem.

Step 3 Since the cascading the filters $F_k(j\Omega)$ and $Y(j\Omega)$ is equivalent to filtering $y(t)$ with $F_k(j\Omega)$, i.e.,

$$Y_k(j\Omega) = Y(j\Omega)F_k(j\Omega) \underset{F^{-1}}{\overset{F}{\rightleftharpoons}} y_k(t) = y(t) * f_k(t), \tag{5.2.4}$$

this relationship is used so that each $y_k(t)$ is convolved with $x_{DWT}(k,n)$.

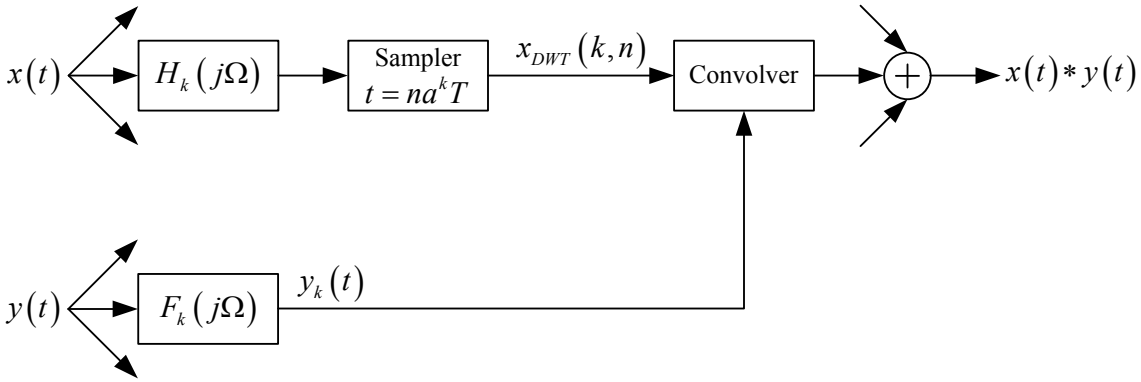

Fig. 5.2.3. Step 3 of the Wavelet Convolution Theorem.

Now, as a complement to the Wavelet Convolution Theorem that has been described, consider that the two signals to be convolved, $x(t)$ and $y(t)$, are square integrable and have bounded energy. The two signals are also of finite time duration.

Let both signals be sampled at a rate of nT, which results in two finite-length signal sequences $x(n)$ and $y(n)$ of lengths N_X and N_Y, respectively, and there exist the z-transforms of both sequences, i.e.,

$$X(z) = \sum_{n=0}^{N_x} x(n) z^{-n} \text{ and} \tag{5.2.5}$$

$$Y(z) = \sum_{n=0}^{N_y} y(n) z^{-n}. \tag{5.2.6}$$

Let $r(n)$ denote the convolution of $x(n)$ and $y(n)$, which gives the transform pair,

$$r(n) = x(n) * y(n) \underset{Z^{-1}}{\overset{Z}{\rightleftharpoons}} R(z) = X(z)Y(z). \tag{5.2.7}$$

Suppose that $x(n)$ is to be expressed using the DWT and then the IDWT, and the synthesized copy of $x(n)$ is to be convolved with $y(n)$. Equivalently, $X(z)$ is to be wavelet transformed using an analysis/synthesis filter bank as seen in Chapter 4, and the synthesized copy of $X(z)$ is to be multiplied with $Y(z)$. This latter scenario is shown in Fig. 5.2.4 with $X(z)$ input to a 1-level DWT and IDWT filter bank.

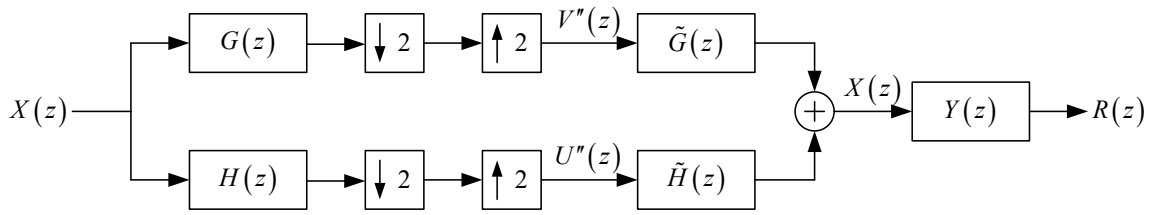

Fig. 5.2.4. 1-level DWT and convolution of $X(z)$.

Within the filter bank, let the variables $U''(z)$ and $V''(z)$ denote the signals that are input to the synthesis HPF, $\tilde{G}(z)$, and the LPF, $\tilde{H}(z)$, respectively. The output of the filter bank is

$$X(z) = V''(z)\tilde{G}(z) + U''(z)H(z) \tag{5.2.8}$$

and therefore,

$$R(z) = \left[V''(z)\tilde{G}(z) + U''(z)H(z)\right]Y(z)$$

$$\Rightarrow R(z) = V''(z)\tilde{G}(z)Y(z) + U''(z)H(z)Y(z) \tag{5.2.9}$$

which implies that the filter $Y(z)$ can be moved inside the summation in Fig. 5.2.4. The order of filtering can also be interchanged since the product of $Y(z)$ with $\tilde{G}(z)$ or $\tilde{H}(z)$ is commutative, i.e.,

$$R(z) = V''(z)Y(z)\tilde{G}(z) + U''(z)Y(z)H(z). \tag{5.2.10}$$

This result is shown graphically in Fig. 5.2.5, and is analogous to Fig. 5.2.2.

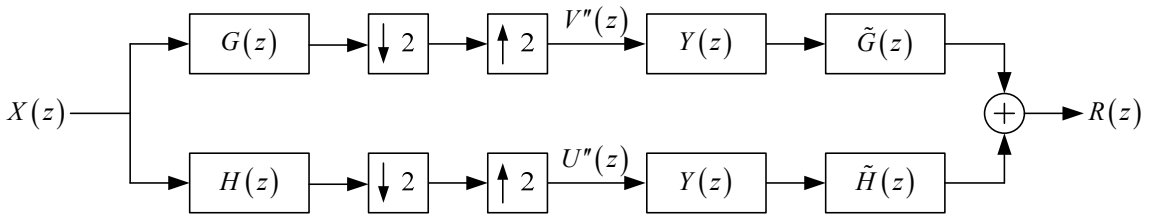

Fig. 5.2.5. The Backward Merge Approach of DWT convolution.

For the purposes of practical implementation there is no need to follow Step 3 of the Wavelet Convolution Theorem, and the system shown in Fig. 5.2.5 can be directly used.

This methodology for DWT convolution involves moving the signal $y(n)$ and the convolution operation from the output of the filter bank to a position inside, and thus essentially causing the cascaded, i.e., merged, filters $Y(z)\tilde{G}(z)$ and $Y(z)\tilde{H}(z)$. Therefore, for the purposes of this dissertation, it is called the Backward Merge Approach of DWT convolution.

The case of analyzing a signal at 2 levels of DWT is shown in Fig. 5.2.6. Recall that the second level of analysis is actually a 1-level DWT of the approximation coefficients at the first level of the overall DWT, $c_1(n)$.

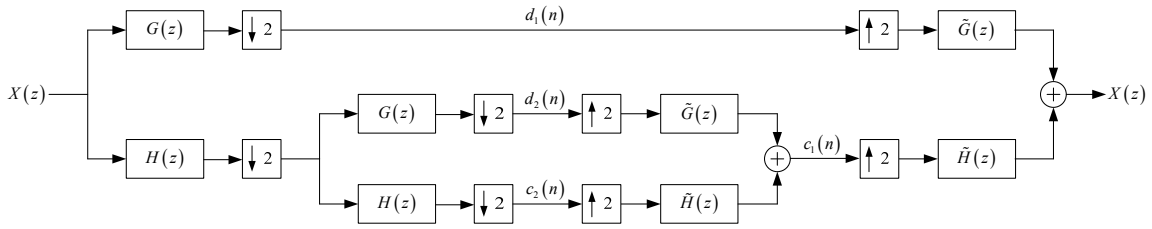

Fig. 5.2.6. 2-level DWT and IDWT.

It is seen in Fig. 5.2.6 that the synthesized output of level-2, i.e., $c_1(n)$, is exactly the sequence of level 1 detail coefficients. After being synthesized, $c_1(n)$ is upsampled by a factor of 2 and filtered. The upsampling operation, however, obeys the distributive property. Therefore, the upsampler that operates on $c_1(n)$ can be moved into the synthesis filter bank at level 2. This move is shown in Fig. 5.2.7.

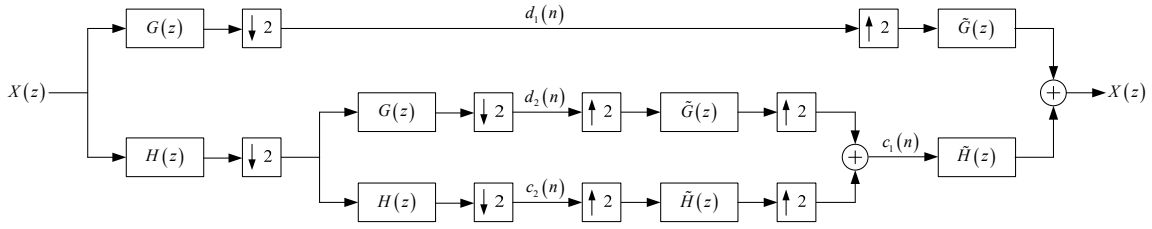

Fig. 5.2.7. Upsampler moved from level 1 to level 2.

This move immediately allows for the use of the second noble identity since the filters $\tilde{G}(z)$ and $\tilde{H}(z)$ in the synthesis bank at level 2 are each followed by an upsampling operation. Furthermore, upsampling a signal by a factor of 2 twice in succession is equivalent to upsampling a signal by a factor of 4 once. Using both of these conditions, the 2-level DWT filter bank in Fig. 5.2.7 is updated as shown in Fig. 5.2.8.

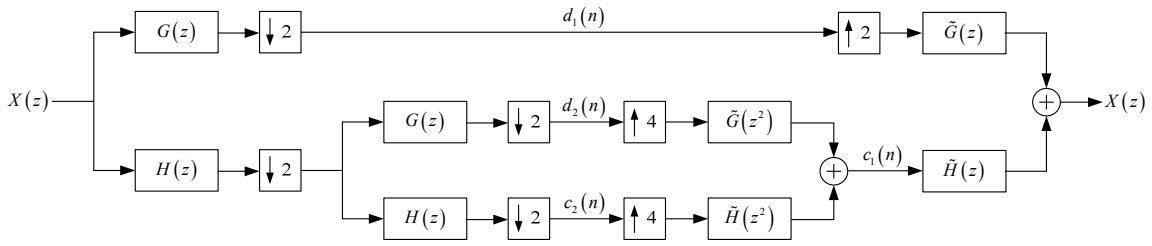

Fig. 5.2.8. Equivalent 2-level DWT.

Note that in Fig. 5.2.8, the order of the synthesis filters is doubled, i.e., the filters are $\tilde{G}(z^2)$ and $\tilde{H}(z^2)$. The coefficients of these filters are $\{\tilde{g}(2n)\}$ and $\{\tilde{h}(2n)\}$, respectively.

Therefore, if $X(z)$ is to be convolved with $Y(z)$, $X(z)$ can be expressed at 2 levels of DWT, and the Backward Merge Approach can once again be used. It is applied in the same way at each level of resolution, and the resulting filter bank is shown in Fig. 5.2.9.

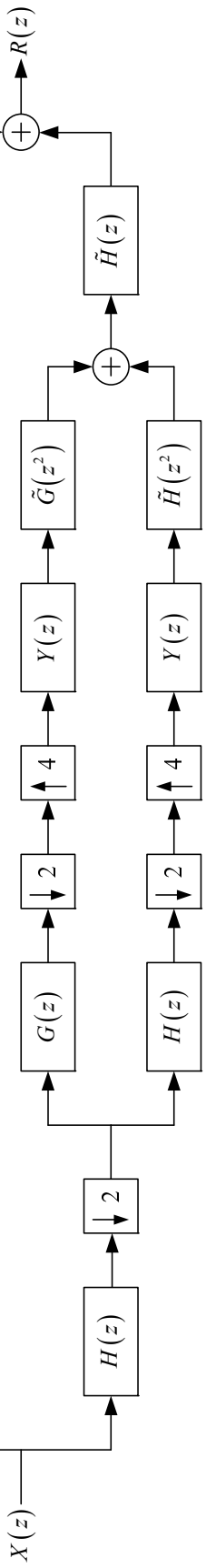

Fig. 5.2.9. The Backward Merge Approach used at two levels of DWT.

In order to gauge the computational complexity of the Backward Merge Approach, let the length of $X(z)$ be N_X, the length of $Y(z)$ be N_Y, and the lengths of all the DWT filters be L. Furthermore, assume that the two signals are much longer discrete-time sequences than the filters, i.e., $N_X \gg L$ and $N_Y \gg L$. Referring to Fig. 5.2.9, the order of complexity required in the level 1 detail subband is

$$O(n) = N_X + N_X N_Y + (N_X + N_Y) \tag{5.2.11a}$$

$$\Rightarrow O(n) \approx N_X N_Y . \tag{5.2.11b}$$

For the level 1 approximation subband, which includes the operations at level 2 as well, the order of complexity is

$$O(n) = 2N_X + 2N_X N_Y + 3(N_X + N_Y) \tag{5.2.12a}$$

$$\Rightarrow O(n) \approx 2N_X N_Y . \tag{5.2.12b}$$

5.3 The Backward Merge Approach with Polyphase Filters

The Backward Merge Approach can be taken one step further by making use of polyphase filtering. Notice in Fig. 5.2.5 that the DWT coefficients are first upsampled by a factor of 2 and then filtered by $Y(z)$. Instead, the polyphase components of $Y(z)$ can be easily generated and used in the DWT convolution process so that the order of the operations of upsampling by a factor 2 and filtering with $Y(z)$ can be interchanged.

As described in (5.1.9) and (5.1.10), $Y(z)$ can be expressed as the 2-component polyphase decomposition

$$Y(z) = E_0(z^2) + z^{-1}E_1(z^2) \tag{5.3.1}$$

where the polyphase components are

$$E_0(z) = \sum_{n=0}^{N_y} y(2n)z^{-n} \text{ and} \tag{5.3.2a}$$

$$E_1(z) = \sum_{n=0}^{N_y} y(2n+1)z^{-n}. \tag{5.3.2b}$$

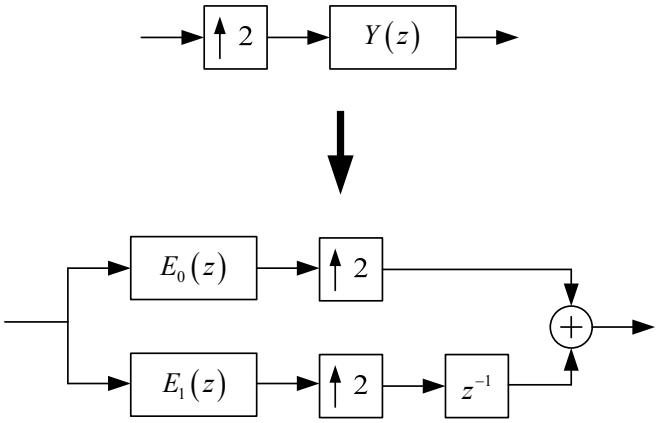

Fig. 5.3.1. Polyphase implementation of the $Y(z)$ interpolation filter.

Note that the same polyphase components can be used in the 1-level DWT filter bank shown in Fig. 5.2.5 since the DWT coefficients in each channel are upsampled by the same factor, i.e., by 2. Therefore, the filter bank implementing the Backward Merge Approach, in Fig. 5.2.5, can be updated to include polyphase filtering as shown in Fig. 5.3.2. This methodology can also be implemented for 2 levels of DWT. In Fig. 5.2.9 it is seen that there are 2-fold upsamplers and 4-fold upsamplers in the 2-level

implementation. Due to this $Y(z)$ must be expressed as a 2-component polyphase decomposition at level 1 and a 4-component polyphase decomposition at level 2.

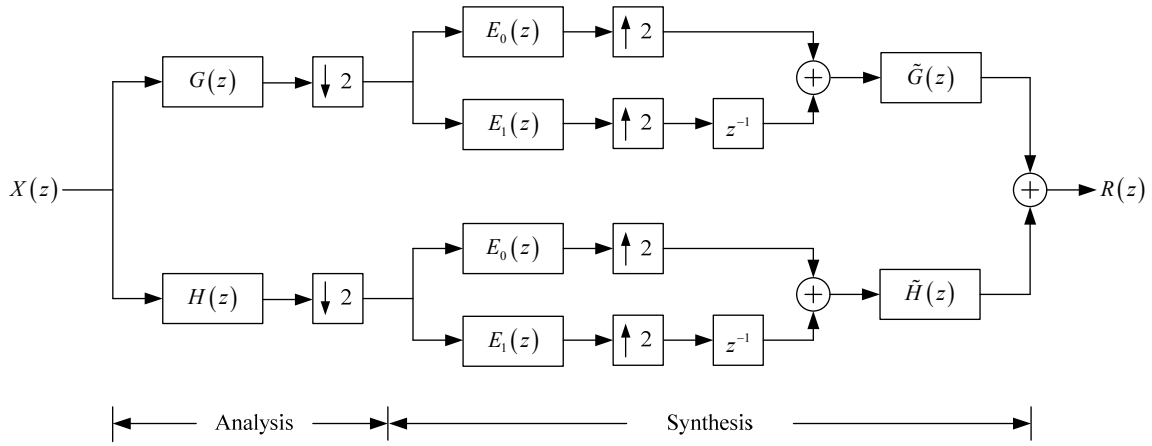

Fig. 5.3.2. The Backward Merge Approach with polyphase implementation at one level of DWT.

To avoid confusion, the m^{th} polyphase component at the k^{th} level of DWT is denoted by $E_m^k(z)$ in the z-domain, and the corresponding discrete time sequence is denoted by $e_m^k(n)$. Using this notation the polyphase components to be used at level 1 of the DWT are $E_0^1(n)$ and $E_1^1(n)$, and the polyphase components for use at level 2 of the DWT are $E_0^2(n)$, $E_1^2(n)$, $E_2^2(n)$ and $E_3^2(n)$.

The resulting filter bank that incorporates the Backward Merge Approach of convolving $X(z)$ and $Y(z)$ at two levels of DWT with the use of polyphase filtering is shown in Fig. 5.3.3.

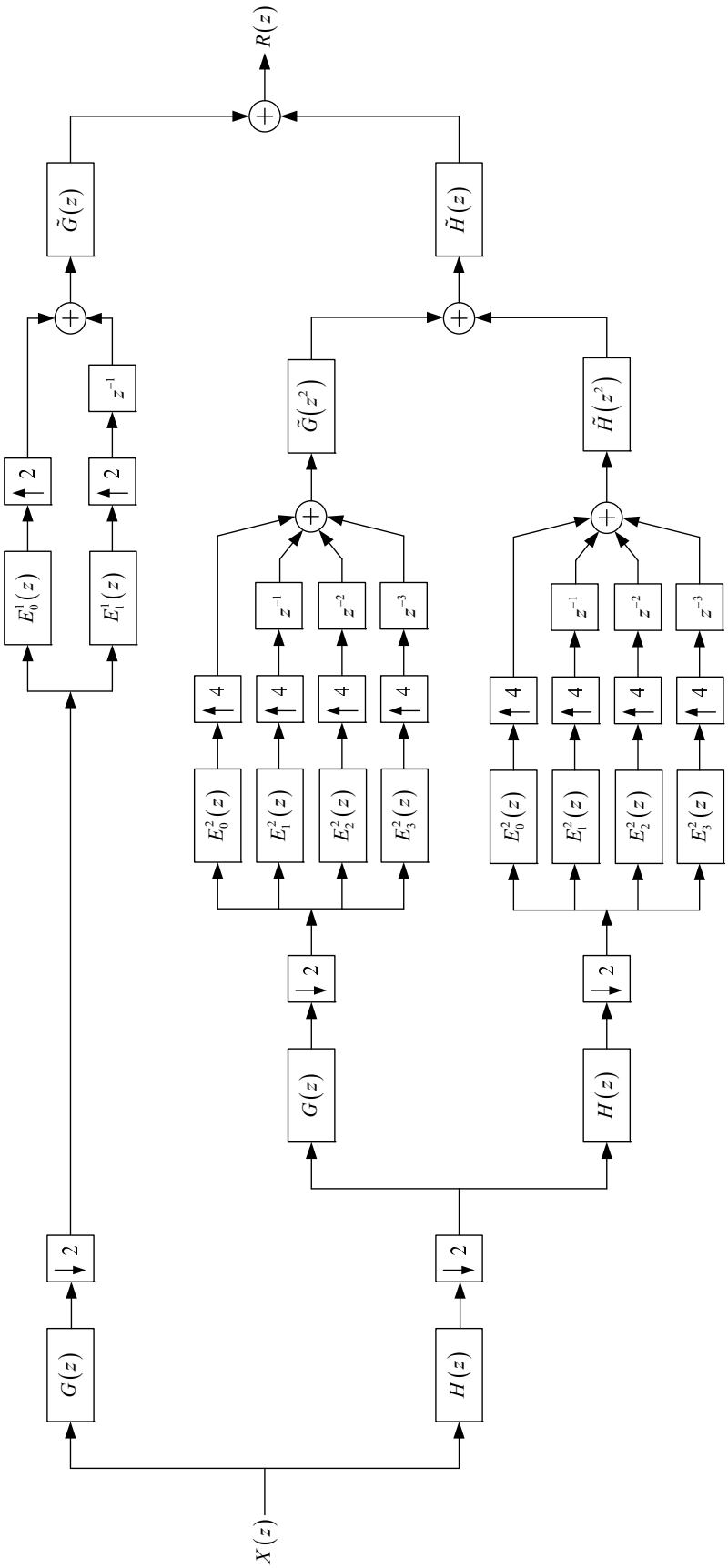

Fig. 5.3.3. The Backward Merge Approach with polyphase implementation at two levels of DWT.

In Fig. 5.3.3, let the length of $X(z)$ be N_X, the length of $Y(z)$ be N_Y, the lengths of all DWT analysis and synthesis filters be L. Assuming that $N_X \gg L$ and $N_Y \gg L$, the number of arithmetic operations that have to be performed in the level 1 detail subband is of the order

$$O(n) = N_X + \frac{N_X N_Y}{2} + (N_X + N_Y) \tag{5.3.3a}$$

$$\Rightarrow O(n) \approx \frac{N_X N_Y}{2}. \tag{5.3.3b}$$

In the level 1 approximation subband, which includes all operations at level 2, the complexity is

$$O(n) = 2N_X + \frac{N_X N_Y}{2} + 3(N_X + N_Y) \tag{5.3.4a}$$

$$\Rightarrow O(n) \approx \frac{N_X N_Y}{2}. \tag{5.3.4b}$$

5.4 The Forward Merge Approach

Using the idea of the Backward Merge Approach an alternative approach can be developed, albeit based essentially on the corollary to the Backward Merge Approach. In this new approach a filter is merged with a DWT filter bank by starting at the input of the filter bank. This procedure, called the Forward Merge Approach, is more intuitively appealing than the Backward Merge Approach because it follows the commonly used diagrammatic direction of signal flow: from left to right.

Once again, starting with two signals, $x(n)$ and $y(n)$, which, when convolved, result in

$$x(n) * y(n) = r(n), \tag{5.4.1}$$

or, equivalently,

$$X(z)Y(z) = R(z). \tag{5.4.2}$$

In the Backward Merge Approach $X(z)$ was transformed using the DWT and IDWT. In this case, however, $R(z)$ is transformed using the DWT and IDWT instead. This scenario is depicted in Fig. 5.3.1 with 1-level DWT.

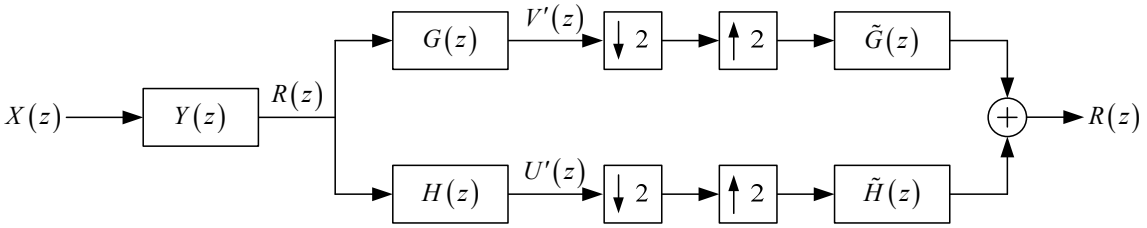

Fig. 5.4.1. 1-level DWT and IDWT of $R(z)$.

From Fig. 5.4.1, the intermediate signals output by the analysis filters are

$$V'(z) = R(z)G(z) \text{ and} \tag{5.4.3}$$

$$U'(z) = R(z)H(z). \tag{5.4.4}$$

Using (5.4.2), these intermediate signals can be rewritten as

$$V'(z) = X(z)Y(z)G(z) \text{ and} \tag{5.4.5}$$

$$U'(z) = X(z)Y(z)H(z). \tag{5.4.6}$$

It is immediately seen in (5.4.5) and (5.4.6) that the orders of filtering, being commutative, can be interchanged. This allows for the signal $Y(z)$ to be embedded within the DWT filter bank that is analyzing $R(z)$. By this action the convolution operation that was originally outside the DWT/IDWT filter bank can be moved inside it and can essentially be merged with the analysis filters. Explicitly, these merged filters would be $G(z)Y(z)$ and $H(z)Y(z)$.

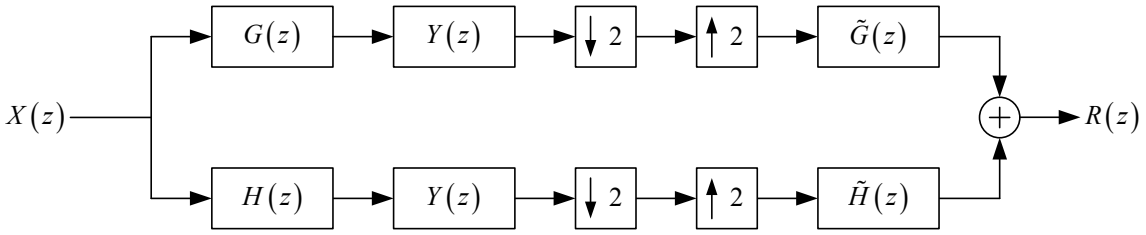

Fig. 5.4.2. The Forward Merge Approach of DWT convolution.

As in the case of the Backward Merge Approach, in order to implement the Forward Merge Approach at 2 levels of DWT a modified form of the 2-level DWT filter bank must be first established. In particular, the 2-fold decimator following $H(z)$ at level 1 has to be moved to level 2. Fortunately, since the decimator precedes the two analysis filters at level 2, the first noble identity can be used. The original 2-level DWT/IDWT filter bank is shown in Fig. 5.4.3. The modified 2-level filter bank is shown in Fig. 5.4.4.

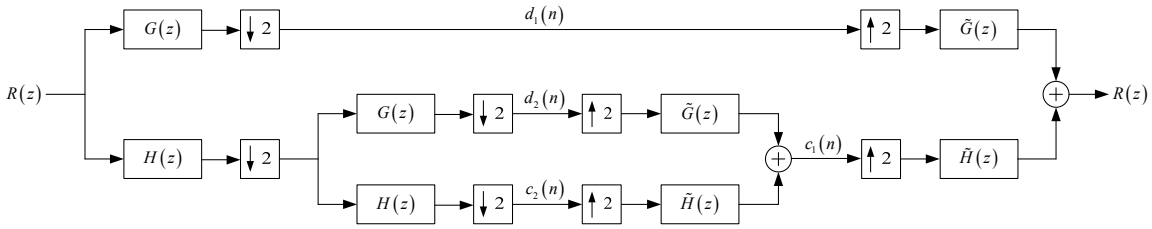

Fig. 5.4.3. Original 2-level DWT/IDWT filter bank.

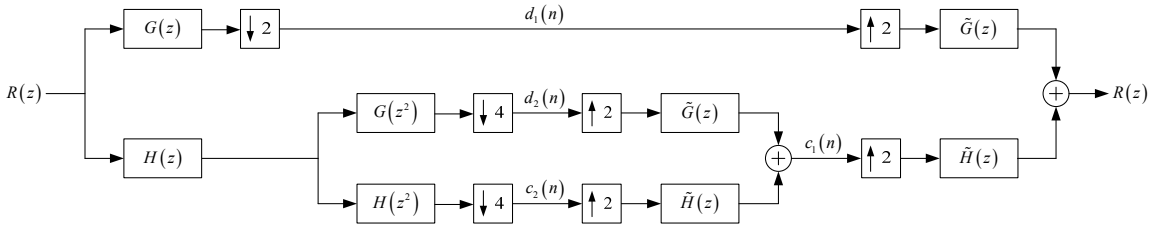

Fig. 5.4.4. Modified 2-level DWT/IDWT filter bank.

The Forward Merge Approach of convolving $X(z)$ and $Y(z)$ can now be implemented by using the modified filter bank in Fig. 5.4.4. The resulting filter bank is shown in Fig. 5.4.5. Using the modified DWT/IDWT filter banks the Forward Merge Approach can be implemented for any number of levels of DWT analysis.

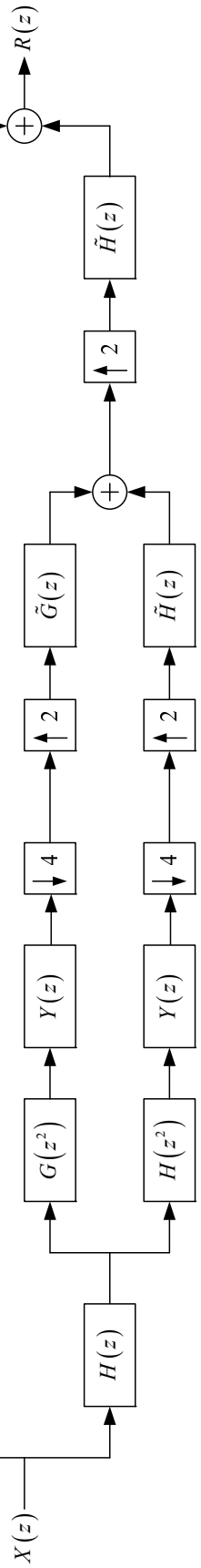

Fig. 5.4.5. The Forward Merge Approach used at two levels of DWT.

Using the same notations for signal lengths as in the Backward Merge Approach, the number of computations required for the Forward Merge Approach at each DWT level can be determined from Fig. 5.4.5. In the level 1 detail subband, the number of computations is

$$O(n) = N_X + N_X N_Y + (N_X + N_Y) \tag{5.4.7a}$$

$$\Rightarrow O(n) \approx N_X N_Y . \tag{5.4.7b}$$

In the level 1 approximation subband, which includes the operations at level 2, the order of complexity is

$$O(n) = 3N_X + 2N_X N_Y + 2(N_X + N_Y) \tag{5.4.8a}$$

$$\Rightarrow O(n) \approx 2N_X N_Y . \tag{5.4.8b}$$

5.5 The Forward Merge Approach with Polyphase Filters

Using polyphase filtering the Forward Merge Approach can be modified into an equivalent form. For the case of 1-level DWT, as seen in Fig. 5.4.2, the output of the $Y(z)$ filter in each channel is decimated by a factor of 2. Such a filtering operation followed by decimation, which is called a decimation filter, may be implemented using the polyphase components of $Y(z)$.

By following the procedure used to generate Fig. 5.1.9, for the case of 2-fold decimation, the 2-component polyphase decomposition of $Y(z)$ is

$$Y(z) = E_0(z^2) + z^{-1}E_1(z^2) \tag{5.5.1}$$

where

$$E_0(z) = \sum_{n=0}^{N_y} y(2n)z^{-n} \text{ and} \tag{5.5.2a}$$

$$E_1(z) = \sum_{n=0}^{N_y} y(2n+1)z^{-n}. \tag{5.5.2b}$$

Note that this polyphase decomposition and the components are exactly the same as in Section 5.3, the Backward Merge Approach with Polyphase Filters. The difference lies in the actual implementation of the filters in conjunction with the decimator. In Section 5.3, the filters were used along with upsamplers instead. The polyphase implementation of the $Y(z)$ decimation filter is shown in Fig. 5.5.1.

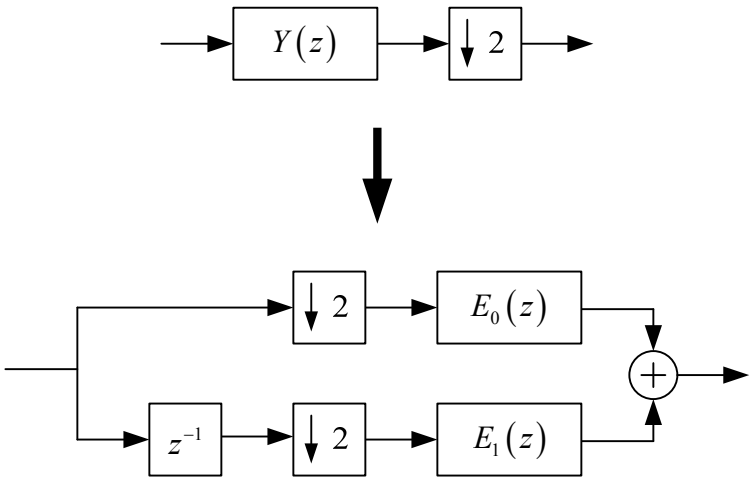

Fig. 5.5.1. Polyphase implementation of the $Y(z)$ decimation filter.

Therefore, the 1-level DWT convolution using the Forward Merge Approach shown in Fig. 5.4.2 is modified by using the polyphase form of the $Y(z)$ interpolation filter shown in Fig. 5.5.1. This equivalent form is illustrated in Fig. 5.5.2.

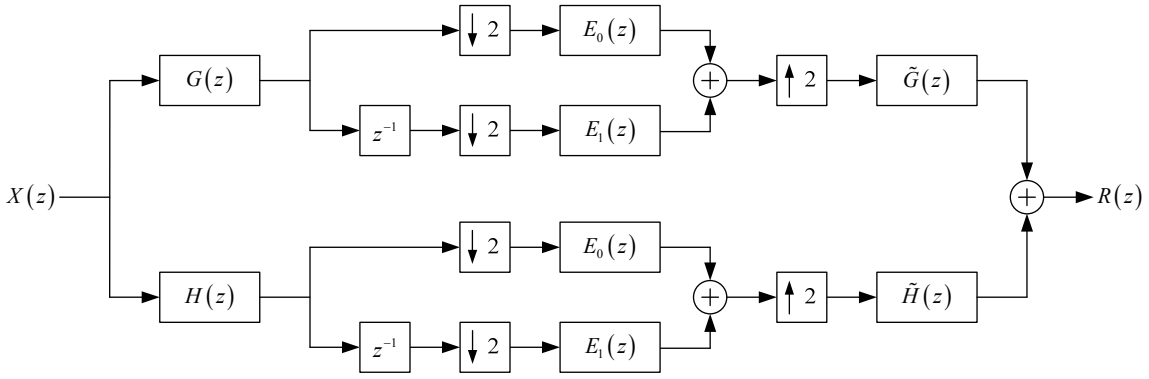

Fig. 5.5.2. The Forward Merge Approach with polyphase implementation at one level of DWT.

Taking into consideration that at two levels of DWT there are 2-fold decimators at level 1 and 4-fold decimators at level 2, two sets of polyphase components are required for the polyphase decomposition of $Y(z)$. The notation established in Section 5.3 is used here as well. For the sake of completeness the coefficients of the two decompositions are provided as follows.

The coefficients of the polyphase components to be used at level 1 are

$$e_0^1(n) = y(2n) \text{ and} \tag{5.5.3a}$$

$$e_1^1(n) = y(2n+1). \tag{5.5.3b}$$

The coefficients to be used at level 2 are

$$e_0^2(n) = y(4n), \tag{5.5.4a}$$

$$e_1^2(n) = y(4n+1), \tag{5.5.4b}$$

$$e_2^2(n) = y(4n+2) \text{ and} \tag{5.5.4c}$$

$$e_3^2(n) = y(4n+3). \tag{5.5.4d}$$

The resulting filter bank is seen in Fig. 5.5.3 in which the convolution of $X(z)$ and $Y(z)$ is implemented using the Forward Merge Approach with polyphase filtering at two levels of DWT. This process can readily be extended for any number of levels of DWT.

Using Fig. 5.5.3, the computational complexity of the Forward Merge Approach with polyphase implementation can be determined. Again, let the length of $X(z)$ be N_X, the length of $Y(z)$ be N_Y, and the lengths of the DWT filters be L. Assuming that $N_X \gg L$ and $N_Y \gg L$, the order of complexity in the level 1 detail subband is

$$O(n) = N_X + \frac{N_X N_Y}{2} + (N_X + N_Y) \tag{5.5.5a}$$

$$\Rightarrow O(n) \approx \frac{N_X N_Y}{2}. \tag{5.5.5b}$$

The complexity in the level 1 approximation subband, which includes all operations at level 2, is

$$O(n) = 3N_X + \frac{N_X N_Y}{2} + 2(N_X + N_Y) \tag{5.5.6a}$$

$$\Rightarrow O(n) \approx \frac{N_X N_Y}{2}. \tag{5.5.6b}$$

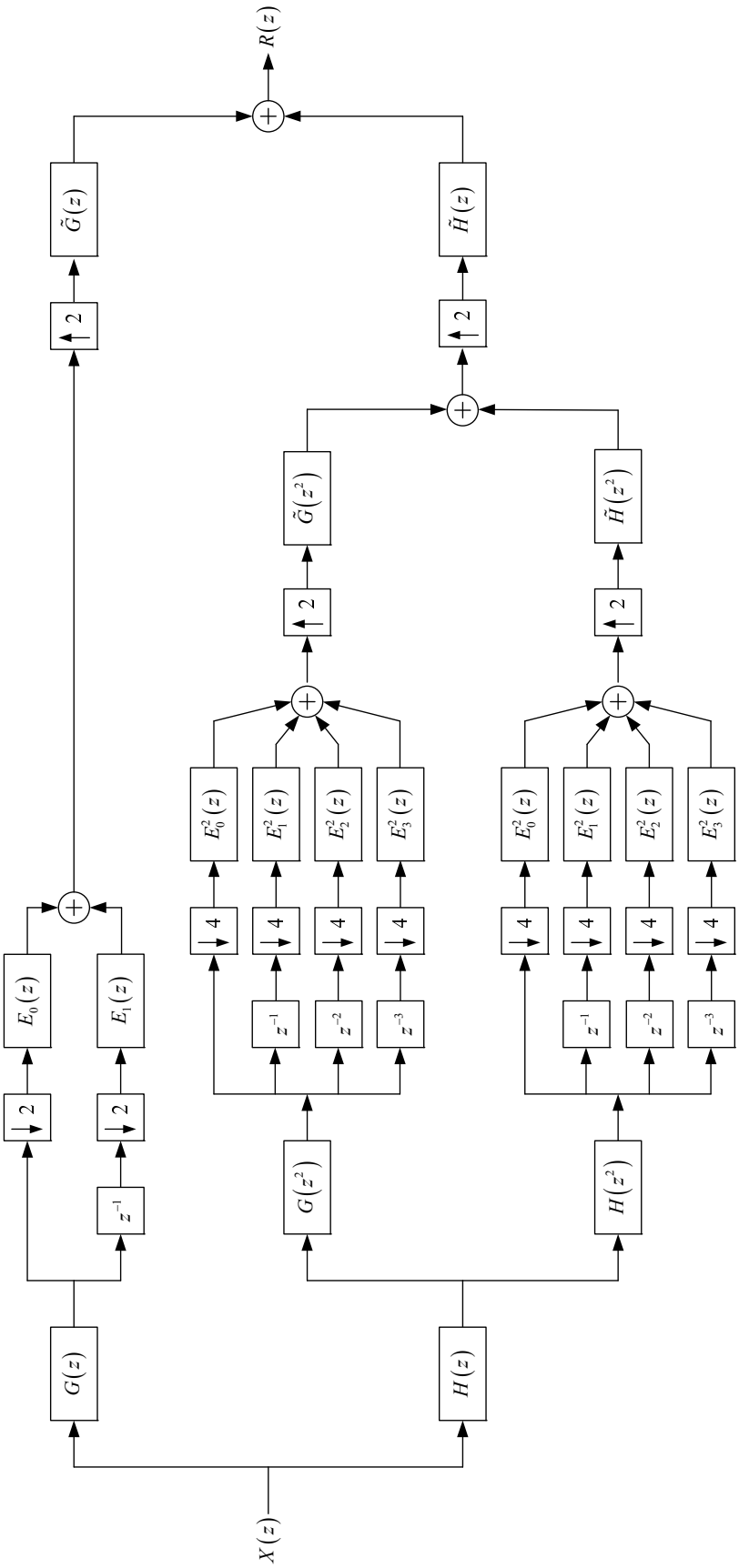

Fig. 5.5.3. The Forward Merge Approach with polyphase implementation at two levels of DWT.

Chapter 6

Discrete Wavelet Transform-Based Channel Estimation

A procedure for the deconvolution of signals using the DWT is developed in this chapter in order to complement the approaches for DWT-based convolution in Chapter 5. The first application of DWT-based convolution and deconvolution is in the estimation of communications channels. In this application pilot-assisted channel estimation is developed.

In the computer simulation experiments, a test signal is first transmitted through a channel and the distorted signal is acquired by a receiver. A copy of the distortion-free pilot signal is available at the receiver, which is deconvolved from the received signal in order to obtain an estimate of the impulse response of the channel.

A point worthy of note is that the procedure of deconvolution using the DWT is not developed here exclusively for the purpose of channel estimation, but rather as a general methodology that can be used in any suitable application.

The methodology for DWT deconvolution is developed in Section 6.1. The procedure for generating analytical forms of channels suitable for use in computer simulation experiments is described in Section 6.2, along with a description of the test signals that are used. The deconvolution procedure is applied to five types of channels, which are

characterized by their PDPs. The results of the simulation experiments are presented in Section 6.3. A discussion of the methodologies used and the results is provided in Section 6.4.

6.1 Deconvolution Using the Discrete Wavelet Transform

Suppose $x(n)$ and $y(n)$ are two finite-length discrete time sequences such that $x(n)$ and $y(n)$ are convolved to produce $r(n)$, i.e.,

$$r(n) = x(n) * y(n). \tag{6.1.1}$$

Using the Forward Merge Approach, let this convolution be performed using the DWT. Specifically, the z-transform equivalents of the signals, $X(z)$ and $Y(z)$, are DWT convolved without using polyphase filters, as shown in Fig. 6.1.1.

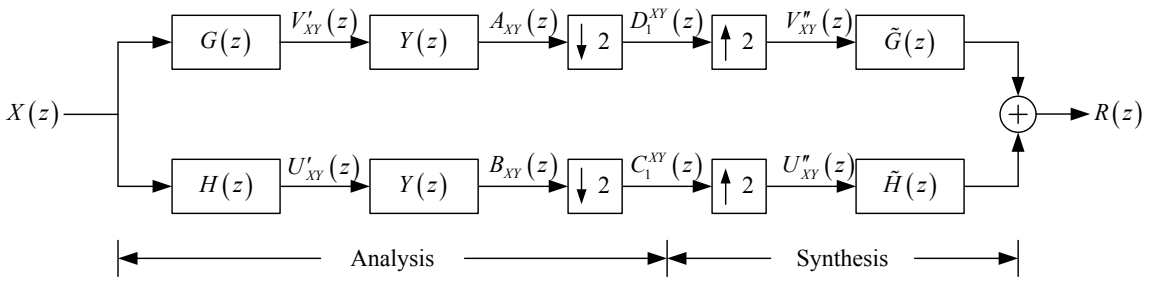

Fig. 6.1.1. DWT convolution of $X(z)$ and $Y(z)$.

Several variables have been shown in Fig. 6.1.1. Among these, $D_1^{XY}(z)$ and $C_1^{XY}(z)$ are the most important as they are the z-transforms of the detail and approximation coefficients, respectively, within the DWT convolution process. Specifically,

$$D_1^{XY}(z) = \sum_{n=0}^{L_{d1}} d_1(n) z^{-n} \text{ and} \tag{6.1.2}$$

$$C_1^{XY}(z) = \sum_{n=0}^{L_{c1}} c_1(n) z^{-n}, \tag{6.1.3}$$

where L_{d1} is the length of $\{d_1(n)\}$ and L_{c1} is the length of $\{c_1(n)\}$. The superscript XY is used to denote that the variables are a part of the DWT convolution of $X(z)$ and $Y(z)$.

In the synthesis filter bank in Fig. 6.1.1, the detail and approximation coefficients, $D_1^{XY}(z)$ and $C_1^{XY}(z)$, are upsampled by a factor of 2, which results in

$$V''_{XY}(z) = D_1^{XY}(z^2) \text{ and} \tag{6.1.4}$$

$$U''_{XY}(z) = C_1^{XY}(z^2). \tag{6.1.5}$$

These signals are then filtered by the synthesis filters and added together to produce the convolved result, i.e.,

$$R(z) = V''_{XY}(z)\tilde{G}(z) + U''_{XY}(z)\tilde{H}(z), \tag{6.1.6}$$

Using (6.1.5) $R(z)$ can be expressed in terms of the detail and approximation coefficients as

$$R(z) = D_1^{XY}(z^2)\tilde{G}(z) + C_1^{XY}(z^2)\tilde{H}(z). \tag{6.1.7}$$

Next, consider the case where $R(z)$ is, by itself, analyzed and then synthesized by a DWT/IDWT filter bank. This scenario is shown in Fig. 6.1.2, along with the intermediate signals in the z-domain.

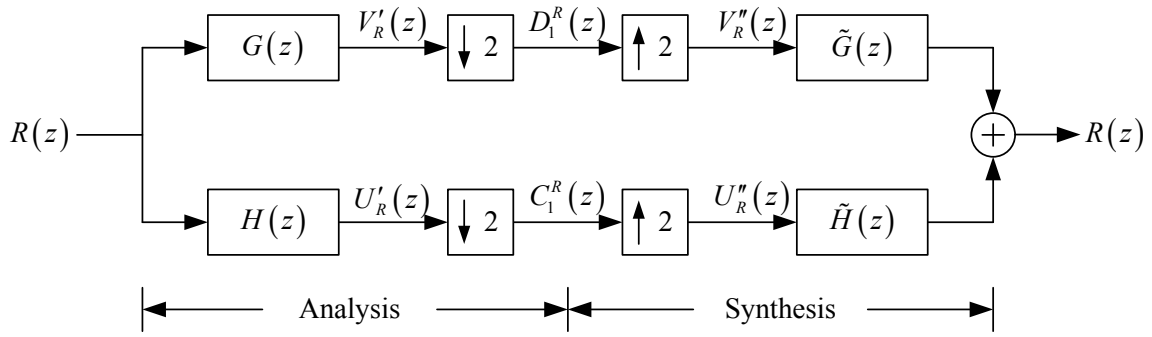

Fig. 6.1.2. DWT and IDWT of $R(z)$.

From the synthesis filter bank in Fig. 6.1.2, $R(z)$ can be expressed in terms of the detail and approximation coefficients, $D_1^R(z)$ and $C_1^R(z)$, as

$$R(z) = D_1^R(z^2)\tilde{G}(z) + C_1^R(z^2)\tilde{H}(z). \tag{6.1.8}$$

Equations (6.1.7) and (6.1.8) now provide two expressions for $R(z)$ in terms of the DWT coefficients. In the first expression, (6.1.7), the DWT coefficients that are used to synthesize $R(z)$ are a result of the DWT convolution of $X(z)$ and $Y(z)$. This case is depicted in Fig. 6.1.1. In the second expression, (6.1.8), the DWT coefficients from which $R(z)$ is synthesized are solely obtained from the DWT of $R(z)$ itself. This case is shown in Fig, 6.1.2.

Based on this observation, the results of the two equations, (6.1.7) and (6.1.8), are equal. Therefore, the coefficients of both equations can be directly compared, and it is seen that

$$D_1^{XY}\left(z^2\right) = D_1^{R}\left(z^2\right) \text{ and} \tag{6.1.9}$$

$$C_1^{XY}\left(z^2\right) = C_1^{R}\left(z^2\right), \tag{6.1.10}$$

which imply that

$$D_1^{XY}\left(z\right) = D_1^{R}\left(z\right) \text{ and} \tag{6.1.11}$$

$$C_1^{XY}\left(z\right) = C_1^{R}\left(z\right). \tag{6.1.12}$$

These two relationships, (6.1.11) and (6.1.12), are significant because they require that in order to synthesize $R(z)$ the DWT coefficients in both cases must be exactly equal.

Revisiting Fig. 6.1.1, the DWT coefficients can be expressed in terms of the intermediate signals just prior to the 2-fold decimation as

$$D_1^{XY}\left(z\right) = \frac{1}{2}\left[A_{XY}\left(z^{1/2}\right) + A_{XY}\left(-z^{1/2}\right)\right] \text{ and} \tag{6.1.13}$$

$$C_1^{XY}\left(z\right) = \frac{1}{2}\left[B_{XY}\left(z^{1/2}\right) + B_{XY}\left(-z^{1/2}\right)\right]. \tag{6.1.14}$$

Similarly, from Fig. 6.1.2, the DWT coefficients can be expressed as

$$D_1^{R}\left(z\right) = \frac{1}{2}\left[V_R'\left(z^{1/2}\right) + V_R'\left(-z^{1/2}\right)\right] \text{ and} \tag{6.1.15}$$

$$D_1^{XY}\left(z\right) = \frac{1}{2}\left[U_R'\left(z^{1/2}\right) + U_R'\left(-z^{1/2}\right)\right]. \tag{6.1.16}$$

Due to the equivalence of DWT detail and approximation coefficients for the 2 cases established in (6.1.11) and (6.1.12), respectively, it follows from (6.1.13)-(6.1.16) that

$$A_{XY}(z) = V'_R(z) \text{ and} \tag{6.1.17}$$

$$B_{XY}(z) = U'_R(z). \tag{6.1.18}$$

These two equations, (6.1.17) and (6.1.18), show that the outputs of the $Y(z)$ filters in the DWT convolution of $X(z)$ and $Y(z)$ are exactly equal to the outputs of the analysis filters in the independent DWT of the convolved signal $R(z)$.

Once again revisiting Fig. 6.1.1, which depicts the DWT convolution of $X(z)$ and $Y(z)$, it is seen that

$$A_{XY}(z) = V'_{XY}(z)Y(z) \text{ and} \tag{6.1.19}$$

$$B_{XY}(z) = U'_{XY}(z)Y(z). \tag{6.1.20}$$

Substituting (6.1.17) into (6.1.19) results in

$$V'_R(z) = V'_{XY}(z)Y(z) \tag{6.1.21}$$

and substituting (6.1.18) in (6.1.20) yields the relationship

$$U'_R(z) = U'_{XY}(z)Y(z). \tag{6.1.22}$$

Expressing $V'_{XY}(z)$ and $U'_{XY}(z)$ as inverses, these two equations can be rewritten as

$$Y(z) = V'^{-1}_{XY}(z)V'_R(z) \text{ and} \tag{6.1.23}$$

$$Y(z) = U'^{-1}_{XY}(z) U'_R(z). \tag{6.1.24}$$

The two equations, (6.1.23) and (6.1.24), provide the means for DWT-based deconvolution of $X(z)$ from $R(z)$ that can be used to obtain estimates of $Y(z)$. In (6.1.23), $Y(z)$ is obtained by deconvolving the DWT detail coefficients of the convolution of $X(z)$ and $Y(z)$ using the Forward Merge Approach from the detail coefficients of $R(z)$. Equation (6.1.24) provides a similar explicit expression of $Y(z)$ except for the fact that the deconvolution involves the approximation coefficients instead.

As with the four approaches to DWT convolution in Chapter 5, this DWT deconvolution procedure may be applied to as many levels of resolution as necessary by extension of the preceding theory. The result of the deconvolution at any level of resolution will be an estimate of $Y(z)$.

Notice that both (6.1.21) and (6.1.22) are expressions of convolution. In (6.1.21) $X(z)$ filtered by $G(z)$, i.e., $V'_{XY}(z)$, is convolved with $Y(z)$ to produce $V'_R(z)$, which is $R(z)$ also filtered by $G(z)$. Equation (6.1.22) expresses a similar procedure, except with the use of $H(z)$ instead of $G(z)$.

Equation (6.2.21) can be expressed in discrete time notation as

$$v'_r(n) = v'_{xy}(n)\, y(n). \tag{6.1.25}$$

Practically, this discrete time convolution can be computed with the use of a Toeplitz matrix formulation.

Matrices with elements that are constant along each diagonal are called Toeplitz matrices. Formally, **T** is a Toeplitz matrix if there exist scalars $p_{-n+1},\ldots,p_0,\ldots p_{n-1}$ such that [95]

$$a_{ij} = p_{j-i} \quad \forall i,j\,. \tag{6.1.26}$$

For example, a 4×4 Toeplitz matrix will have the form

$$\mathbf{T} = \begin{bmatrix} p_0 & p_1 & p_2 & p_3 \\ p_{-1} & p_0 & p_1 & p_2 \\ p_{-2} & p_{-1} & p_0 & p_1 \\ p_{-3} & p_{-2} & p_{-1} & p_0 \end{bmatrix}. \tag{6.1.27}$$

Suppose that $\left\{v'_{xy}(n)\right\}$ and $\left\{y(n)\right\}$ are composed of four elements each. The convolution operation in (6.1.25) for this case can be implemented as the familiar matrix equation

$$\mathbf{V}'_{\mathbf{xy}}\mathbf{y} = \mathbf{v}'_{\mathbf{r}} \tag{6.1.28}$$

where

$$\mathbf{V}'_{\mathbf{xy}} = \begin{bmatrix} v'_{xy}(0) & 0 & 0 & 0 \\ v'_{xy}(1) & v'_{xy}(0) & 0 & 0 \\ v'_{xy}(2) & v'_{xy}(1) & v'_{xy}(0) & 0 \\ v'_{xy}(3) & v'_{xy}(2) & v'_{xy}(1) & v'_{xy}(0) \\ 0 & v'_{xy}(3) & v'_{xy}(2) & v'_{xy}(1) \\ 0 & 0 & v'_{xy}(3) & v'_{xy}(2) \\ 0 & 0 & 0 & v'_{xy}(3) \end{bmatrix}, \tag{6.1.29}$$

$$\mathbf{y} = \begin{bmatrix} y(0) & y(1) & y(2) & y(3) \end{bmatrix}^{\mathrm{T}} \text{ and} \tag{6.1.30}$$

$$\mathbf{v}'_{\mathbf{r}} = \begin{bmatrix} v'_r(0) & v'_r(1) & v'_r(2) & v'_r(3) & v'_r(4) & v'_r(5) & v'_r(6) \end{bmatrix}^{\mathrm{T}}. \tag{6.1.31}$$

It is immediately seen that (6.1.28) is an overdetermined equation and can be reduced by selecting a suitable square sub-matrix of $\mathbf{V}'_{\mathbf{xy}}$. The vector $\mathbf{v}'_{\mathbf{r}}$ must also be truncated correspondingly. An example of this step is

$$\begin{bmatrix} v'_{xy}(0) & 0 & 0 & 0 \\ v'_{xy}(1) & v'_{xy}(0) & 0 & 0 \\ v'_{xy}(2) & v'_{xy}(1) & v'_{xy}(0) & 0 \\ v'_{xy}(3) & v'_{xy}(2) & v'_{xy}(1) & v'_{xy}(0) \end{bmatrix} \begin{bmatrix} y(0) \\ y(1) \\ y(2) \\ y(3) \end{bmatrix} = \begin{bmatrix} v'_{r}(0) \\ v'_{r}(1) \\ v'_{r}(2) \\ v'_{r}(3) \end{bmatrix}. \tag{6.1.32}$$

The matrix in (6.1.32) is in lower triangular form and the unknown values of **y** can be readily found by forward substitution. It should be noted that in (6.1.32) the leading transient elements of $\mathbf{v}'_{\mathbf{r}}$ are selected, which is the reason why the lower triangular square sub-matrix of $\mathbf{V}'_{\mathbf{xy}}$ is obtained.

Generally, however, the elements of the central portion of $\mathbf{v}'_{\mathbf{r}}$ could be considered and a square sub-matrix of $\mathbf{V}'_{\mathbf{xy}}$ that is not in lower triangular form would result. Solving for the unknown **y** in these cases can be accomplished with the use of an efficient procedure such as the Levinson-Durbin algorithm for solving Toeplitz matrices. Appendix A contains the Levinson-Durbin algorithm for the case of non-Hermitian Toeplitz matrices, an example of which is in (6.1.32). The computational complexity of the algorithm is on the order of $O\left(n^2\right)$ [95].

For the purposes of this dissertation, i.e., to simply verify that DWT-based deconvolution is possible, it is, however, sufficient to use the Least Squares Inversion (LSI) routine built into MATLAB [96].

Computational Complexity

As described in this section, DWT-based deconvolution minimally requires two partial DWT analyses, with each DWT analysis in a single subband. Specifically, two functions are required for the deconvolution:

1. The signal $V'_{XY}(z)$, which is the output of the high-pass analysis filter, $G(z)$, when excited by the known signal $X(z)$.
2. The signal $V'_{R}(z)$, which is the output of the high-pass analysis filter, $G(z)$, when excited by the known signal $R(z)$

The signal $V'_{XY}(z)$ is to be deconvolved from $V'_{R}(z)$ to provide the unknown $Y(z)$.

In order to evaluate the computational complexity involved in this operation, first let the length of the filter $G(z)$ be L. Next, let the length of the signal $X(z)$ be N_X, and the length of the signal $R(z)$ be N_R. Hence, the length of $V'_{XY}(z)$ is $N_X + L - 1$, and the length of $V'_{R}(z)$ is $N_R + L - 1$. Making the assumption that the input signal $X(z)$ is much longer than the filter $G(z)$, i.e., $N_X \gg L$, the length of $V'_{XY}(z)$ can be approximated to is N_X, and the length of $V'_{R}(z)$ to N_R.

Now, the DWT-based deconvolution operation to obtain an estimate of $Y(z)$ has been shown in (6.1.23) to be

$$Y(z) = V'^{-1}_{XY}(z) V'_R(z)$$

while standard z-domain deconvolution of $X(z)$ from $R(z)$ is

$$Y(z) = X^{-1}(z) R(z). \tag{6.1.33}$$

Comparing the DWT-based deconvolution in (6.1.23) and standard z-domain, or discrete-time domain, deconvolution in (6.1.33), it is seen that the lengths of the respective functions involved are approximately the same. Specifically,

length of $V'_{XY}(z)$ = length of $X(z)$ = N_X

and

length of $V'_R(z)$ = length of $R(z)$ = N_R.

Therefore, the computational complexity of DWT-based deconvolution is almost equal to the complexity of standard deconvolution. The exact order of complexity depends on the specific deconvolution technique used in both cases. If a technique such as LU decomposition is used the order of complexity is $O(N_X^3)$, while a technique such as the Levinsion-Durbin algorithm possesses complexity on the order of $O(N_X^2)$.

6.2 Setup and Design of Computer Simulation Experiments

In order to test the theory of DWT deconvolution that has been established in Section 6.1 by way of computer simulation experiments there are two critical factors that have to be addressed. The first is the generation of impulse responses of channels. The second is the generation of test signals.

For implementation in a simulation environment, such as MATLAB, the impulse response of a communications channel is necessary. As mentioned in Chapter 2, channels are not, however, typically characterized by a time-domain impulse response in either analytical or empirical models as well as in measurements. Instead, the power delay profile of a channel is established, either as an analytical model or empirically by channel sounding measurements.

The procedure of generating an impulse response of a channel from a PDP is described in Section 6.2.1. The test signals that will be used in all simulations are defined analytically in Section 6.2.2.

6.2.1 Generation of Channels for Computer Experiments

The channel impulse response at any discrete-time instant nT can be described by its In-phase (I) and Quadrature (Q) components as

$$c(n) = c_I(n) + jc_Q(n). \tag{6.2.1.1}$$

The PDP of the channel is denoted by $p(n)$. The channel impulse response, $c(n)$, is a complex zero-mean Gaussian random process with variance $p(n)$. Therefore, $c_I(n)$ and $c_Q(n)$ are uncorrelated Gaussian random processes as well [97].

Now, according to the Bienaymé equality, the variance of the sum of uncorrelated random variables is the sum of the variances of each random variable, i.e.,

$$\operatorname{var}\left(\sum_{i=1}^{n} X_i\right) = \sum_{i=1}^{n} \operatorname{var}(X_i). \tag{6.2.1.2}$$

Hence, the variance of each component of the channel impulse response, i.e., of $c_I(n)$ and of $c_Q(n)$, is $p(n)/2$.

Next, a Gaussian random vector, **c**, of length 2*N* can be composed of the I and Q components of $c(n)$ for various values of n, i.e.,

$$\mathbf{c} = \left\{c_I(n_1), c_Q(n_1), c_I(n_2), c_Q(n_2), \ldots, c_I(n_N), c_Q(n_N)\right\}. \tag{6.2.1.3}$$

Now, the covariance of two real-valued processes, X and Y, is

$$\operatorname{cov}(X,Y) = E\left[\left(X - E(X)\right)\left(Y - E(Y)\right)\right]. \tag{6.2.1.4}$$

$$\Rightarrow \operatorname{cov}(X,X) = \operatorname{var}(X). \tag{6.2.5}$$

Hence, by applying (6.2.1.5) to (6.2.1.3), the covariance matrix of **c** is given by

$$\mathbf{M} = \begin{bmatrix} \frac{p(n_1)}{2} & & & & \\ & \frac{p(n_1)}{2} & & 0 & \\ & & \ddots & & \\ & 0 & & \frac{p(n_N)}{2} & \\ & & & & \frac{p(n_N)}{2} \end{bmatrix}. \tag{6.2.1.6}$$

In a computer simulation environment the vector **c** can now be generated from a Gaussian distribution that satisfies the covariance matrix **M**. In this manner all of the N I and Q components of the channel impulse response may be generated. A test signal is then convolved with the channel impulse response to emulate the physical process of transmission, and the real part of the convolved result is taken to be the received signal.

It should be noted that for a particular PDP, every time this procedure is run the actual channel impulse response that is generated will be different. This is due to the generation of pseudo-random numbers taken from a Gaussian distribution. A single PDP may, therefore, be common to a very large number of channel impulse response realizations. This fact is easily seen if the channel is considered to be a continuous time function, $c(t)$. By definition,

$$\left\langle c^*(t)c(t')\right\rangle = p(t)\delta(t-t') \tag{6.2.1.7}$$

where $\langle\ \rangle$ denotes an ensemble average, and

$$p(t) = \left\langle \left|c(t)\right|^2 \right\rangle. \tag{6.2.1.8}$$

6.2.2 Test Signals

The test signals that are used in all simulation experiments are composed of superimposed sinusoids. Each test signal is the sum of a specific number of odd harmonics of a fundamental sinusoidal component. The general form of the signal sequence is described in discrete time as

$$s(n) = \sum_{k=1}^{K} A_k \cos\left[(2k-1)2\pi f_0 n T_s + \phi_k\right] \tag{6.2.2.1}$$

where

$s(n)$ is the n^{th} element of the test signal sequence,

K is the number of sinusoidal harmonic components in the test signal,

A_k is the amplitude of the k^{th} harmonic component,

f_0 is the frequency of the fundamental harmonic,

T_s is the sampling rate, and

ϕ_k is the additional phase offset for the k^{th} harmonic.

The values of the amplitude and the phase of each harmonic component, A_k and ϕ_k, respectively, are obtained from uniform distributions of each parameter. The values of the amplitudes are limited to the numerical range 0 to 10, while the phase offsets range from 0 to 2π radians. The frequency of the fundamental harmonic, f_0, is fixed at a nominal value of 2 Hz, and the number of odd harmonics, K, is chosen to be 7.

6.2.3 Procedure of Experiments

The procedure for DWT-based deconvolution theorized in Section 6.1 is examined via simulation experiments for the following scenarios:

1. Five channel PDP models;
2. Two cases of fading per channel;
3. Addition of white Gaussian noise to every received signal.

In each experiment a test signal is convolved with a channel impulse response, which creates the received signal. WGN is then added to the received signal. The noisy received test signal is then transformed using the DWT without decimation. The resulting DWT coefficients are then used for DWT-based deconvolution as described in Section 6.1.

The noise that is added to all transmitted signals is Additive White Gaussian Noise (AWGN) with a double-sided Power Spectral Density (PSD) of $N_0/2$. The metric of E_b/N_0 is used throughout this work to provide a relative measure of the energy contained in every "bit" that is transmitted, E_b, to the power of the noise that is added to the signal.

Each received signal is analyzed to four levels of resolution, which gives five estimates of $\phi_c(n)$, i.e., $\hat{\phi}_c(n)$. Four of these estimates are obtained from the detail coefficients at

each of the four levels of resolution and the fifth estimate from the approximation coefficients at the fourth level of resolution.

The Haar wavelet is used in all simulations. For the first channel, viz., the channel defined by a Gaussian PDP in Section 6.3.1, 3 additional wavelets are used for the purposes of comparisons. These are the Daubechies2 (db2), Daubechies3 (db3) and Daubechies 4 (db4) wavelets.

In every simulation experiment the Mean-Squared Error (MSE) between the actual channel impulse response and each estimate is computed. For each channel scenario a total of 1,001 test signals are transmitted for each value of E_b/N_0. An average of the resulting ensemble of 1,001 MSEs for each value of E_b/N_0 is then computed. The results are illustrated graphically in Figs. 6.3.2 - 6.3.9.

6.3 Simulation Experiments and Results

Five different channel PDP models are considered:

1. Gaussian PDP
2. Exponential PDP
3. Equal Amplitude Two-Ray PDP
4. Unequal Amplitude Three-Ray PDP
5. Hilly Area PDP

Two fading scenarios are considered for each channel profile. The first is a case of fast fading, which is implemented by selecting the normalized delay time of the channel, *d*, to be 0.2. The second case is of a slow fading channel, in which case a normalized delay time of $d = 0.2$ is used.

Consider, for the sake of illustration, a channel with a Gaussian PDP, which is defined as

$$\phi_c(t) = \frac{1}{\sqrt{2\pi\tau}} e^{\frac{(t/\tau)^2}{2}} . \tag{6.3.1}$$

In (6.3.1) the quantity τ denotes the Root-Mean-Squared (RMS) delay spread, and is defined by

$$\tau = dT_{sym} , \tag{6.3.2}$$

where T_{sym} is the period of the baseband digital symbols on which the transmitted signals are based. In all experiments the baseband symbol period, T_{sym}, is set as 1 s.

Before proceeding further it must be noted that the channel PDPs, and, therefore, the channel impulse responses require the definition of a baseband symbol period, T_{sym}. For this reason the test signals that are used are several units of $s(n)$, defined in (6.2.10), concatenated one after the previous. Each unit may be considered to be a "baseband symbol."

The control experiment is a direct deconvolution of a copy of the uncorrupted test signal from the noisy received signal in the discrete time-domain. Such deconvolution generates an estimate of the channel impulse response. The normalized MSE of the

estimate so obtained and a copy of the channel impulse response is then computed. This process is repeated 1,001 times for each value of E_b/N_0 and an ensemble average of the 1,001 MSEs for each value of E_b/N_0 is then computed. These ensemble-averaged MSEs are then compared with the corresponding MSEs obtained from the DWT deconvolution.

6.3.1 Channel 1: Gaussian Power Delay Profile

The Gaussian PDP used as a model for channel 1 was defined previously in (6.3.1) as

$$\phi_c(t) = \frac{1}{\sqrt{2\pi\tau}} e^{\frac{(t/\tau)^2}{2}}.$$

The duration of $\phi_c(t)$ is fixed as 5 s for all simulations using this Gaussian channel. The baseband symbol period for the test signal is 1 s, and the test signal is composed of 10 symbols. Each symbol is represented by a sinusoidal signal defined by (6.2.10). Furthermore, each symbol period is sampled at a rate of 10 samples/symbol. Due to this condition the test signal is composed of 100 numerical sample values, and the channel impulse response is composed of 50 sample values.

Two PDPs defined by (6.3.1) are shown in Fig. 6.3.1. In Fig. 6.3.1a the case of a slow fading channel, with $d = 2.5$, is illustrated while the case of a fast fading channel, with $d = 0.2$, is shown in Fig. 6.3.1b.

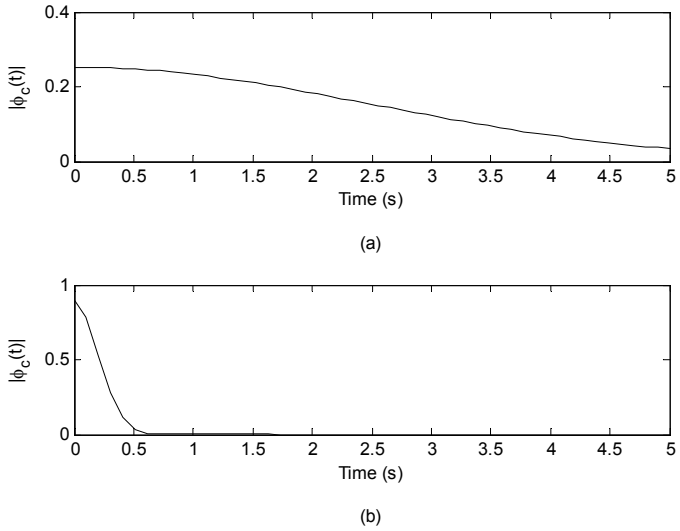

Fig. 6.3.1. Gaussian PDP for the (a) slow fading case of $d = 2.5$; (b) fast fading case of $d = 0.2$.

In Fig. 6.3.2, the results from the case of a slow fading channel are shown. DWT analysis is carried out with the Haar wavelet to four levels of resolution. The MSEs between the five DWT-based estimates and the actual channel impulse response are plotted using the various colored lines, and datum markers. The phrase "Level 1 Detail" in the legend in Fig. 6.3.2 indicates the MSEs between the estimate of the channel impulse response obtained from the detail coefficients at the 1st level of resolution and the actual channel impulse response. The other captions in the legend can be interpreted in a similar manner.

The MSE of the control experiment is plotted as a solid black line, with the data marked by asterisks. The phrase "time-domain" is used in the legend to indicate the control data

obtained by deconvolving the received signal from a copy of the uncorrupted transmitted signal directly in the discrete time-domain.

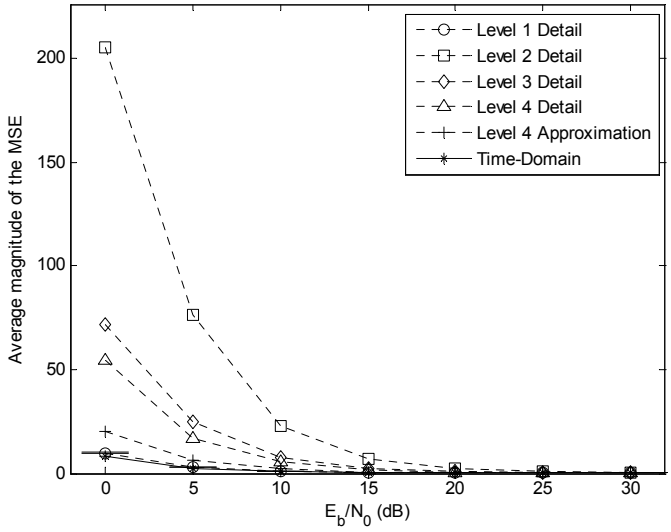

Fig. 6.3.2. Normalized ensemble-averaged MSEs between the actual channel impulse response and the estimates using the Haar wavelet (for $d = 2.5$).

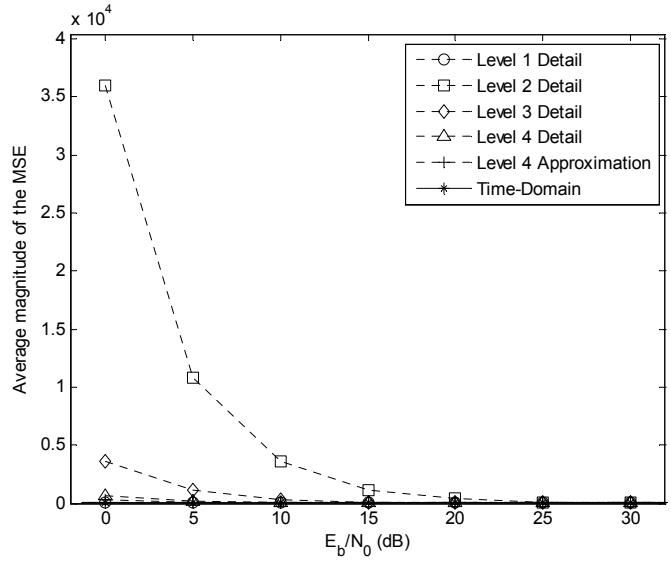

Fig. 6.3.3. Normalized ensemble-averaged MSEs between the actual channel impulse response and the estimates using the Daubechies2 wavelet (for $d = 2.5$).

The 95% confidence intervals for the MSE data of the level 1 Detail estimates are also shown. A 95% confidence interval [99] for a mean value, μ, is an interval $\mu - k \le \mu \le \mu + k$ that contains μ with a probability of 0.95.

The second set of simulations involved the use of the Daubechies2 wavelet instead of the Haar. The normalized MSEs that resulted from this experiment are plotted in Fig. 6.3.3. By comparing Figs 6.3.2 and 6.3.3 it is seen that the estimation errors in the latter plot (using the Daubechies2 wavelet) are significantly greater that the errors in the former plot, in which case the Haar wavelet was used.

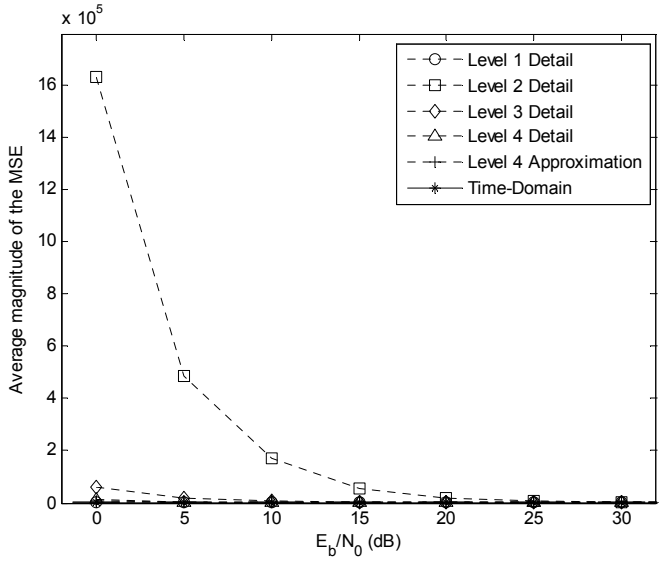

Fig. 6.3.4. Normalized ensemble-averaged MSEs between the actual channel impulse response and the estimates using the Daubechies3 wavelet (for $d = 2.5$).

The Monte Carlo simulation experiment for the slowly fading case of $d = 2.5$ was repeated a third time, but in this iteration the Daubechies3 wavelet was used. Following

the trend seen from the cases of the Haar and the Daubechies2 wavelets, in Figs. 6.3.2 and 6.3.3, the estimation errors increase even more.

The last experiment for the Gaussian channel with $d = 2.5$ involves the use of the Daubechies4 wavelet. Once again the estimation errors at every level of resolution increased as the values of E_b/N_0 increased. The estimation errors are also seen in Fig,. 6.3.5 to be collectively greater in the case of the Daubechies4 wavelets, than when the previous three wavelets were used.

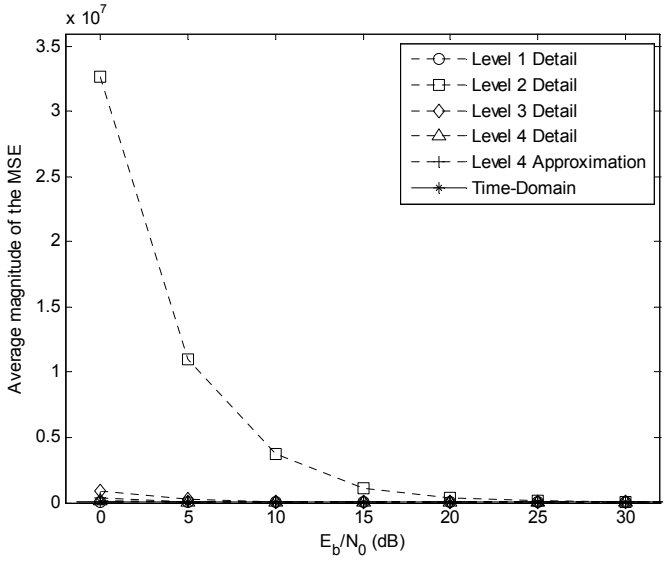

Fig. 6.3.5. Normalized ensemble-averaged MSEs between the actual channel impulse response and the estimates using the Daubechies4 wavelet (for $d = 2.5$).

The second set of simulation experiments for estimating the Gaussian channel were based on the channel having a normalized delay time, *d*, of 0.2. This condition results in a fast fading channel for the test signals previously defined. As with the case of the slow

fading channel, with $d = 2.5$, the same four wavelets are used in succession so as to compare the performance of DWT-based deconvolution for the different wavelets.

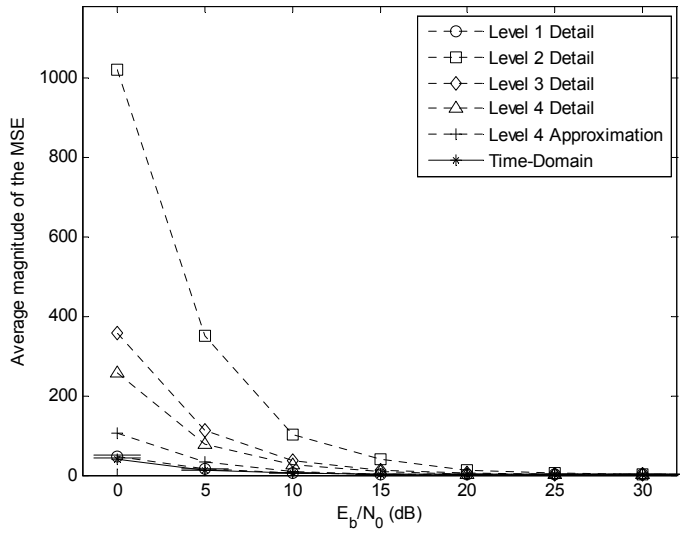

Fig. 6.3.6. Normalized ensemble-averaged MSEs between the actual channel impulse response and the estimates using the Haar wavelet (for $d = 0.2$).

The results of the simulations that used the Haar wavelet are plotted in Fig. 6.3.6. As expected, the MSEs of the estimates increase as the power of the noise added increases. A comparison of results is now in order. In Figs. 6.3.1 and 6.3.6 the errors in estimating the Gaussian channel with the use of the Haar wavelet are presented. The results in Fig. 6.3.1, however, are for the slowly fading Gaussian channel while the results in Fig. 6.3.6 are for the fast fading Gaussian channel. It is seen from the two figures that the estimation errors at all levels of resolution are greater in the case of the fast fading channel than in the case of the slow fading channel.

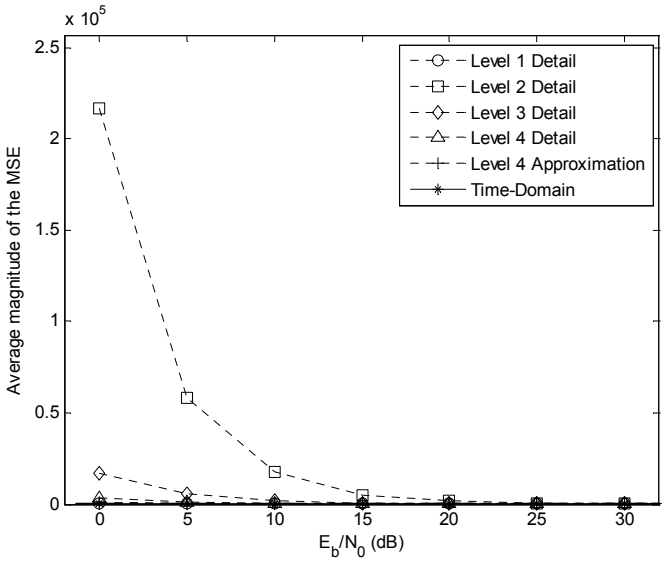

Fig. 6.3.7. Normalized ensemble-averaged MSEs between the actual channel impulse response and the estimates using the Daubechies2 wavelet (for $d = 0.2$).

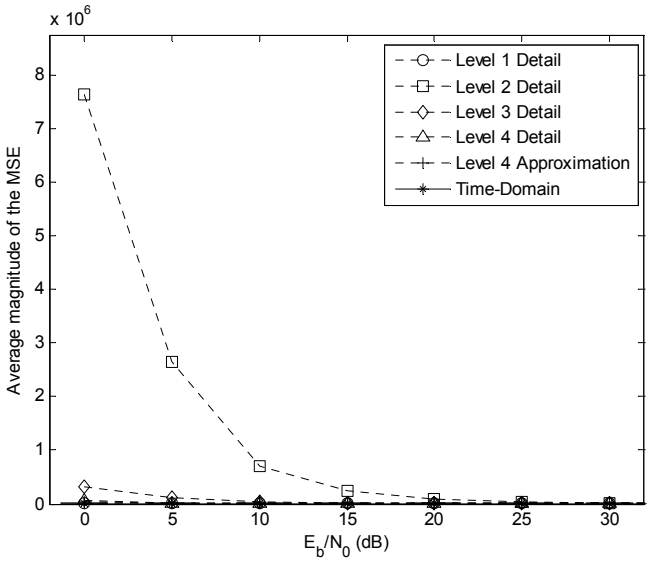

Fig. 6.3.8. Normalized ensemble-averaged MSEs between the actual channel impulse response and the estimates using the Daubechies3 wavelet (for $d = 0.2$).

In Figs. 6.3.7 and 6.3.8 the estimation errors that resulted from the use of the Daubechies2 and Daubechies3 wavelets, respectively, are plotted. In both cases it is seen that the errors in estimating the channel from the detail coefficients at level 2 are significantly larger than the errors in the channel estimates obtained from any other level of resolution.

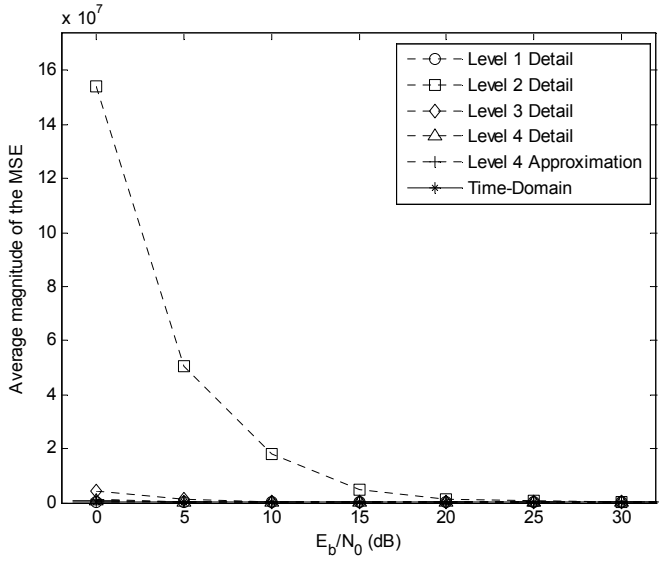

Fig. 6.3.9. Normalized ensemble-averaged MSEs between the actual channel impulse response and the estimates using the Daubechies4 wavelet (for $d = 0.2$).

The final simulation experiment involving the Gaussian channel made use of the Daubechies4 wavelet. The estimation errors from this case are shown in Fig. 6.3.9. The results follow the trends that are readily apparent in Figs. 6.3.2-6.3.8.

6.3.2 Channel 2: Exponential Power Delay Profile

The second channel considered in this dissertation has the functional form of an exponential decay. The PDP is defined as

$$\phi_c(t) = \begin{cases} \frac{1}{\tau} e^{-t/\tau}, & t \geq 0 \\ 0, & \text{otherwise} \end{cases} . \tag{6.3.2}$$

As with the Gaussian PDP in (6.3.1), this channel model is also a one-sided, strictly causal, function.

The duration of the channel impulse response was fixed at 5 s. The numerical values of the impulse response were generated at a rate of 10 samples/s, which resulted in the length of the discretized impulse response being 50 samples.

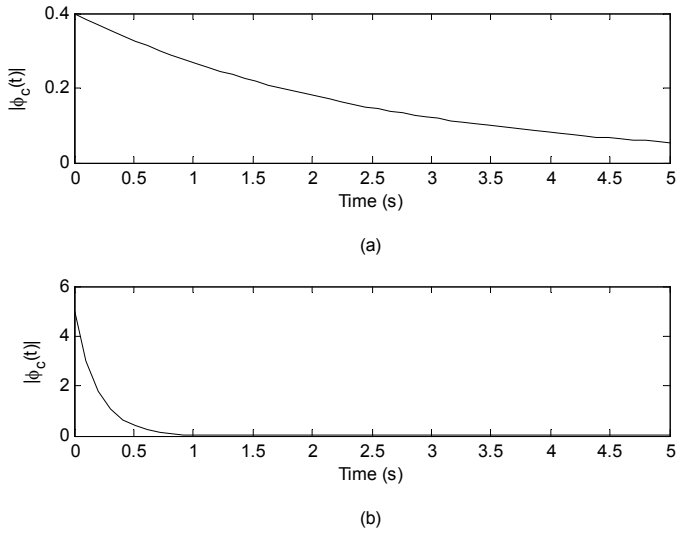

Fig. 6.3.10. Exponential PDP for the (a) slow fading case of $d = 2.5$; (b) fast fading case of $d = 0.2$.

For this channel two cases of fading are considered: slow fading with $d = 2.5$, and fast fading with $d = 0.2$. Plots of the channel impulse response for these two conditions are shown in Fig. 6.3.10 (a) and (b), respectively.

For both cases of fading the channel estimates are obtained at four levels of resolution with the use of the Haar wavelet. Unlike in Section 6.3.1, no other wavelets are used for this channel.

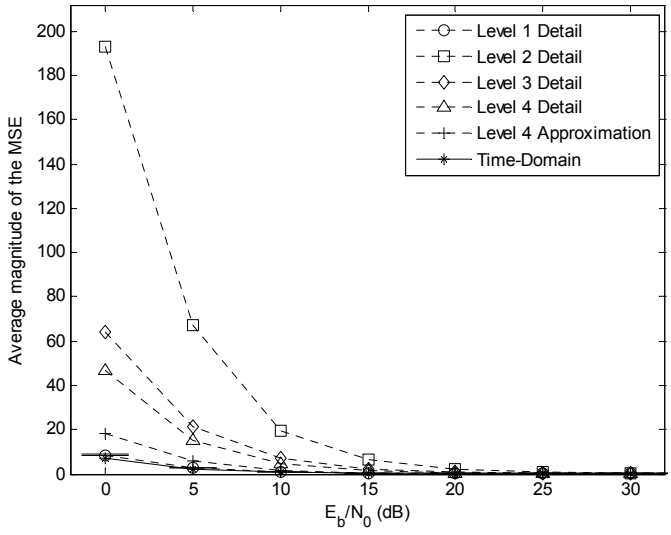

Fig. 6.3.11. Normalized ensemble-averaged MSEs between the actual channel impulse response and the estimates using the Haar wavelet (for $d = 2.5$).

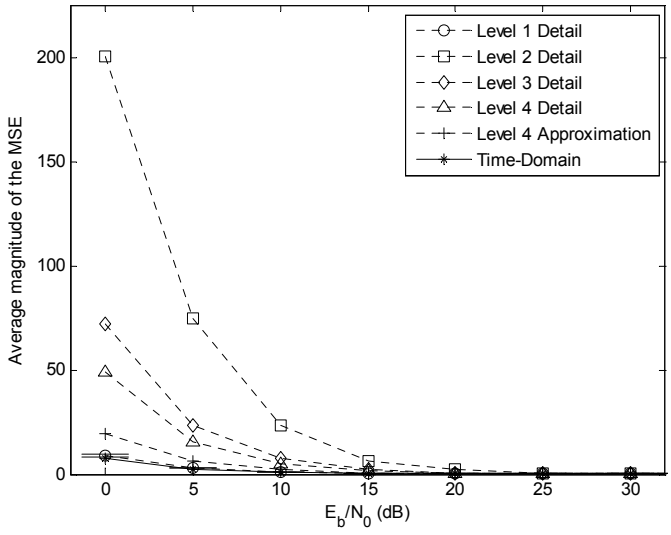

Fig. 6.3.12. Normalized ensemble-averaged MSEs between the actual channel impulse response and the estimates using the Haar wavelet (for $d = 0.2$).

As expected the errors in the channel estimates at each level of resolution increase with the addition of increasing amounts of noise to the received signals in both cases of fading. It is also seen from Figs. 6.3.11 and 6.3.12 that the estimation error is generally larger for the case of the fast fading channel than for the slow fading channel. It is also seen, however, that the differences in the MSEs at corresponding levels in the two plots are only slightly different. This latter observation is subjective but can be placed into context by comparisons with Figs. 6.3.2 and 6.3.6, in which the estimation errors of the Gaussian channels for the same two cases of fading are shown.

6.3.3 Channel 3: Equal Amplitude Two-Ray Power Delay Profile

Although practically unrealizable, a channel impulse response consisting of impulses is an interesting case to consider theoretically. The third channel considered is, therefore, a simple model of a double echo. Each echo of a transmitted test signal is facilitated analytically and numerically, with the use of delta functions. The particular channel PDP that is used in this set of experiments is composed of two equal-amplitude impulses, and is defined by

$$p(t) = \frac{1}{2}\left[\delta(t-\tau) + \delta(t-2\tau)\right]. \tag{6.3.3}$$

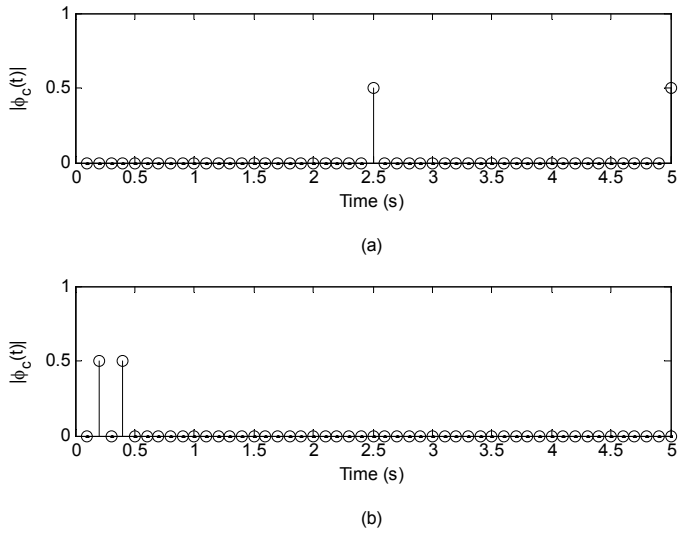

Fig. 6.3.13. Equal amplitude two-ray PDP for the (a) slow fading case of $d = 2.5$; (b) fast fading case of $d = 0.2$.

It should be noted that in (6.3.3) the PDP is defined as a continuous time function, and, therefore, Dirac delta functions are used. Equivalently, however, in a discrete-time implementation Kronecker delta functions are used.

The equal-amplitude two-ray PDPs for the cases of slow and fast fading, with $d = 2.5$ and $d = 0.2$, respectively, are shown in Fig. 6.3.13. Each channel is set to be 5 s in duration, and evaluated numerically at a rate of 10 samples/s. The test signals are the same as in Sections 6.3.1 and 6.3.2.

The errors in estimating the channel from the DWT coefficients at four levels of resolution, using the Haar wavelet, are shown graphically in Figs. 6.3.14 and 6.2.15. Although the results display general trends of increasing error magnitudes with increasingly powerful AWGN, it is immediately seen that the estimation errors for this channel are larger than for the Gaussian or the exponential channels in Sections 6.3.1 and 6.3.2, respectively.

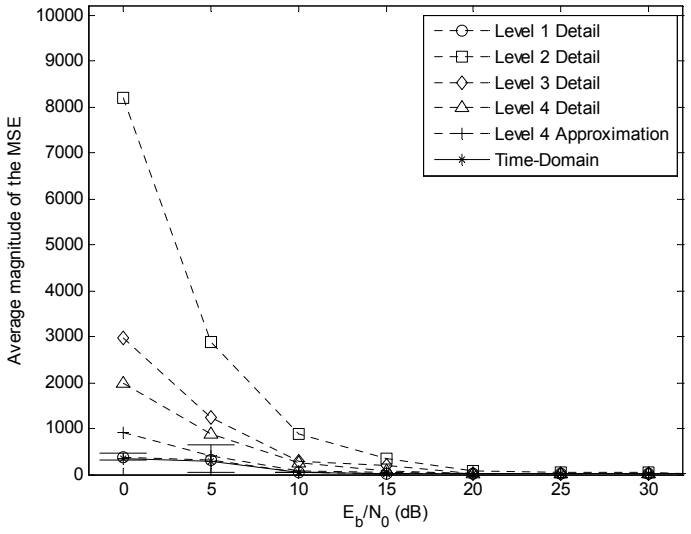

Fig. 6.3.14. Normalized ensemble-averaged MSEs between the actual channel impulse response and the estimates using the Haar wavelet (for $d = 2.5$).

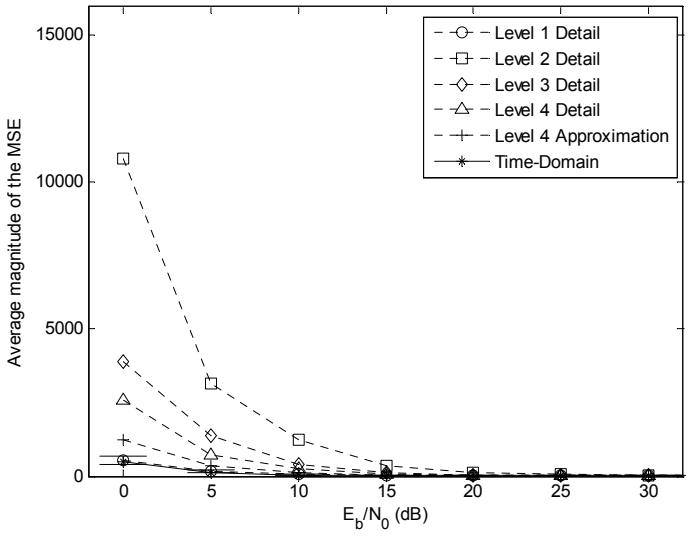

Fig. 6.3.15. Normalized ensemble-averaged MSEs between the actual channel impulse response and the estimates using the Haar wavelet (for $d = 0.2$).

6.3.4 Channel 4: Unequal Amplitude Three-Ray Power Delay Profile

In keeping with the concept of echo delays, a second channel PDP is considered. This channel, however, results in three echoes of the transmitted test signal. By design, the amplitudes of the delta functions in this channel model are unequal.

The PDP of this unequal-amplitude three-ray channel is defined in continuous-time as

$$\phi_c(t) = 0.8\delta(0) + 0.2\delta(t-\tau) + 0.5\delta(t-2\tau). \tag{6.3.4}$$

Once again, the cases of slow and fast fading, with $d = 2.5$ and $d = 0.2$, respectively, are considered. The PDP of the channel for each of these cases is illustrated graphically in Fig. 6.3.16.

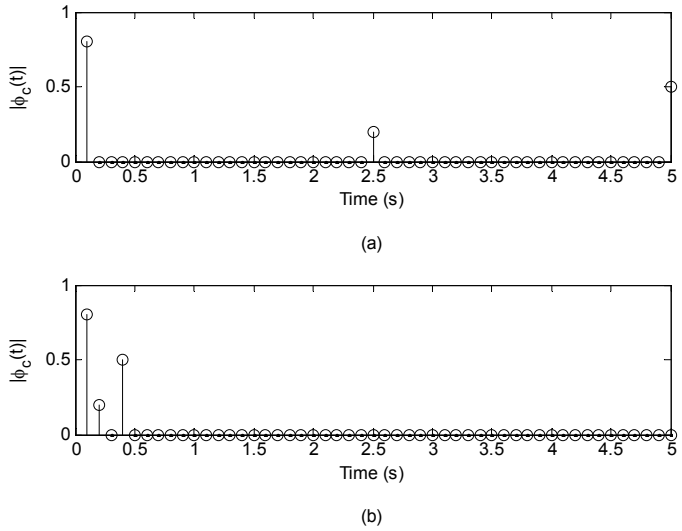

Fig. 6.3.16. Unequal amplitude three-ray PDP for the (a) slow fading case of $d = 2.5$; (b) fast fading case of $d = 0.2$.

As seen in Fig. 6.3.16, the duration of the channel PDP, and, therefore, impulse response is 5 s, and is numerically evaluated at a rate of 10 samples/s. The discrete-time sequence representing the channel impulse response is, therefore, 50 samples in length.

The estimation errors for both cases of fading are shown graphically in Figs. 6.3.17 and 6.3.18. As with the previous three channels, the errors in estimating this channel increase rapidly as the power of the WGN increases.

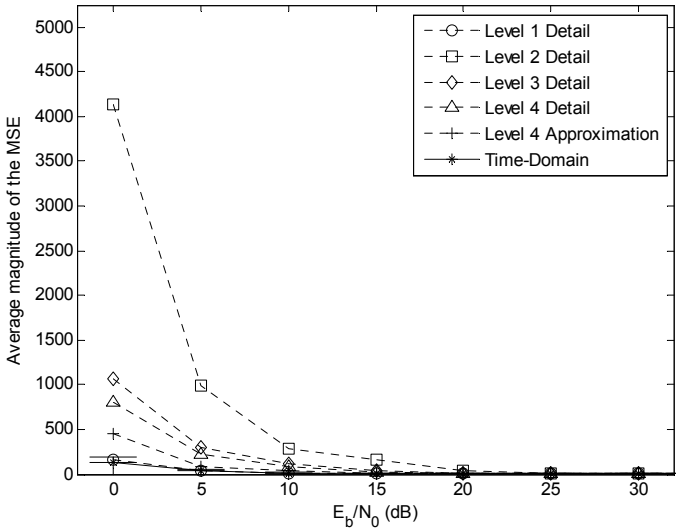

Fig. 6.3.17. Normalized ensemble-averaged MSEs between the actual channel impulse response and the estimates using the Haar wavelet (for $d = 2.5$).

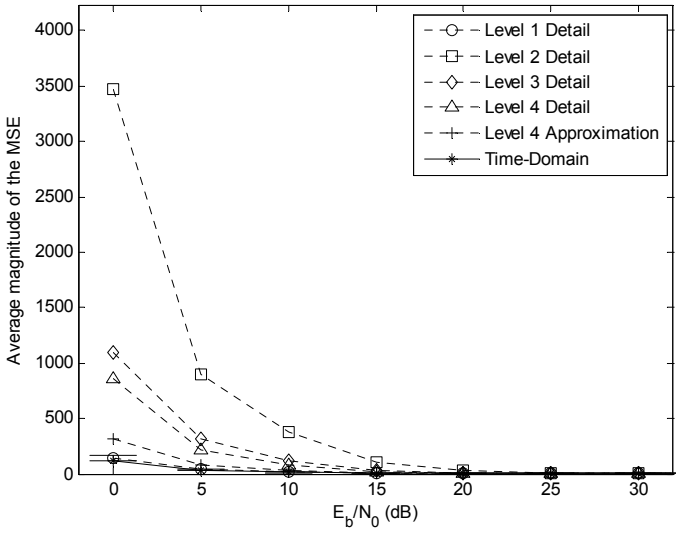

Fig. 6.3.18. Normalized ensemble-averaged MSEs between the actual channel impulse response and the estimates using the Haar wavelet (for $d = 0.2$).

6.3.5 Channel 5: Hilly Area Power Delay Profile

The final channel model that is considered is based on the exponent function. Under a program called European Cooperation in Science and Technology (COST), several multipath channel models have been developed. The particular sub-program of interest in this dissertation is the COST Action 207. Of interest here are the channel PDP models for signal transmission in hilly areas.

Specifically, the COST 207 reference PDP model for a hilly urban area is

$$\phi_c(t) = \begin{cases} e^{-t/1\text{ ms}}, & 0 \le t < 5\text{ ms} \\ 0.5e^{-(5\text{ ms}-t)/1\text{ ms}}, & 5\text{ ms} \le t < 10\text{ ms}, \end{cases} \tag{6.3.5}$$

and the PDP for a hilly rural area is

$$\phi_c(t) = \begin{cases} e^{-3.5\text{ ms}\,t/1\text{ ms}}, & 0 \le t < 2\text{ ms} \\ 0.1e^{-(15\text{ ms}-t)/1\text{ ms}}, & 15\text{ ms} \le t < 20\text{ ms}. \end{cases} \tag{6.3.6}$$

The two models in (6.3.5) and (6.3.6) cannot, however, be used in conjunction with test signals of any arbitrary fundamental frequency since the durations of the PDPs are defined in milliseconds. Furthermore, the RMS delay spread parameter, τ, is also absent from these models.

Therefore, a new model having a functional form similar to the COST 207 PDPs in (6.3.5) and (6.3.6) is defined as

$$\phi_c(t) = \begin{cases} e^{-10t/\tau}, & 0 \le t < 0.5\tau \\ 0.5e^{-5(0.5\tau-t)/\tau}, & 0.5\tau \le t < \tau \end{cases}, \tag{6.3.7}$$

which may be with any test signal. Since this PDP is based in the two "hilly area" PDPs from COST 207, it is referred to as a Hilly Area PDP in this work.

As seen in Fig. 6.3.19, the duration of this channel was fixed at 2 s, and (6.3.7) was evaluated at a rate of 16 samples/s. The previous four channels, however, were each 5 s in duration and evaluated at a rate of 10 samples/s. This change in parameters was required in order to generate meaningful hilly area channel PDPs and impulse responses for the cases of $d = 2.5$ and $d = 0.2$.

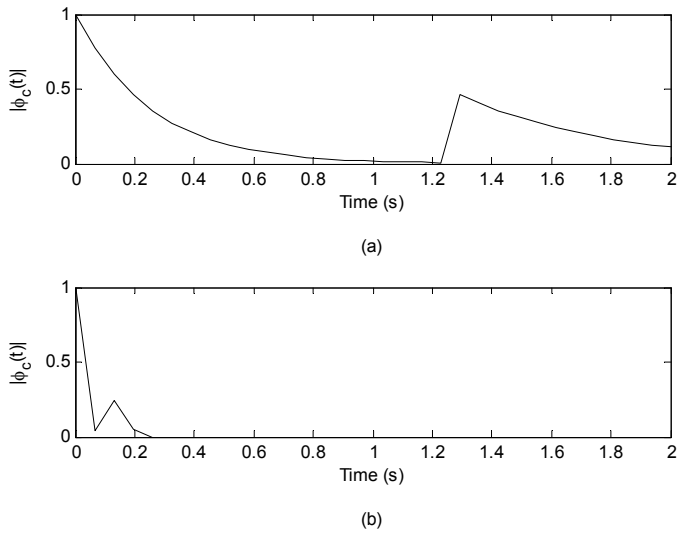

Fig. 6.3.19. Hilly area PDP for the (a) slow fading case of $d = 2.5$; (b) fast fading case of $d = 0.2$.

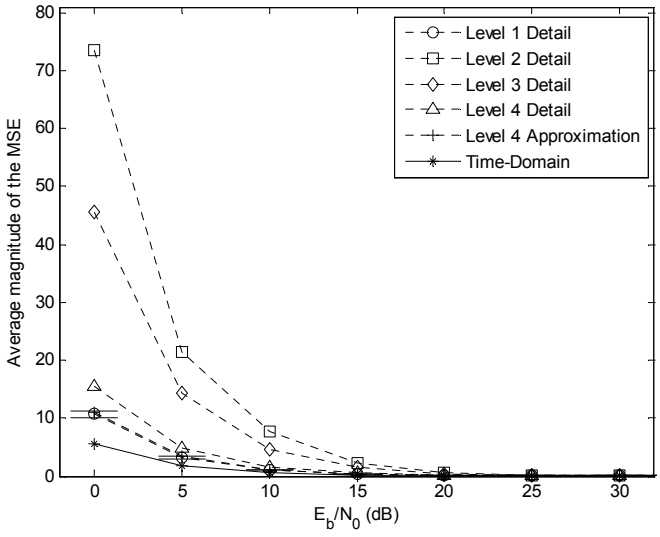

Fig. 6.3.20. Normalized ensemble-averaged MSEs between the actual channel impulse response and the estimates using the Haar wavelet (for $d = 2.5$).

The noisy received signals were analyzed to four levels of resolution using the Haar wavelet. The MSEs of the channel estimates at each level for both fading conditions are provided in Figs. 6.3.20 and 6.3.21.

Although the MSE curves in Fig. 6.3.20 appear similar to all other MSE plots in this chapter, there is one striking difference: the magnitudes of the estimation errors at all four levels are much smaller that the corresponding MSEs in all of the other graphs. The reasons for this anomaly may be two-fold. First, when using this channel there are fewer samples of the received signal than when the previous 4 channels were used. Second, this channel does not consist of long durations with zero amplitude. These two reasons will be examined in detail in Section 6.4.

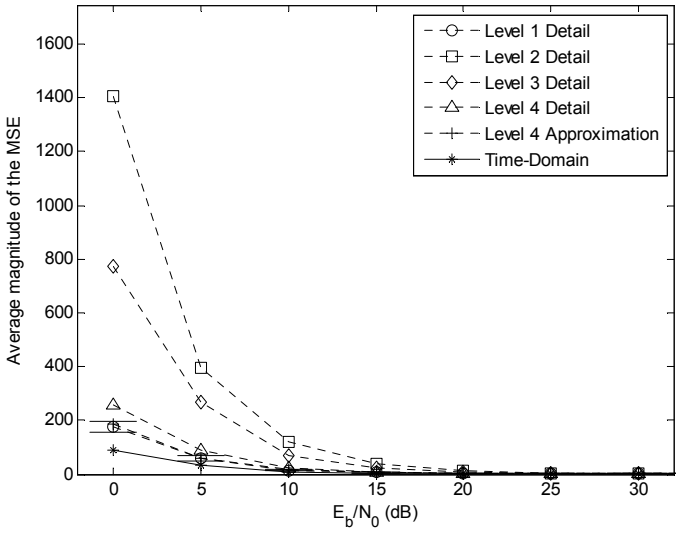

Fig. 6.3.21. Normalized ensemble-averaged MSEs between the actual channel impulse response and the estimates using the Haar wavelet (for $d = 0.2$).

6.4 Discussion

General comparisons with time-domain control experiments

The estimation of the impulse response of a channel is implemented by way of DWT-based deconvolution. In Section 6.1 such a deconvolution methodology is described analytically. Estimates of the channel impulse response are obtained by direct deconvolution of appropriate detail and approximation coefficients from undecimated DWT analyses of received pilot signals and uncorrupted original pilot signals.

The control experiment is the deconvolution of an uncorrupted pilot signal from a received signal in the discrete time-domain. The signals and channels used in the control experiments follow the same setup as those used for the DWT-based deconvolution

experiments. In all control experiments 1,000 Monte Carlo trials have been used for each value of E_b/N_0, which is also the case in all DWT-based deconvolution simulations. The results of all simulation experiments that yield channel estimates from DWT deconvolution have been compared with the results of the corresponding control experiments in Section 6.3.

It can be observed from every plot of error estimates in Section 6.3 that deconvolution in the discrete time-domain outperforms DWT deconvolution at low values of E_b/N_0. This trend is clearly seen in all MSE plots in Section 6.3 especially when the values of E_b/N_0 approach 0 dB. At higher values of E_b/N_0, however, the estimation errors from both techniques converge asymptotically. Such convergence is seen to occur at around 30 dB, and improves as the power of the WGN decreases.

From one level of resolution to the next, the errors in channel estimation appear to follow a particular order regardless of the actual channel impulse response or the wavelet used. Arranged in order of increasing difference with the time-domain estimates the wavelet coefficients are:

1. Level 1 detail
2. Level 4 approximation
3. Level 4 detail
4. Level 3 detail
5. Level 2 detail.

A general inference can be drawn from this ordered list: the best channel estimate is obtained from the detail coefficients at the first level of resolution. Also, a channel estimate obtained from the approximation coefficients at the N^{th} level of resolution will usually be as robust as an estimate from the level 1 detail coefficients. In addition, it is seen from the results in Section 6.3 that channel estimates obtained from the detail coefficients at any level except the first are always inferior to the estimates obtained from the level 1 detail and level N approximation coefficients. A cause of this phenomenon may be due to the high- and low-pass filtering performed on the received signal. In all of the results shown in this chapter it is seen that the MSEs of the channel estimates obtained from DWT coefficients at all levels of resolution converge towards 0 as the values of E_b/N_0 increase. This observation suggests that the accuracy DWT-based deconvolution depends on the filtering operations performed on a noisy received signal.

As evidenced from the MSE plots in Figs. 6.3.2-6.3.9, these trends of the level-by-level accuracy of DWT deconvolution are the same regardless of whether the Haar, the Daubechies2, Daubechies3, or the Daubechies4 wavelet was used.

Trends of MSEs with respect to the wavelets used

In the case of the Gaussian channel in Section 6.3.1 the Monte Carlo simulation experiments were repeated so that four wavelets were used. For both fading scenarios the best results were obtained with the Haar wavelet, followed by the Daubechies2 wavelet, the Daubechies3 wavelet, and then Daubechies4 wavelet.

From a numerical computational standpoint, the only differences between each of the 4 cases are the lengths of the analysis and synthesis filters. The lengths of the filters associated with each wavelet are:

Haar - 2 elements

Daubechies2 - 4 elements

Daubechies3 - 6 elements

Daubechies4 - 8 elements.

It is seen in Figs. 6.3.2-6.3.5, for the case of the slowly fading Gaussian channel, that as the length of the wavelet filters increased, from Haar to Daubechies4, the quality of the channel estimates from DWT deconvolution deteriorated rapidly. The best results were obtained by using the shortest filter, and the worst by the longest of the four. The same observations can be made by viewing Figs. 6.3.6-6.3.9, which depict the case of the fast fading Gaussian channel.

Trends of MSEs with respect to lengths of channel impulse responses

One anomalous set of results is seen in Fig. 6.3.20, which is the case of the slowly fading hilly area channel. The lengths of test signals used in the simulations involving this channel are the same as in all other simulations, and the Haar wavelets is used as well. The difference in this particular experiment is the length of the channel, which was chosen to be 2 s long. At a rate of 16 samples/s, hilly area channel impulse responses that were generated contained 32 numerical elements, as opposed to 50 for the other four channels.

The errors in the channel estimates for this slow fading channel, seen in Fig. 6.3.20, are significantly smaller than the errors obtained from estimating the other four slow fading channels with the Haar wavelet.

Since the length of the discrete-time channel is shorter than in the other corresponding cases, it follows that the MSE of the channel estimate will generally be smaller as well since there are fewer elements.

Possible erroneous MSE trends due to amplitude nulls in channel impulse responses

One source of systematic errors in the results of the simulations is the fact that some of the channels have very small, or even zero-valued, amplitudes for long durations. Ideally, any estimates of these channels should reproduce all of these small amplitudes faithfully. The addition of WGN to the received signals renders this idea practically impossible, and errors in estimation necessarily occur.

In the cases of the channels in Section 6.3.3 and 6.3.4, the two channels modeled with sparse impulse responses, this problem of mostly zero-valued elements is particularly problematic. The MSEs between channel estimates and the actual channels at all levels of DWT resolution can be reduced if fewer samples are used.

Chapter 7

Discrete Wavelet Transform-Based Channel Equalization

The underlying hypothesis of this chapter is that the equalization of signals is possible in the wavelet-domain by using linear equalizer methodologies used in the time-domain. The two types of equalization that are considered are Zero-Forcing Equalization (ZFE) and Minimum Mean-Squared Error (MMSE) equalization in the wavelet-domain.

Viewed with a different perspective, in this chapter the typical formulations of ZFE and MMSE equalization methodologies in time-domain are translated into wavelet-domain formulations.

To this end, the focus of this chapter is on demonstrating the possibility and, subsequently, the efficacy of wavelet-domain channel equalization. Such a demonstration is provided by the development of theories that support the hypothesis made above and empirical evidence that supports the hypothesis.

Expression of these linear equalization techniques in the wavelet-domain is facilitated by mathematical treatments as well as pictorial derivations. The latter consist of series of systems-level block diagrams that provide logical insight into the evolution of wavelet-domain ZFE and MMSE equalization methodologies from their corresponding precursor time-domain block diagram structures.

This chapter does not, however, attempt to adapt the aforementioned methodologies for use in communications systems. Instead, such adaptations are examined in Chapter 8, Communications Receivers with Wavelet-Domain Sub-Systems.

In Section 7.1 the general methodology of channel equalization in the wavelet-domain is documented. The development of the methodology from the typical time-domain implementation to two types of wavelet-domain implementations are described both analytically as well as in the form of block diagrams. The first type of wavelet-domain implementation does not make use of the concept of polyphase filtering while the second type does. Also included in Section 7.1 are the algorithms for MMSE equalization and ZFE using the implementation with polyphase filtering.

Section 7.2 is devoted to the computer simulations of the performance of the methodologies devised in Section 7.1. First, parameters such as the control experiments, test signals, types of wavelets, etc., that are used in the Monte Carlo simulations are presented. This is followed by the results of the simulations of the MMSE equalization experiments and then the results of the ZFE experiments.

The possibility of extending these methodologies towards the formulation of adaptive equalization in the wavelet-domain is explored in Section 7.4. Finally, a discussion of the results and the techniques presented follows in Section 7.5.

7.1 Methodology for Wavelet-Domain Channel Equalization

Both of the types of equalization that have been described in Chapter 2 are implemented with the use of pilot signals to train the equalizers, i.e., to determine the transfer functions of the equalizer filters.

The equalizer is actually an FIR filter that is implemented in the direct form, which is called known as a tapped delay line. The coefficients of the z-domain polynomial are then simply the weights assigned to each tap of the tapped delay line filter, and are referred to either as tap weights or tap coefficients.

In the process of pilot-assisted equalization, particularly in the context of communications receivers, a pilot signal is first transmitted through a channel and is subsequently acquired by the receiver. The pilot signal is used to generate the tap coefficients of the channel equalizer. The message signal is then transmitted through the same channel, and upon being acquired by the receiver is immediately equalized.

A generalized depiction of this equalization process is shown pictorially in Fig. 7.1.1. Although not shown, the message signal, $x(n)$, is transmitted after the pilot, $p(n)$, with a deliberate time-lapse in between to allow for the necessary signal processing at the receiver.

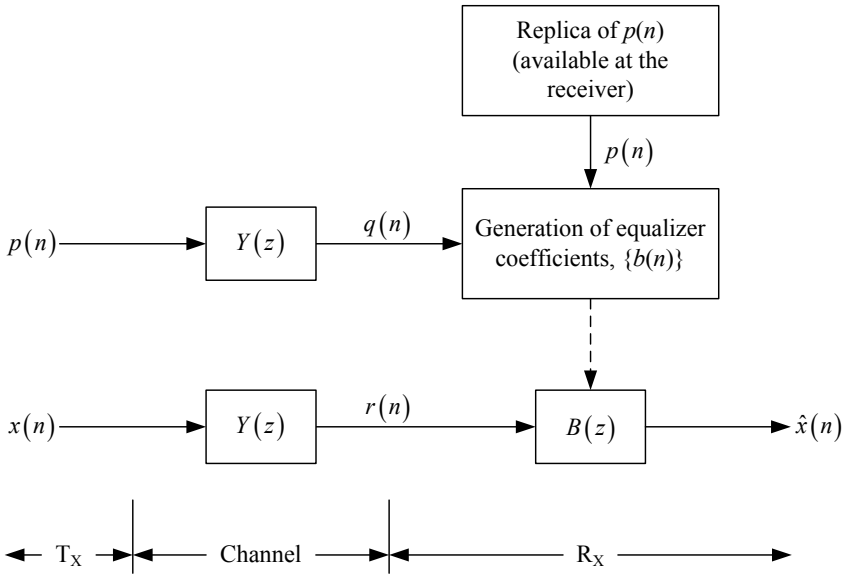

Fig. 7.1.1. System-level description of a typical pilot-assisted channel equalization procedure.

The quantities appearing in Fig. 7.1.1 are described as follows:

$p(n)$ is the transmitted pilot signal, expressed in discrete-time notation,

$q(n)$ is the received pilot signal,

$x(n)$ is the transmitted message signal,

$r(n)$ is the received message signal,

$\hat{x}(n)$ is the equalized received message signal,

$Y(z)$ is the transfer function of the channel, expressed in the z-domain, with the corresponding channel impulse response denoted by $y(n)$, and

$B(z)$ is the transfer function of the channel equalizer, expressed in the z-domain, which corresponds to the impulse response of the filter denoted by $b(n)$.

As seen in Fig. 7.1.1, the received pilot signal can be expressed in the z-domain as

$$Q(z) = P(z)Y(z). \tag{7.1.1}$$

The received message signal can be expressed in the form

$$R(z) = X(z)Y(z), \tag{7.1.2}$$

while the estimate of the message signal, i.e., the output of the equalizer, is

$$\hat{X}(z) = R(z)B(z). \tag{7.1.3}$$

Therefore, the estimate of the message signal can be expressed as

$$\hat{X}(z) = X(z)Y(z)B(z). \tag{7.1.4}$$

This concise expression, viz., (7.1.4), can be expressed as the system-level block diagram shown in Fig. 7.1.2.

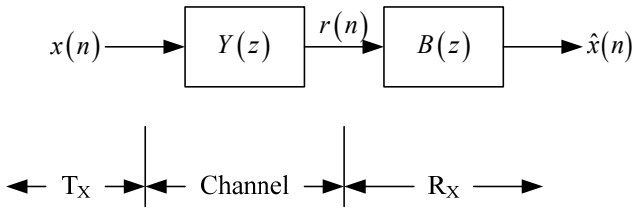

Fig. 7.1.2. Concise block diagram of signal transmission and equalization.

The estimate of the message signal, i.e., $\hat{x}(n)$, can be expressed in the wavelet-domain with the use of the DWT. Specifically, $\hat{x}(n)$ is analyzed by the high-pass and low-pass filters $G(z)$ and $H(z)$, respectively. $G(z)$ and $H(z)$ comprise the analysis filter bank for this 1-level DWT operation. The outputs of these two analysis filters, which are in

the discrete time-domain, are then dyadically decimated. Subjecting these resulting DWT coefficients to an IDWT synthesis filter bank again yields the original signal, which, in this case, is $\hat{x}(n)$. This procedure is depicted in Fig. 7.1.3

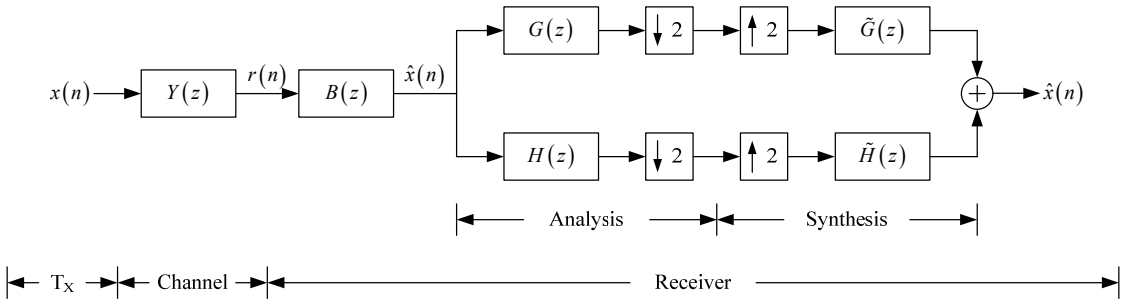

Fig. 7.1.3. DWT and IDWT of the estimated message signal, $\hat{x}(n)$.

The Forward Merge Approach for DWT-based convolution, devised in Chapter 5, can now be applied to the wavelet-domain representation of $\hat{x}(n)$, shown in Fig. 7.1.3. The resulting system, which is seen in Fig. 7.1.3, is essentially a representation of channel equalization using the DWT.

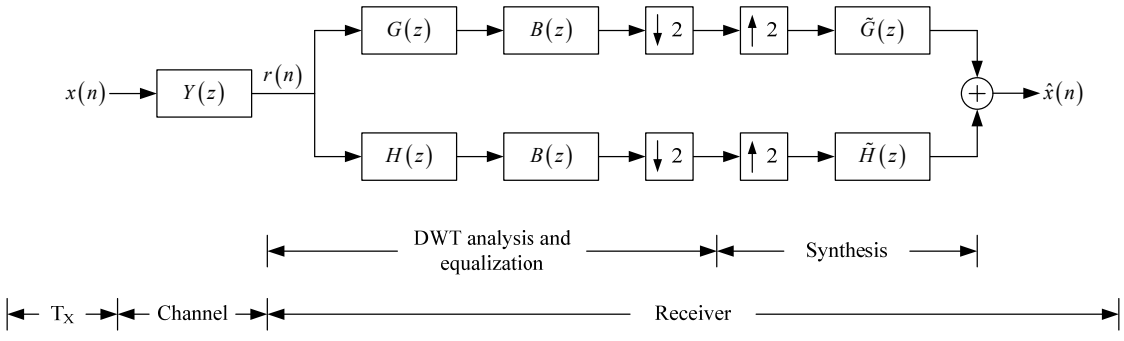

Fig. 7.1.4. A general topology for DWT-based channel equalization.

The equalizer filter, $B(z)$, can also be expressed in the wavelet-domain with the use of the Forward Merge Approach with polyphase implementation. For this purpose it must be described in terms of polyphase components, as described in Chapter 5. Specifically, for 1-level DWT, the two polyphase components of $B(z)$ are defined in the discrete time-domain as

$$b_0(n) = b(2n) \text{ and} \tag{7.1.5}$$

$$b_1(n) = b(2n+1). \tag{7.1.6}$$

Using the z-transforms of (7.1.5) and (7.1.6), the filter $B(z)$ can be expressed as

$$B(z) = B_0(z^2) + z^{-1}B_1(z^2). \tag{7.1.7}$$

The block diagram representation of channel equalization based on the Forward Merge Approach with polyphase implementation at one level of DWT resolution is, therefore, shown in Fig. 7.1.5. The 2-level block diagram is provided in Fig. 7.1.6.

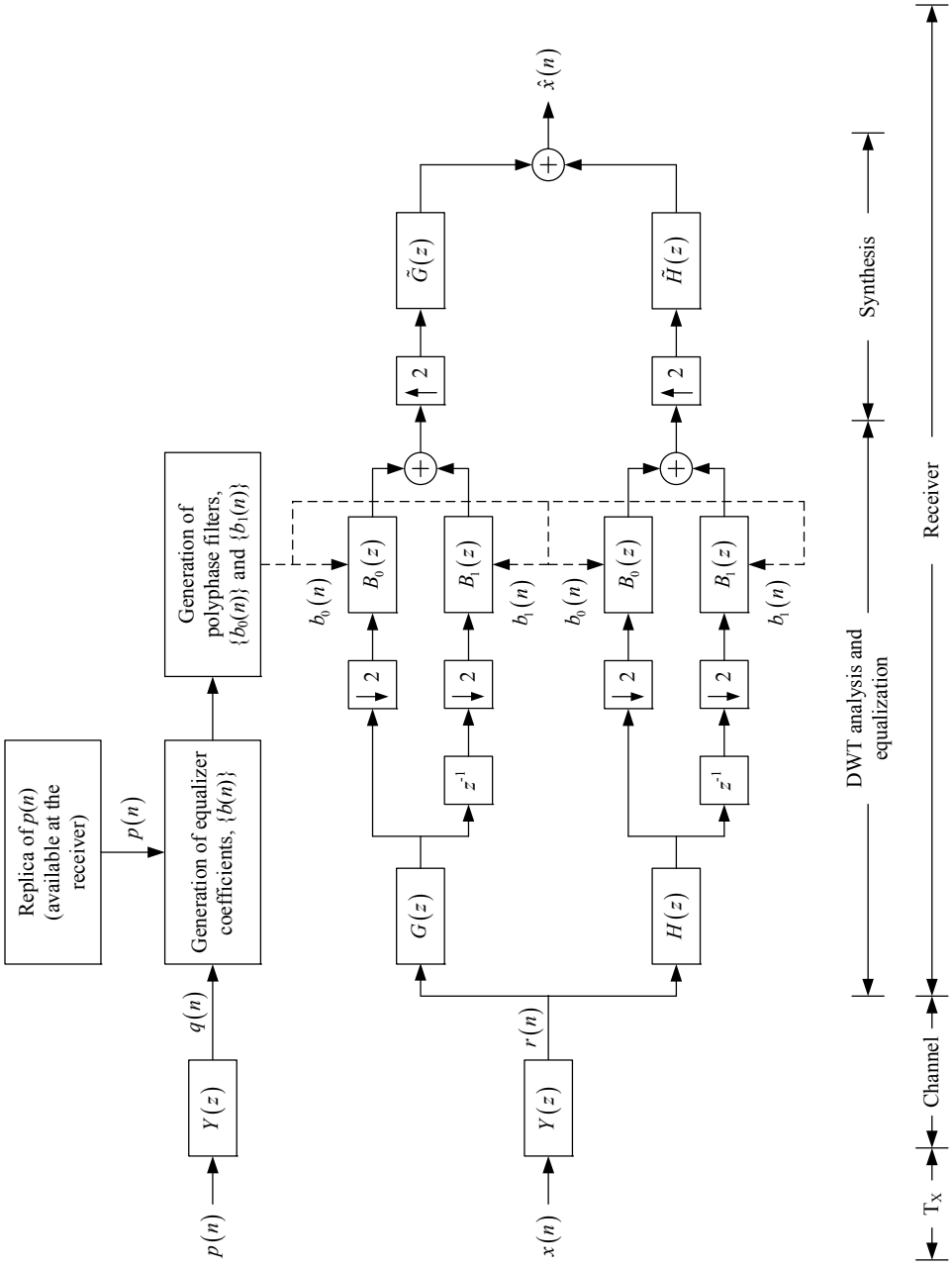

Fig. 7.1.5 Block diagram of the DWT-based equalization procedure, with polyphase filters and using 1-level DWT.

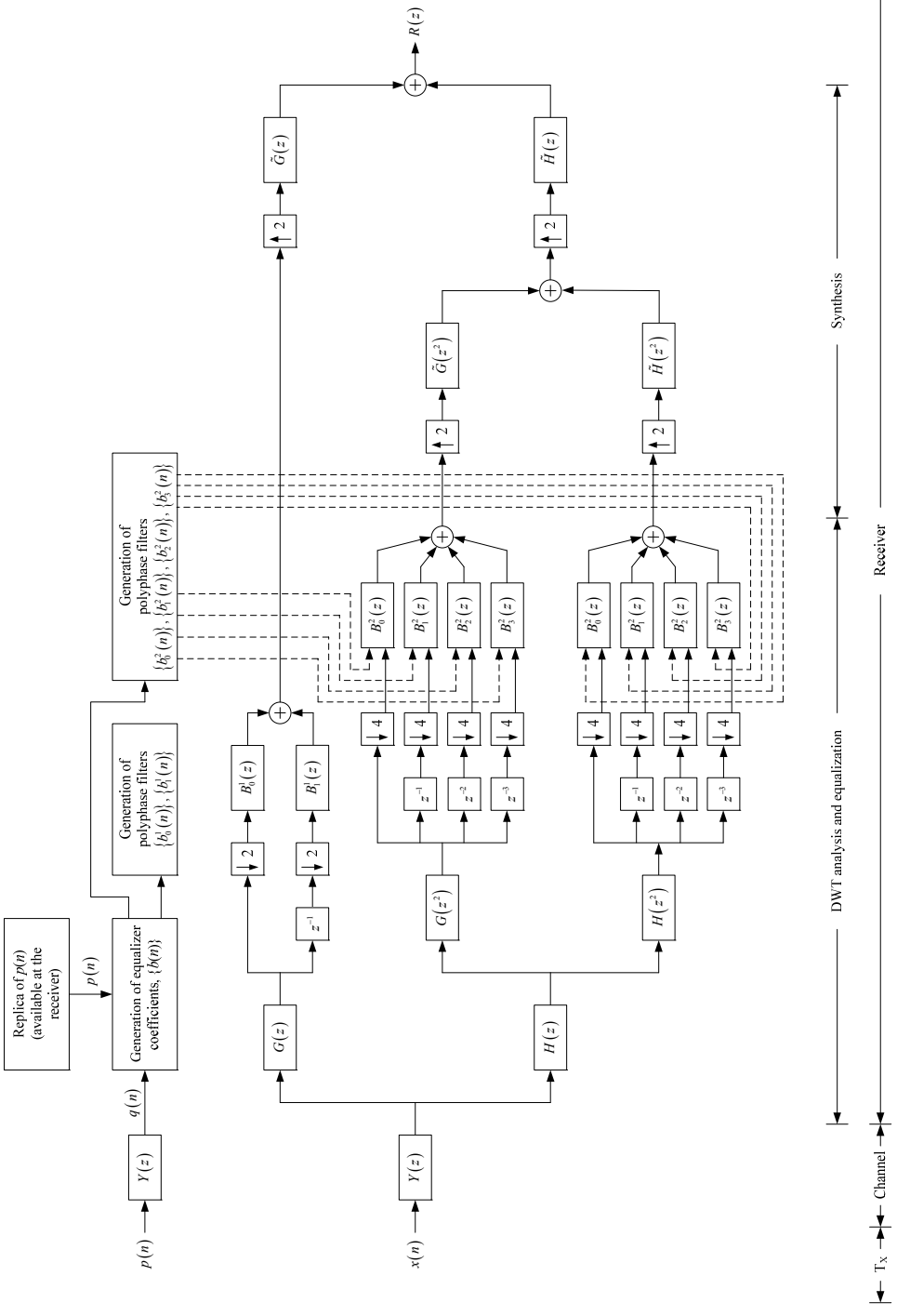

Fig. 7.1.6 Block diagram of the DWT-based equalization procedure, with polyphase filters and using 2-level DWT.

Algorithm for Wavelet-Domain Channel Equalization

1. A pilot signal is transmitted through a channel, and the corrupted pilot signal is acquired by the receiver.
2. The filter coefficients of the equalizer are then generated with the use of the received pilot signal and a locally-stored replica of the uncorrupted pilot.
3. Depending on the number of levels of DWT, polyphase filters are then derived from the filter generated in Step 2. The number of phases, N_p, (i.e., the number of polyphase filters) is related to the number of levels of DWT required, M, by the formula $N_p = 2^M$.
4. After a time delay sufficient to allow the completion of Steps 2 and 3, the message signal is transmitted through the channel and is subsequently also acquired by the receiver.
5. The message signal is analyzed, i.e., decomposed, to as many levels of DWT as desired but are not decimated.
6. The signals in Step 5 are then delayed and decimated as necessary, and then filtering by the polyphase equalizer filters generated in Step 3.
7. The output of the polyphase filters at each level DWT are then summed element-wise, to form the equalized detail and approximation coefficients of what will be the estimate of the message signal.
8. IDWT is performed on the detail and approximation coefficients obtained in Step 7, which results in the final output of the entire process: the equalized estimate of the message signal.

Computational Complexity

Let the length of the received signal, $R(z)$, be denoted by N_R, the length of the channel equalizer, $B(z)$, be denoted by L_B, and the lengths of the DWT filters by L. The assumption is made that both the received signal and the channel equalizer filter sequences are longer than the DWT filters, i.e., $N_R \gg L$ and $L_B \gg L$.

For the case of DWT-based equalization at 1 level of resolution, as depicted in Fig. 7.1.5, the computational complexity is

$$O(n) = 2N_R + N_R L_B + (N_R + L_B) \tag{7.1.8a}$$

$$\Rightarrow O(n) \approx N_R L_B . \tag{7.1.8b}$$

When equalization at two levels of DWT resolution is considered, as in Fig. 7.1.6, the order of complexity for the level 1 detail subband is

$$O(n) = N_R + \frac{N_R L_B}{2} + (N_R + L_B) \tag{7.1.9a}$$

$$\Rightarrow O(n) \approx N_R L_B \tag{7.1.9b}$$

and for the level 1 approximation subband, which includes the level 2 operations as well, is

$$O(n) = 3N_R + \frac{N_R L_B}{2} + 2(N_R + L_B) \tag{7.1.10a}$$

$$\Rightarrow O(n) \approx N_R L_B . \tag{7.1.10b}$$

7.2 Computer Simulations

The general methodology that has been presented theoretically in Section 7.1 has been implemented using the MATLAB simulation software package. It has then been adapted for use with both the ZFE and MMSE equalization techniques. The efficacy of these two resulting wavelet-domain equalization methodologies is demonstrated by using Monte Carlo simulation experiments. This approach enables verification of the techniques.

7.2.1 Setup of the Simulations

The test signals that are used for all Monte Carlo trials are sums of sinusoids. Specifically, the signals are the sums of a user-defined number of odd harmonics of a fundamental sinusoidal component. The signal itself is of the general form

$$s(n) = \sum_{k=1}^{K} A_k \cos\left[(2k-1)2\pi f_0 n T_s + \phi_k\right] \tag{7.2.1}$$

where

$s(n)$ is the n^{th} element of the test signal, expressed in the discrete time-domain,

K is the number of sinusoidal harmonic components in the test signal,

A_k is the amplitude of the k^{th} harmonic component,

f_0 is the frequency of the fundamental harmonic,

T_s is the sampling rate, and

ϕ_k is the additional phase offset for the k^{th} harmonic.

The values of the amplitude and the phase of each harmonic component are obtained from uniform distributions of each parameter. In this work the values of the amplitudes

are limited to the range from 0 to 10, and the values of the phase offsets range from 0 to 2π. The frequency of the fundamental harmonic, f_0, was chosen to be a nominal 2 Hz, and the number of odd harmonics, *K*, was chosen to be 7.

In order to emulate the transmission of data symbols that are represented by finite-length sinusoidal signals, every pilot and message signal that was generated was a packet of 10 successively concatenated signals described by (7.2.1).

A channel with a Gaussian PDP, $\phi_c(t)$, of the form

$$\phi_c(t) = \frac{1}{\sqrt{2\pi\tau}} e^{\frac{(t/\tau)^2}{2}}, \tag{7.2.2}$$

where τ is the Root-Mean-Square (RMS) delay spread, and is defined as

$$\tau = dT_{sym}. \tag{7.2.3}$$

In this definition, *d* is the normalized delay time of the channel and T_{sym} is the period of the baseband symbols on which the transmitted signals are fundamentally based. The channels were selected to have a normalized delay time of $d = 0.2\,\text{s}$. Since the symbol period, T_{sym}, is selected to be 1 s, this normalized delay time corresponds to fast-fading channels. For the purposes of numerical implementation, the actual values of the magnitude of each channel are generated for a length of 2 baseband symbol periods.

The noise that is added to all transmitted signals is AWGN with a double-sided power spectral density of $N_0/2$. The metric of E_b/N_0 is used throughout this work to provide

a relative measure of the energy contained in every "bit" that is transmitted, E_b, to the power of the noise that is added to the signal.

The metric of Signal-to-Noise Ratio (SNR), which is the ratio of signal power to noise power, was not used since ultimately the performance of the equalizers is examined with the use of Symbol Error Rate (SER) curves. The SER curves generated in this dissertation use the metric of E_b/N_0 instead of SNR. These SER curves indicate the performance of the communications systems that have wavelet-domain equalizers embedded within, are the subject of Chapter 9.

For every value of E_b/N_0 the MSE between the output of the equalizer and the uncorrupted message signal is computed and recorded. This procedure is repeated 1,001 times to mimic 1,001 successive transmissions and equalizations. The signals and channel generated for each Monte Carlo trial may be considered as an independent event. The MSE is normalized to the power contained by the corresponding uncorrupted message signal.

The average MSE of every ensemble of 1,001 MSEs recorded for each value of E_b/N_0 is also computed and then presented graphically.

7.2.2 Minimum Mean-Squared Error Equalization

For each Monte Carlo trial the coefficients of the MMSE equalizer filter are generated based on the minimization of the MSE between the received pilot signal and a replica of the uncorrupted transmitted pilot signal, which is stored in the receiver. The length of the MMSE equalizer is chosen to be equal to the length of the received message signal in discrete time, L_{Rxm} (or the next odd integer if L_{Txm} is even). For the simulation setup described in Section 7.2.1, each such MMSE equalizer has 49 taps.

Three experiments are performed with the MMSE equalizer that is generated.

1. The first is the control experiment in which the received message signal is equalized in the discrete time-domain. The output of the MMSE equalizer is an estimate of the transmitted message signal. This is the output that is expected with the standard formulation and implementation of MMSE equalization in the z-domain and, equivalently, in the discrete time-domain.

2. The second experiment involves the implementation of the MMSE equalizer as polyphase filters. The received message signal is transformed using a 1-level DWT filter bank, and the resulting approximation and detail coefficients are equalized by the polyphase MMSE equalizer filters. The output of the polyphase equalizers are estimates of the approximation and detail coefficients of the transmitted message signal at 1 level of DWT resolution. An IDWT operation is performed on these estimates of the coefficients, which produces the estimate of the transmitted message signal, in the discrete time-domain.

3. The third experiment is similar to the second experiment in every aspect except one: DWT and MMSE equalization are carried out at two levels of analysis instead of just one level.

The mother wavelet used in all three experiments is the Daubechies3 wavelet. Plots of the mother wavelet and the corresponding scaling function are provided in Fig. 7.2.1.

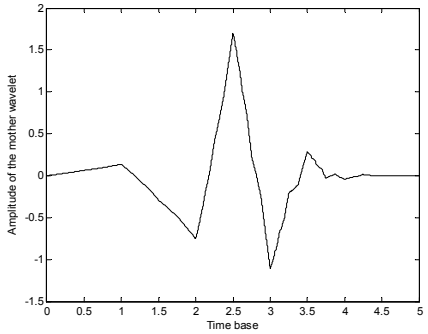

Fig. 7.2.1a. The Daubechies3 wavelet.

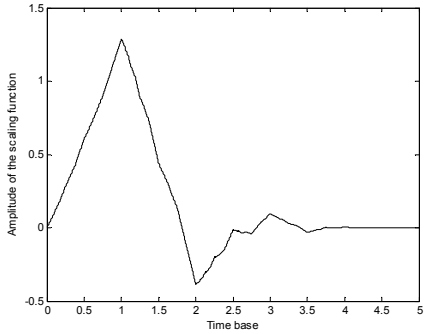

Fig. 7.2.1b. The Daubechies3 scaling function.

The ensemble-averaged MSEs for E_b/N_0 values ranging from 60 dB down to 0 dB for both the control experiment, i.e., MMSE equalization in the discrete time-domain, and at 1-level of DWT are shown graphically in Fig. 7.2.2. Each datum that comprises the

graph represents the average MSE between the estimated message signal and the transmitted message signal over 1,001 independent trials.

Also shown on the graph are the 95% confidence intervals [99] for each of the wavelet-domain MSE data. A 95% confidence interval for a mean value, μ, is an interval $\mu - k \le \mu \le \mu + k$ that contains μ with a probability of 0.95.

Furthermore, all MSE values shown in Fig. 7.2.2 are normalized to the average variance of the transmitted message signal, which can also be viewed as normalization to the average power of the transmitted message signal.

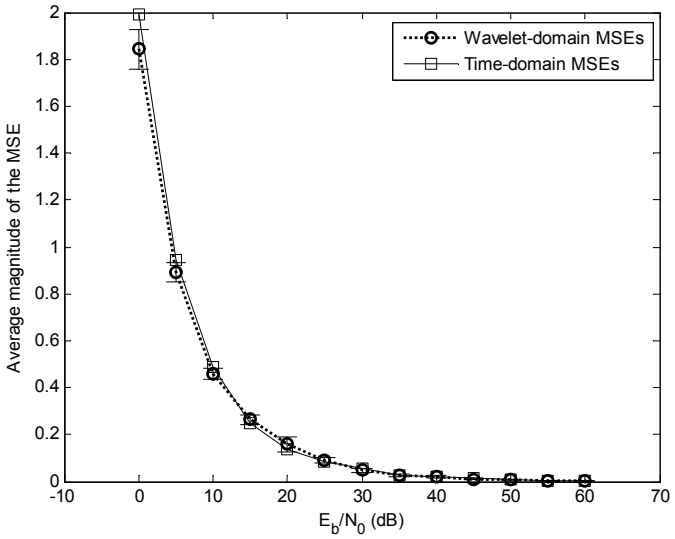

Fig. 7.2.2. Normalized ensemble-averaged MSE plot for 1-level wavelet-domain MMSE equalization.

It is seen in Fig. 7.2.2 that the average errors of the wavelet-domain estimates are close to the average errors in the time-domain control equalization experiment, which is standard MMSE, implemented in the discrete time-domain. It can also be inferred from the graph that wavelet-domain MMSE equalization at 1 level of DWT performs as well as time-domain MMSE equalization for the entire range of E_b/N_0 values. Another point of note is that the 95% confidence intervals, depicted by the horizontal bars, become smaller as E_b/N_0 increases.

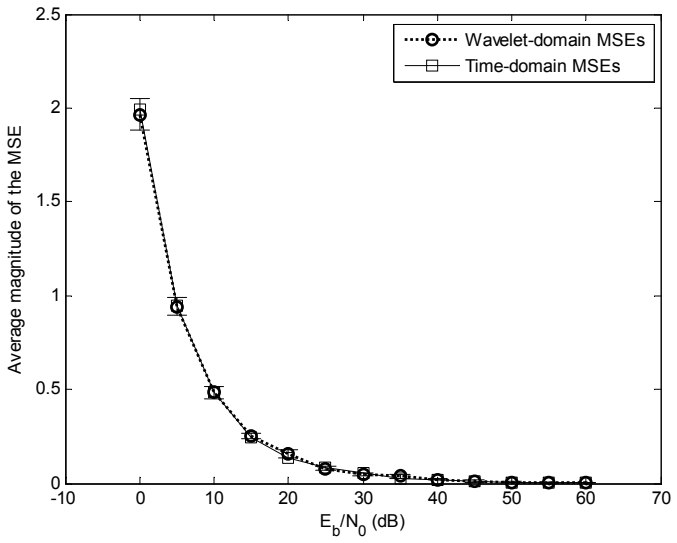

Fig. 7.2.3. Normalized ensemble-averaged MSE plot for 2-level wavelet-domain MMSE equalization.

In Fig. 7.2.3 the graphs of the MMSE equalization results at 2 levels of DWT and from the control experiment are shown. As in the case of MMSE equalization at 1-level, the average errors between wavelet-domain and discrete time-domain MMSE equalization

are statistically convergent. The 95% confidence intervals also follow the same trend of decreasing in size as noise of decreasing power is added to the faded signals.

7.2.3 Zero-Forcing Equalization

Following the same procedure for MMSE equalization, the coefficients of the ZFE are first generated by using the received message signal and an uncorrupted replica of the transmitted message signal. The length of the ZFE is chosen to be $6L_h + 1$, i.e., six times the length of the discrete time channel. Hence, according to the setup described in Section 7.2.1, each ZFE is a 55-tap filter. The mother wavelet used in all three experiments is the Haar wavelet, which plotted along with the corresponding scaling function in Fig. 7.2.4.

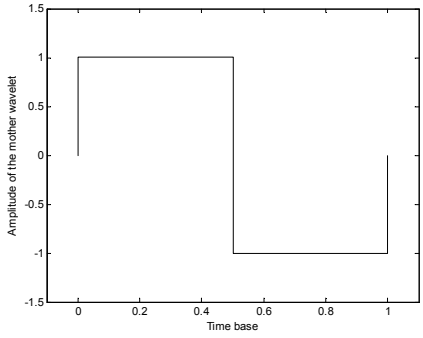

Fig. 7.2.4a. The Haar wavelet.

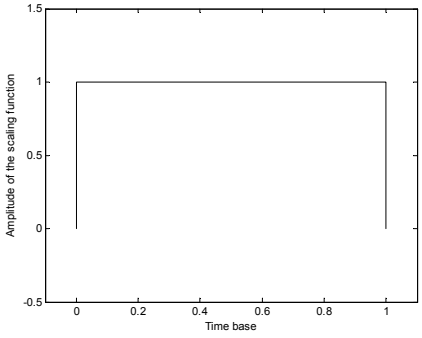

Fig. 7.2.4b. The Haar scaling function.

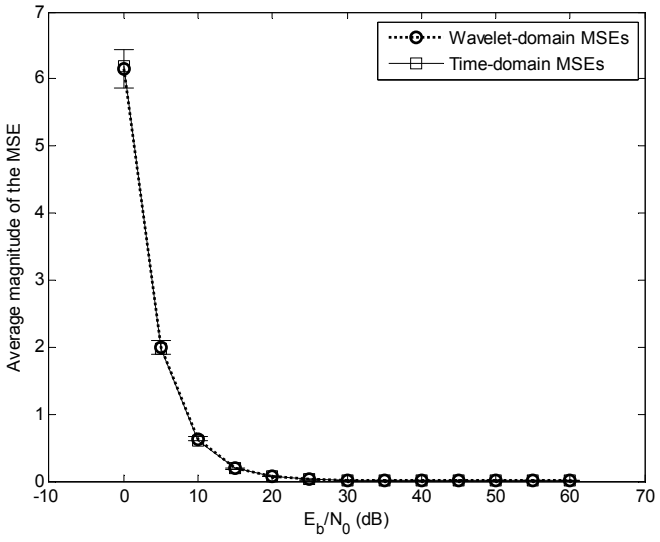

Fig. 7.2.5. Normalized ensemble-averaged MSE plot for 1-level wavelet-domain ZFE.

In Fig 7.2.5 it is seen that the average MSE values for each value of E_b/N_0 obtained using ZFE at 2 levels of DWT correlate very well with the average MSE values obtained in the time-domain. As expected, the magnitude of the errors resulting from wavelet -domain equalization are greatly diminished as the power of the noise added to the faded transmitted message signals decreases. The 95% confidence intervals also decrease in size as the values of E_b/N_0 increase.

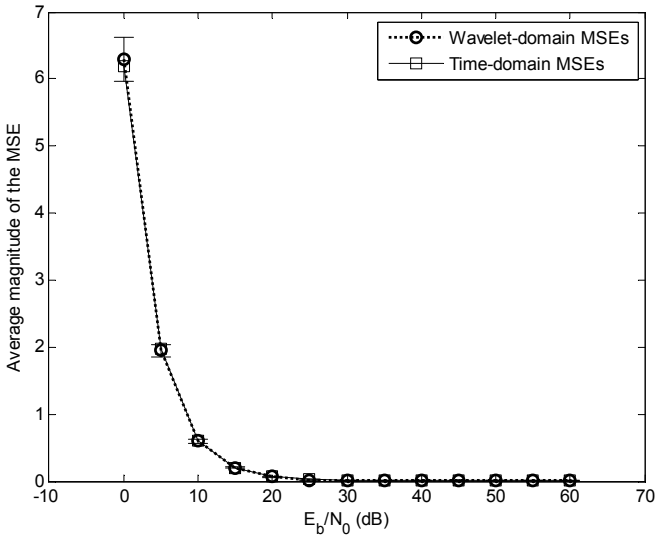

Fig. 7.2.6. Normalized ensemble-averaged MSE plot for 2-level wavelet-domain ZFE.

The results of the experiment of ZFE in 2-level DWT are shown in Fig. 7.2.6. Again it is seen that the ZFE in the wavelet-domain performs as well as ZFE in the time-domain even if an additional level of DWT is used.

7.3 Strategies for Discrete Wavelet Transform-Based Adaptive Equalization

In this dissertation the assumption that channels are time-invariant has been made. Specifically, it is the impulse responses, $c(t)$, of such channels that are considered to be constant. In practical situations, however, time-varying channels are more likely to be encountered. In order to equalize the effects of time-varying channels adaptive filters are necessary. Adaptive filters are equipped with the ability to change the filter tap coefficients automatically.

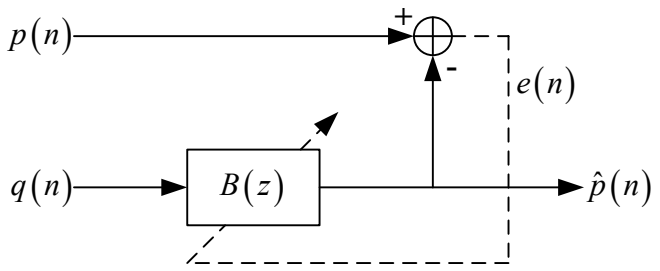

Fig. 7.3.1. Feedback structure of an adaptive equalizer [100].

Consider the general topology of an adaptive equalizer shown that is in Fig. 7.3.1. The discrete time signal $p(n)$ denotes a pilot signal that is transmitted through an unknown channel, and a copy of which is available at the receiver for use by the equalizer. The signal $q(n)$ is the received pilot signal, $B(z)$ is the transfer function of the equalizer filter, and $\hat{p}(n)$ is the equalized pilot signal. The error between the original pilot signal and the received pilot signal, denoted by $e(n)$, is

$$e(n) = p(n) - \hat{p}(n). \tag{7.3.1}$$

As in the case of the MMSE equalizer, by minimizing the error between the uncorrupted pilot signal and equalized received pilot signal the equalizer coefficients can be obtained. The procedure of MMSE , which has been described in Chapter 2, requires the inversion of the autocorrelation matrix of the received pilot signal, $q(n)$. A different, popular, procedure for minimizing the error, $e(n)$, is the LMS algorithm, in which the filter coefficients are recursively updated instead of being obtained by direct matrix inversion

[3]. For the purposes of adaptive equalization either MMSE equalization or the LMS algorithm may be used [101].

In this section, however, the structures of adaptive equalizers using a DWT-based framework are the subject of interest, rather than the well-established algorithms that may be used for the realization of these structures. Two strategies for DWT-based adaptive equalization are identified.

The first strategy involves the use of the original pilot signal, $p(n)$, and the equalized pilot signal, $\hat{p}(n)$, directly. The received pilot signal, $q(n)$, is, transformed using the DWT, and the resulting wavelet coefficients are equalized, as described in Section 7.1. The error between $p(n)$ and $\hat{p}(n)$ is then computed and a suitable algorithm, such as MMSE or LMS, can be used to obtain the coefficients of the equalizer, $\{b(n)\}$. This strategy merges the DWT-based equalization described in Section 7.1 with the feedback structure depicted in Fig. 7.3.1, and is shown in Fig. 7.3.2.

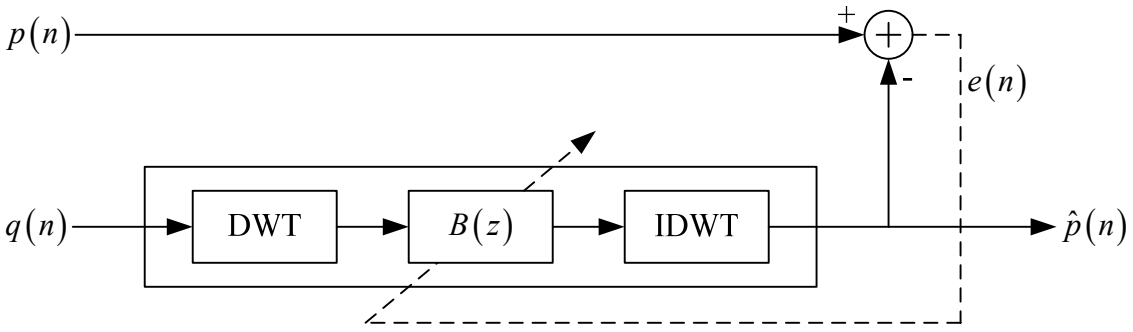

Fig. 7.3.2. DWT-based adaptive equalization using the synthesized signal estimate.

In the second strategy, both the copy of the original pilot signal and the received pilot signal are transformed using the DWT. The undecimated DWT coefficients at corresponding levels of resolution of the two signals are then compared to produce error signals. Each error signal could then be used to generate the coefficients of an independent equalizer. In this manner each set of DWT coefficients of the received pilot signal has a dedicated equalizer, and is equalized separately. All equalized DWT coefficients are then synthesized by the IDWT filter bank, which results in the equalized estimate of the pilot signal. This second strategy is depicted in Fig. 7.3.3 for 1 level of DWT resolution.

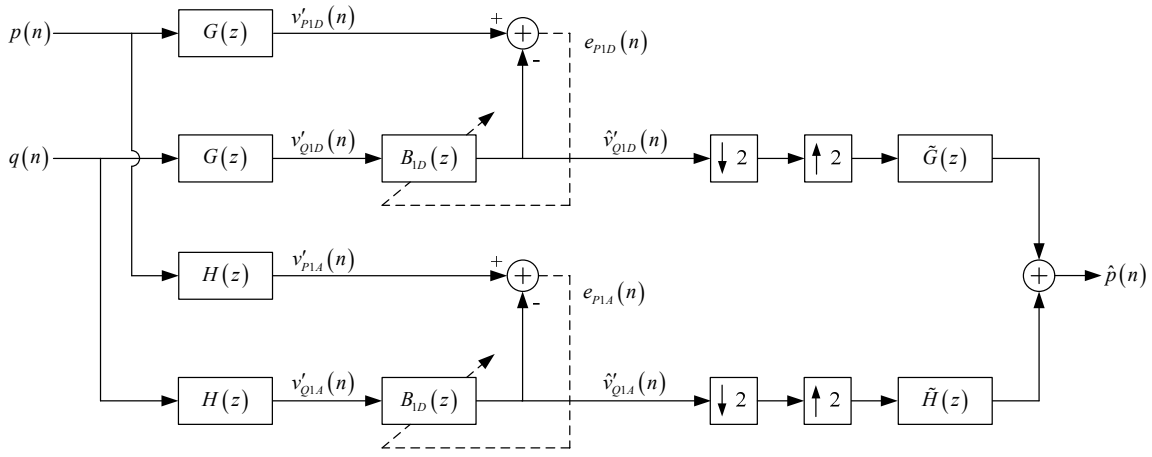

Fig. 7.3.3. DWT-based adaptive equalization directly using wavelet coefficients.

As seen in Fig. 7.3.3, 1 level of DWT resolution requires 2 subbands, both of which yield a set of DWT coefficients. The level-1 detail and approximation coefficients of the original pilot signal, $p(n)$, are labeled $v'_{P1D}(n)$ and $v'_{P1A}(n)$, respectively. Similarly, the level-1 detail and approximation coefficients of the received pilot signal are denoted by

$v'_{Q1D}(n)$ and $v'_{Q1A}(n)$, respectively. The error signal that results from the detail coefficients is

$$e_{P1D}(n) = v'_{P1D}(n) - \hat{v}'_{Q1D}(n) \tag{7.3.2}$$

and the error that results from the approximation coefficients is

$$e_{P1A}(n) = v'_{P1A}(n) - \hat{v}'_{Q1A}(n). \tag{7.3.3}$$

The signals $\hat{v}'_{Q1D}(n)$ and $\hat{v}'_{Q1A}(n)$ are the equalized undecimated DWT coefficients of the received pilot signal, $q(n)$.

Using a suitable equalization algorithm, the equalizer filters $B_{1D}(z)$ and $B_{1A}(z)$, corresponding to the level-1 detail and approximation coefficients, respectively, can be generated.

7.4 Discussion of Results

In this chapter, a framework for wavelet-domain channel equalization has been developed. The initial hypothesis was that discrete time-domain equalization could be moved into the wavelet-domain by the use of suitable analytical means. An implication of this hypothesis was, however, that verification must also be provided by implementing specific equalization methodologies using the framework. ZFE and MMSE equalization, being fundamental as well as popular, methodologies were selected for this purpose. Such verification is a necessary condition required to prove that the framework for wavelet-domain equalization is correct.

The average MSE graphs seen in Figs. 7.2.2, 7.2.3, 7.2.5 and 7.2.6 provide evidence that the wavelet-domain equalization framework that was developed in Section 7.1 is indeed accurate. In addition, these results also show that both MMSE equalization and ZFE can be implemented as effectively with the use of the DWT as in the discrete time-domain. In Figs. 7.2.2 and 7.2.3, the good convergence of the average errors of wavelet- and time-domain estimates indicates that the use of 1,001 Monte Carlo trials for each value of E_b/N_0 produces statistically significant results. This inference is further validated by the results of the ZFE experiments, which are shown in Figs. 7.2.5 and 7.2.6.

Another notable trend evidenced in both types of equalization is that the 95% confidence intervals decrease in size as the value of E_b/N_0 increases. A plausible explanation for this observation is that the magnitude of outliers, which in this case are errors in estimation that are several standard deviations from an average MSE, reduces as less powerful noise is added to the faded signal.

Such containment of outliers is expected since the equalizer filters are generated partly based on the pilot signal that is received. The noise added to the transmitted pilot signal in every simulation trial is independent of the noise added in any other trial. Due to this pseudo-random generation and implementation of AWGN, it is reasonable to assume that for a particular value of E_b/N_0 the numerical value(s) of the noise process may cause an equalizer that is sub-optimal. Such sub-optimality of filter coefficients may arise due to

the necessary solution of equations that contain ill-conditioned matrices in both MMSE equalization and ZFE procedures.

Another factor along these lines that does not allow perfect convergence of the time- and wavelet-domain results is the generation of the channels. As with the AWGN, the impulse responses of the fading channels that are used in every trial are independent of the impulse responses in every other trial, and are also pseudo-randomly generated with the aid of a Gaussian distribution. Due to this setup sometimes channels that lead to ill-conditioned matrix equations are generated.

The result of "unfavorable" noise or channels, as explained above, is non-convergent filters. To minimize this problem heuristic limits of convergence were set for the ZFE and MMSE filters. For all ZFE experiments,

$$\sum_{n=1}^{N} |b_n| < 2$$

and for all MMSE equalization experiments

$$\sum_{n=1}^{N} |b_n| < 5 .$$

The application of these upper bounds on filter convergence resulted in the reduction of the outliers in the time- and wavelet-domain experiments.

The outcomes of this chapter are summarized as follows.

1. A general framework for pilot-assisted wavelet-domain channel equalization has been established, specifically by making use of the techniques of wavelet-domain convolution developed in Chapter 5.
2. Two variations of the framework are provided: one with polyphase filtering and the other without.
3. The techniques of MMSE equalization and ZFE have been successfully applied to the wavelet-domain framework.
4. Simulation experiments have shown that signals propagated through fast-fading multipath channels can be equalized as well using wavelet-domain equalization as with time-domain equalization.
5. The experiments also show that the performance of time- and wavelet-domain equalization procedures is comparable for a large range of AWGN power levels.

Chapter 8

Communications Receivers with Wavelet -Based Sub-Systems

The concepts of DWT-based channel estimation and equalization have been developed in Chapters 6 and 7, respectively. The analytical and algorithmic formulations of these estimation and equalization methodologies have been presented as general signal processing strategies that can be adapted for use in appropriate applications.

One area in which these strategies can be applied is communications receivers. The primary hypothesis of this chapter is that the DWT-based channel estimation and equalization strategies can be used in communications receivers.

Furthermore, it is postulated that the performance of communications receivers composed partially of DWT-based sub-systems is comparable to the performance of receivers with discrete time-domain sub-systems that perform the same signal processing tasks. This second hypothesis stems the results of the computer simulations in Chapters 6 and 7. In these results it was seen that the performance of each DWT-based sub-system is indeed similar to the performance of the corresponding discrete time-domain sub-system.

8.1 Communications Systems

The typical form of a communications system that is composed of a transmitter, a channel, and a receiver is provided in Fig. 8.1.

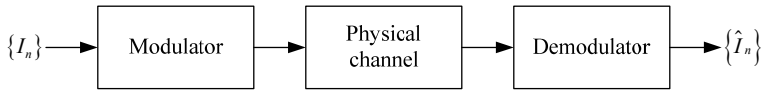

Fig. 8.1. Basic communications system.

Note that in Fig. 8.1 the transmit filter referred to in previous chapters of this dissertation is now called the modulator. This change in nomenclature is simply to emphasize the actual application of a transmit filter in a communications system, which is to modulate a carrier signal in a specific manner dictated by each symbol in the baseband message sequence, $\{I_n\}$.

Similarly, the basic system in Fig. 8.1 also now contains a demodulator, which is fundamentally composed of three operations:

1. A receive filter, with an impulse response matched to the impulse response of the transmit filter
2. A sampler, with sampling intervals defined by the baseband symbol rate
3. A decision-making device, which ultimately yields an estimate of the transmitted baseband message sequence.

The ideal, basic, system illustrated in Fig. 8.1 can be readily augmented to include the case of additive noise, and the compensation for the effects of the channel, which is an equalizer. This augmented system is depicted in Fig. 8.2.

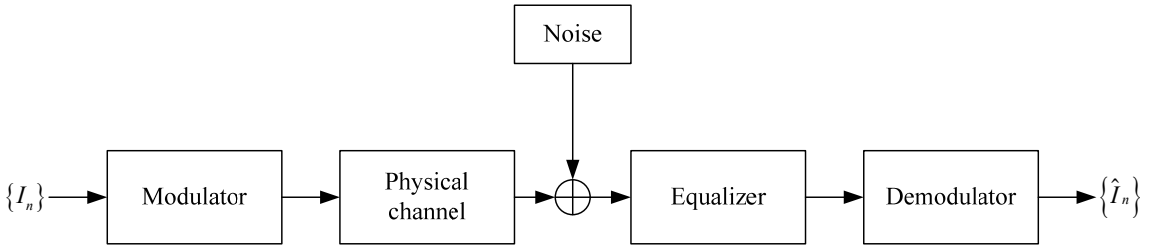

Fig. 8.2. Augmented communications system.

Although the communications signal processing strategy presented in Fig. 8.2 is intuitively appealing, an alternative approach can also be used. In this alternative approach, the transmitted signals are designed in such a manner that the signal processing effort in equalizing the received signals is greatly reduced. Specifically, instead of equalizing and restoring the fidelity of a complete received signal, only discrete samples of the received signal after matched filtering are equalized.

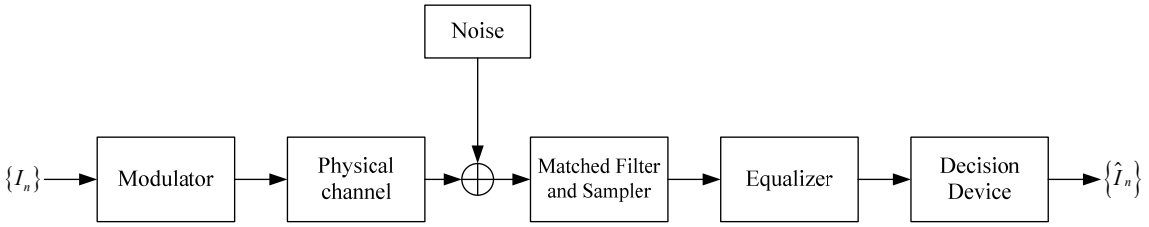

Fig. 8.3. Traditional discrete-time communications system.

This alternative approach [3] has been described in detail in Chapter 2, and is shown in Fig. 8.3 for convenient reference. In this chapter, however, the traditional system in Fig. 8.3 is not implemented. Instead, the more intuitive approach of equalizing the complete received signal, seen in Fig. 8.2, is used.

In the preceding chapters channel estimation is performed with the use of deconvolution procedures, in the discrete time- and wavelet-domains. Channel equalization is implemented using MMSE equalization and ZFE, both in the discrete time- and wavelet-domains. Between these two equalization strategies, MMSE does not require an estimate of the channel impulse response, but ZFE does.

Therefore, there are three combinations of these signal processing strategies considered in this chapter. These are introduced as sub-systems in communications receivers, and are:

1. MMSE equalization of received signals, in both discrete time- and wavelet-domains.
2. ZFE of received signals, in both discrete time- and wavelet-domains, with ***a priori*** **knowledge** of the channel impulse responses.
3. ZFE of received signals, in both discrete time- and wavelet-domains, with ***a posteriori*** **estimation** of the channel impulse responses.

Block diagram illustrations of these three cases are provided in the respective sections that follow.

All of the receiver structures are evaluated in communications systems that use the BASK, BFSK, and 16-QAM modulation schemes. The transmitted signals are corrupted by AWGN resulting in the E_b/N_0 range of $[0\,\text{dB}, 20\,\text{dB}]$.

Setup of Simulations

All results presented in this chapter have been obtained from simulations performed in MATLAB. The specific parameters used in the simulations are listed as follows. These parameters are largely common for all cases of MMSE equalization and ZFE, with and without channel estimation.

Signal Parameters

1. Modulation schemes: BASK, BFSK, 16-QAM
2. Carrier frequency (f_c): 1 Hz (BASK, 16-QAM),
   1 Hz and 2 Hz (BFSK basis functions)
3. Carrier amplitude (A): 1 V (BFSK),
   1 V and 2 V (BASK basis functions),
   1 V and 3 V (16-QAM basis functions)
3. Baseband symbol period (T_s): 1 s
4. Samples per symbol (N_s): 4 (BASK, 16-QAM),
   8 (BFSK)

Channel Parameters

1. Power Delay Profile: Gaussian
2. Normalized delay spread (d): 2.5 (slow fading condition)
3. Channel length (L_c): 2 baseband symbol periods

Noise Parameters

1. Type of Noise: Additive White Gaussian
2. E_b/N_0 range: 0 dB to 20 dB

Wavelet Parameters

1. Wavelet: Haar
2. Levels of resolution (N): 1

Monte Carlo Simulation Parameters

1. Number of trials: 1,000
2. Symbols per transmission: 10

Equalizer Filter Parameters

1. Filter length: $2L_c + 1$ (MMSE equalizers)

   $6L_c + 1$ (ZFE)
2. Upper bound: 100 (max. sum of filter tap coefficients)

   (for filter convergence)

8.2 Receiver with Wavelet-Based Minimum Mean -Squared Error Equalization

It has been established in Chapter 7, Discrete Wavelet Transform-Based Channel Equalization, that the performance of the DWT-based MMSE equalization procedure is similar to the performance of discrete time-domain-based MMSE equalization.

In this section the DWT-based MMSE equalization strategy is applied to three communications systems. Each communications system implements one of the three

modulation schemes - BASK, BFSK, and 16-QAM. The effect of DWT-based MMSE equalization in each system is evaluated with the use of SER curves.

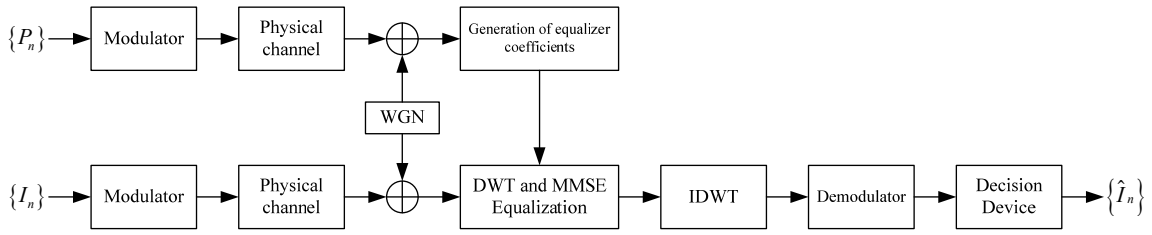

Fig. 8.2.1. Experimental system #1, with DWT-based MMSE equalization.

In a similar fashion, a second set of simulation experiments is performed, but with the use of standard, discrete time-domain-based, MMSE equalization instead of DWT-based MMSE equalization. The effect of using discrete time-domain-based MMSE equalization in each of the three systems is also determined with the aid of SER curves.

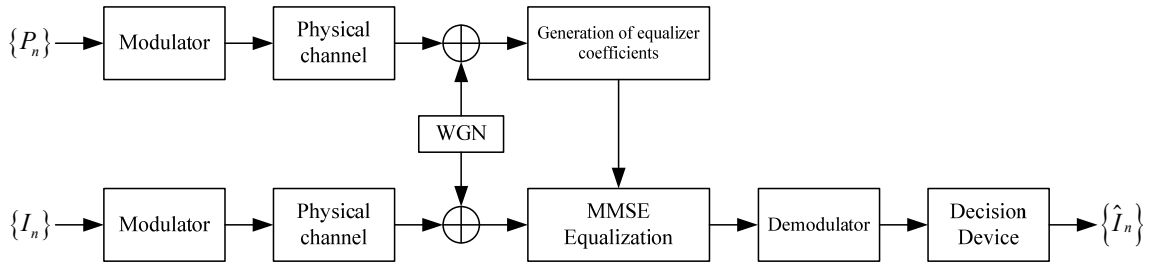

Fig. 8.2.2. Experimental system #2, with discrete time-domain-based MMSE equalization.

The control experiment for each of the three cases is the operation of each communications system without the use of any equalization procedure. Thus, a third set

of SER curves is obtained, which represents the worst-case scenario from the perspective of robust recovery of the transmitted baseband symbols.

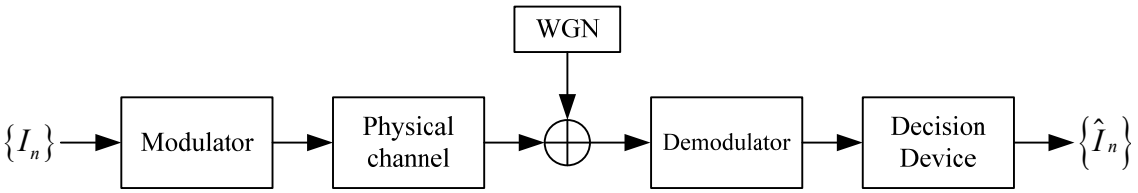

Fig. 8.2.3. Control experiment - communications system with no equalization.

These three sets of SER curves for each modulation scheme are overlaid and compared graphically.

Results

The results of the Monte Carlo simulations for BASK are illustrated graphically in Fig. 8.2.4, for BFSK in Fig. 8.2.5, and for 16-QAM in Fig. 8.2.6.

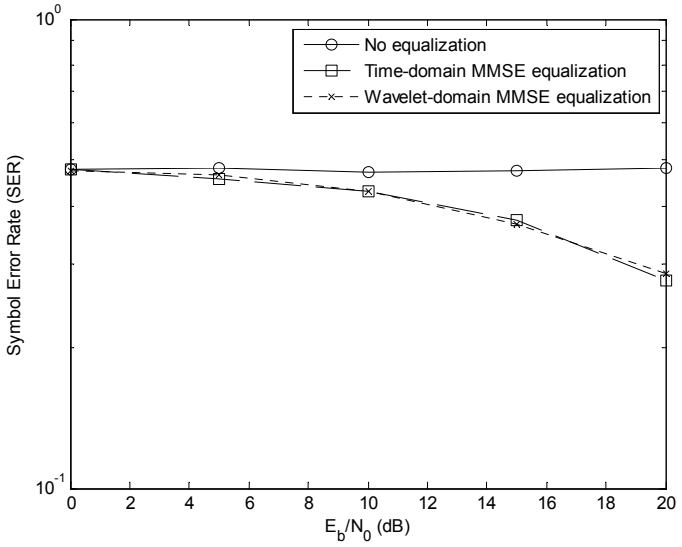

Fig. 8.2.4. SER curves for BASK, with MMSE equalization.

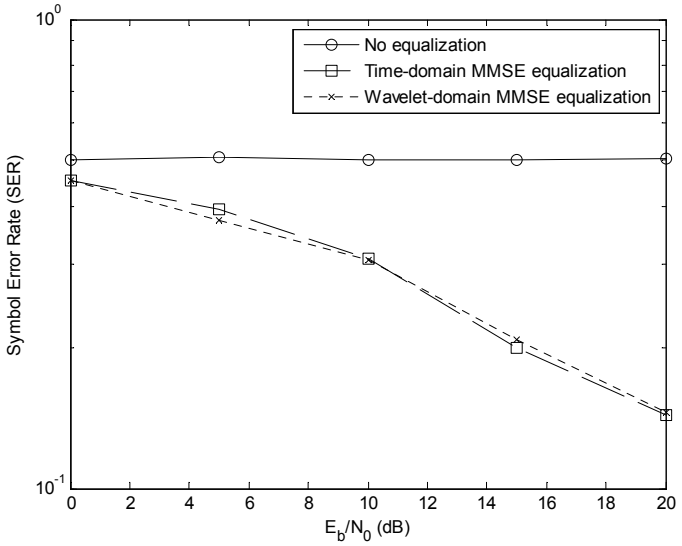

Fig. 8.2.5. SER curves for BFSK, with MMSE equalization.

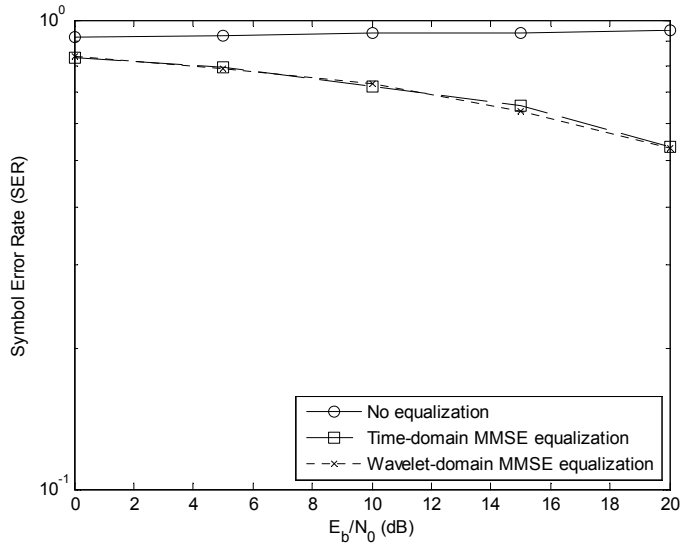

Fig. 8.2.6. SER curves for 16-QAM, with MMSE equalization.

It is seen in Figs. 8.2.1-8.2.3 that the errors in symbol recovery for all three modulation schemes reduce in number as the noise power decreases. In all three cases the systems using DWT-based MMSE equalization perform as well as corresponding systems that use discrete time-domain-based equalization.

These results, being statistically significant, verify the predictions that were made based on the underlying hypothesis of this chapter, i.e., communications systems that use DWT-based MMSE equalization performs as well as similar systems that use discrete time-domain-based MMSE equalization.

8.3 Receiver with Wavelet-Based Zero-Forcing Equalization

Having validated the predictions of the performance DWT-based MMSE equalization in communications systems, the next prediction involves DWT-based ZFE. An important consideration in this case is that the impulse response of the channel is assumed to be known *a priori*, and is available at the receiver for the generation of the equalizer filter tap coefficients.

It has been demonstrated in Chapter 7 that DWT-based ZFE is a perfectly viable and practicable signal processing strategy that performs as well as discrete time-domain-based ZFE. Therefore, the natural progression stemming from this observation, in the context of this dissertation, is to place a DWT-based ZFE in a communications system and to evaluate the performance of such the new system. Such a system can be compared with one that contains a discrete time-domain-based ZFE instead of a DWT-based ZFE.

The prediction in this case is that the performance of both systems, implemented for BASK, BFSK, and 16-QAM modulation schemes, will be statistically similar. The performance of the systems is characterized once again with the use of SERs.

The control experiments are the operation of communications systems implementing BASK, BFSK, and 16-QAM, that do not implement any equalization strategy.

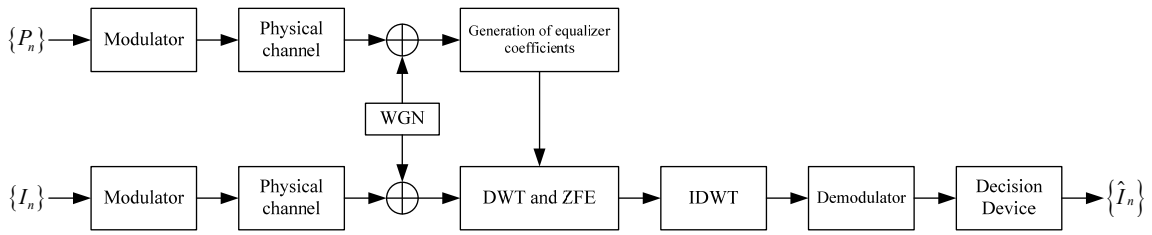

Fig. 8.3.1. Communications system with DWT-based ZFE.

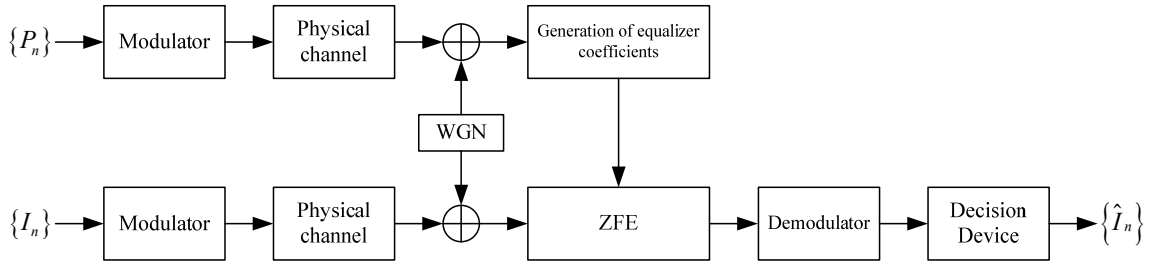

Fig. 8.3.2. Communications system with discrete time-domain-based ZFE.

System-level block diagrams of the two communications systems that are used in this section are illustrated in Figs. 8.3.1 and 8.3.2. The system used in the control experiment is exactly same as the one used in Section 8.2, and is shown in Fig. 8.2.3.

Results

The SERs obtained for the systems implementing BASK, BFSK, and 16-QAM with ZFE equalization are presented graphically in Figs. 8.3.3-8.3.5, respectively.

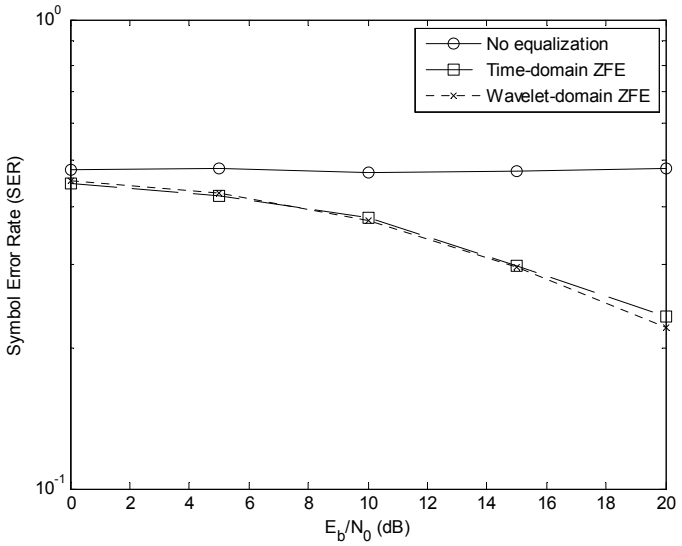

Fig. 8.3.3. SER curves for BASK, with ZFE but no channel estimation.

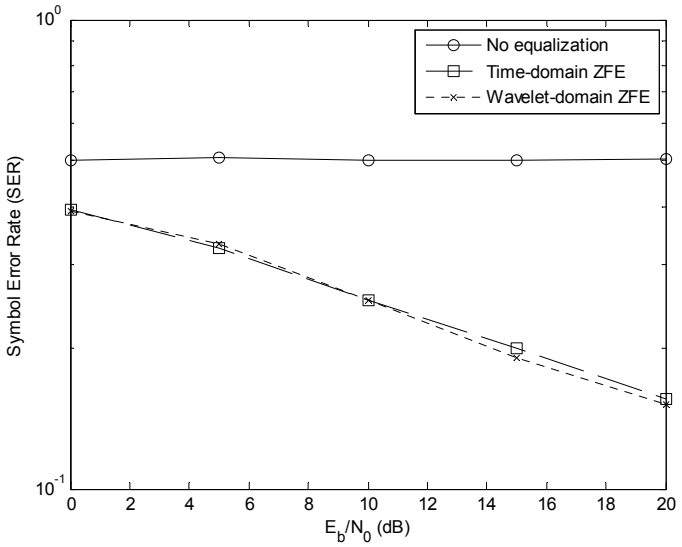

Fig. 8.3.4. SER curves for BFSK, with ZFE but no channel estimation.

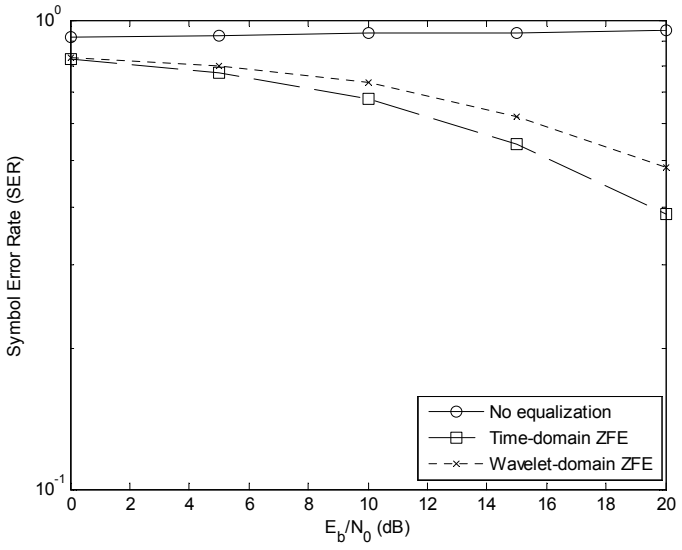

Fig. 8.3.5. SER curves for 16-QAM, with ZFE but no channel estimation.

Again, the results of the simulations validate the prediction that was postulated: the performance of communications systems using DWT-based ZFE, such that the channel impulse response is known *a priori*, is essentially identical to systems using, standard, discrete time-domain-based ZFE.

8.4 Receiver with Wavelet-Based Zero-Forcing Equalization and Channel Estimation

This final application of DWT-based signal processing strategies in communications systems involves the use of the DWT-based channel estimation procedure developed in Chapter 6 and the DWT-based ZFE procedure from Chapter 7.

In this case the impulse response is assumed to not be known *a priori*, but must be estimated by the receiver *a posteriori*. As is required to accomplish this task, pilot signals are used. The specific procedures have been described in Chapter 6.

In Chapter 6 it was shown that DWT-based deconvolution is statistically comparable in performance to standard discrete time-domain deconvolution at all levels of resolution when signals are corrupted by low-power noise. It was also seen, however, that when more powerful noise is added to signals, resulting in E_b/N_0 values in the range of 0 dB to 20 dB, DWT-based deconvolution at high levels of resolution is very prone to errors.

The prediction for this experiment is: DWT-based channel estimation at a low level of resolution and DWT-based ZFE can be implemented in communications systems such that the performance of the systems is statistically comparable to similar systems with discrete time-domain-based channel estimation and ZFE.

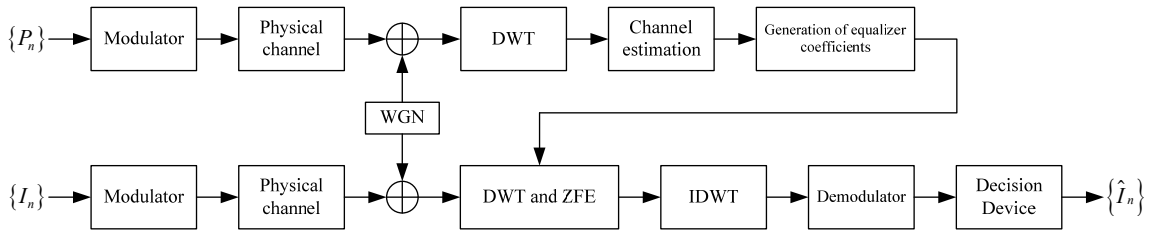

Fig. 8.4.1. Communications system with DWT-based channel estimation and ZFE.

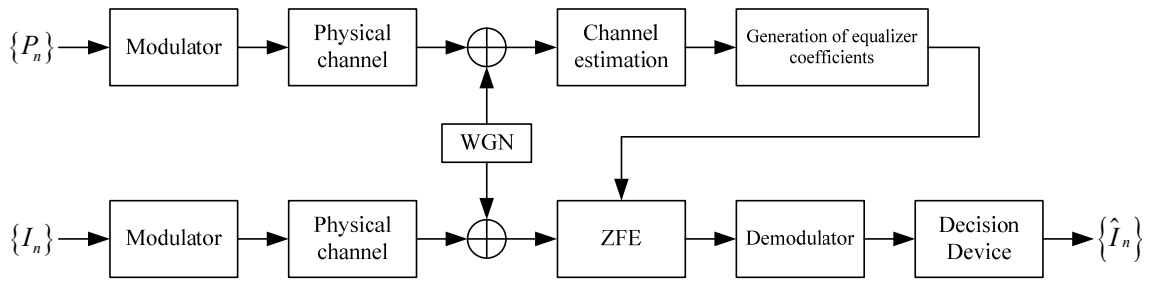

Fig. 8.4.2. Communications system with discrete time-domain-based channel estimation and ZFE.

Block diagrams of these systems are provided in Figs. 8.4.1 and 8.4.2. The control experiment is, again, the case where no equalization is implemented for any of the three modulations schemes. The general block diagram for this system is illustrated in Fig. 8.1.3.

The DWT is carried out to one level of resolution, and the estimate of channel impulse responses are obtained by deconvolution of the undecimated detail coefficients of the received pilot signal and the corresponding coefficients of an uncorrupted copy of pilot signal. This procedure was described in Chapter 6.

Results

The SERs obtained from simulations of the BASK system are illustrated graphically in Fig. 8.4.3, of BFSK in Fig. 8.4.4, and of 16-QAM in Fig. 8.4.5.

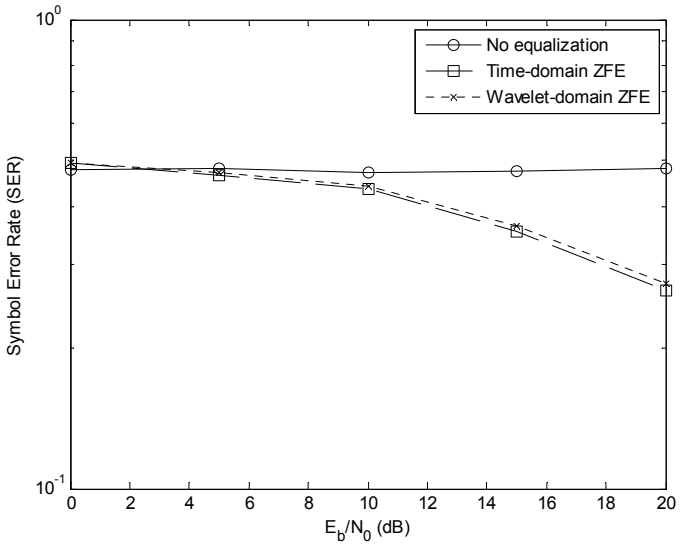

Fig. 8.4.3. SER curves for BASK, with ZFE and channel estimation.

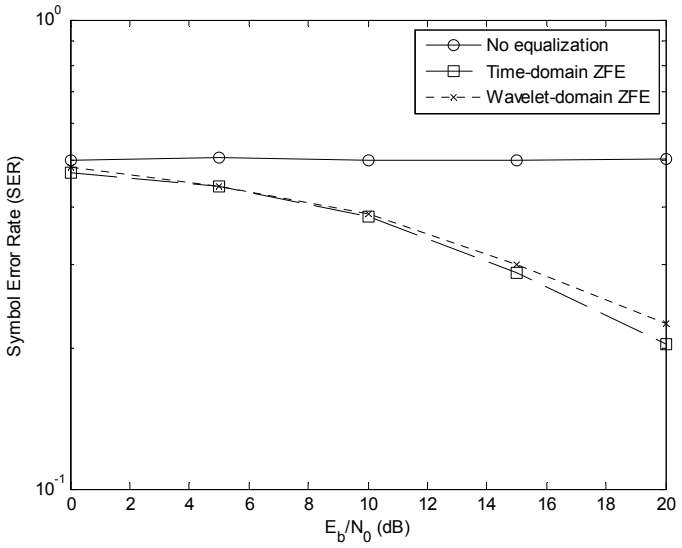

Fig. 8.4.4. SER curves for BFSK, with ZFE and channel estimation.

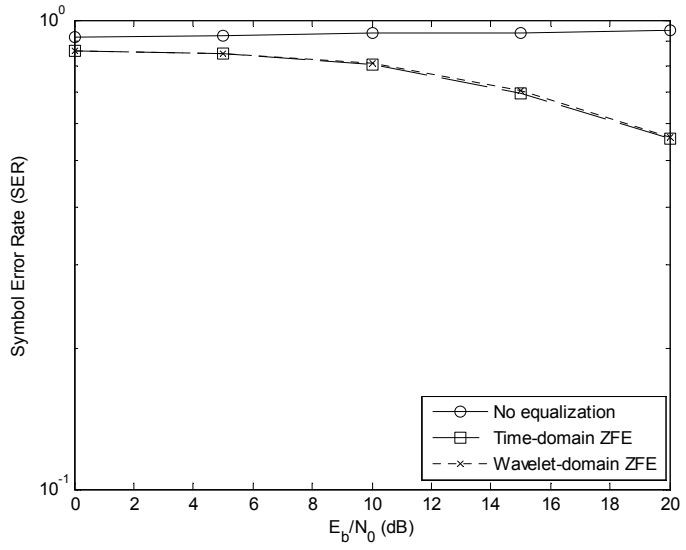

Fig. 8.4.5. SER curves for 16-QAM, with ZFE and channel estimation.

In this third scenario as well the Monte Carlo simulation results verify the predictions that were made. Communications systems that implement both DWT-based channel estimation and DWT-based ZFE offer identical performance as systems that contain discrete time-domain-based channel estimation and ZFE, as seen in Figs. 8.4.3-8.4.5.

This is the case regardless of whether the modulation scheme implemented is BASK, BFSK, or 16-QAM, as evidenced by the SER curves in Figs. 8.4.3-8.4.5. Also, as expected, the systems that include channel estimation and equalization perform better than systems that do not use these signal processing strategies.

.

8.5 Summary

The primary hypothesis posited at the beginning of this chapter was that DWT-based channel estimation and equalization strategies can be successfully introduced into communications systems. The secondary hypothesis dealt with the degree of such success. In particular, it was predicted that the performance of communications systems with DWT-based sub-systems would be comparable to the performance of corresponding systems with discrete time-domain-based channel estimation and equalization.

The results of the simulation experiments presented in this chapter validate both hypotheses. The performance of the two classes of communications systems, with DWT-based sub-systems and with discrete time-domain-based sub-systems, is consistently similar for the cases of:

1. BASK, BFSK, and 16-QAM modulation schemes.
2. AWGN resulting in the range of E_b/N_0 values from 0 dB to 20 dB
3. Slow fading Gaussian channel (d = 2.5).

It has thus been shown that DWT-based channel estimation, MMSE equalization, and ZFE can indeed be used within communications systems as replacements for the corresponding time-domain sub-systems. The drawback in the utility of these signal processing strategies is the additional computation complexity of the DWT and the IDWT. The accuracy of these alternative methods, however, is statistically identical to similar discrete time-domain-based strategies.

Chapter 9

Conclusions

The conclusion of this dissertation is composed of three sub-sections. Each is a reflection of the research that has been presented from differing points of view.

In the first section, 9.1, is a summary in which the salient features of each research topic addressed in this dissertation are highlighted. Insight that has been gained during the development of each topic, as well as regarding the efficacy and utility of the Wavelet Platform for communications systems is discussed as well.

Section 9.2 is a commentary on the limitations of the work in its current state. The individual parts as well as the dissertation as a whole are viewed critically in order to provide a measure of objectivity in evaluating the success of the research. Possible extensions of this thesis are discussed in the final section, Section 9.3.

9.1 Summary

In response to the six primary objectives that were identified in Section 1.2, the following observations are in order:

1. It is indeed possible to estimate the time-domain impulse response on an unknown communications channel using a DWT-based approach, in Chapter 6.

2. A methodology for DWT-based channel estimation has been subsequently developed, in Chapter 6.
3. It has been shown that DWT-based channel equalization is indeed possible, as shown in Chapter 7.
4. A procedure for DWT-based channel equalization has been developed and verified in Chapter 7.
5. Combinations of DWT-based channel equalization and estimation procedures have been incorporated into communications systems, and the efficacy of these new systems has been established in Chapter 8.
6. The performance of DWT-based estimation and equalization techniques, as well as communications systems that include such techniques, have been compared in Chapters 6, 7, and 8, respectively.
7. All analytical formulations been verified and simulations experiments have been carried using the MATLAB simulation environment [102-107].

Convolution Using the DWT

Four equivalent methods for convolving discrete time-domain signals within a DWT framework have been described in Chapter 5. Three of these four methods have been developed in this dissertation. These are the Forward Merge Approach, and the Backward and Forward Merge Approaches with the use of polyphase filtering. Each method has been described with the aid of analytical formulations using system-theoretic concepts, and has also been presented in the form of filter bank block diagrams as well.

A useful feature of the DWT-based convolution procedures presented in this dissertation is that they make use of a filter bank approach, and can be readily implemented in engineering applications. This fact is significant since none of the alternative wavelet transform-based convolution methods surveyed in Chapter 3 lend themselves to use in practical applications such as the Wavelet Platform for reconfigurable radios.

DWT-Based Channel Estimation

Following the development of DWT-based convolution a procedure for DWT-based deconvolution was developed in Chapter 6. The method of deconvolution makes use of one of the four equivalent methods of convolution, viz., the Forward Merge Approach. The procedure has been described analytically, and has also been depicted pictorially using block diagrams.

This deconvolution procedure uses a partial DWT analysis operation instead of standard DWT analysis. In the partial DWT analysis the wavelet coefficients at all levels of resolution are not decimated by the appropriate dyadic factor. Instead, the undecimated DWT coefficients are used for the purposes of deconvolution, which immediately yield the desired channel impulse response.

Deconvolution of the DWT coefficients is then carried out at each level of resolution, as explained in Section 6.1, in the same manner that standard discrete time-domain deconvolution is performed, e.g., with Toeplitz matrix formulations coupled with Gaussian elimination or the Levinson-Durbin algorithm.

The resulting methodology has been applied to test signals in conjunction with ten different channel scenarios. Five channel models have been used, with each channel defined to reflect fast fading and for slow fading conditions. The faded test signals have also been corrupted by AWGN of varying power levels. Results of Monte Carlo computer simulations of the DWT-based deconvolution procedure applied to each of the ten scenarios provided consistent results that were both statistically significant and interesting.

It is seen that an unknown channel impulse response can be obtained completely by applying the deconvolution procedure to the wavelet coefficients at any one level of resolution. It is also seen that the accuracy of the estimate differs between levels.

In the case where very small amounts of WGN have been added to a signal the channel estimates at all levels of resolution are asymptotically identical to within a small degree of uncertainty. In the cases of powerful AWGN, however, the most accurate channel estimates are obtained from the detail coefficients at the first level of resolution. The estimates obtained from the approximation coefficients at the finest level of resolution are also almost as accurate. The accuracy of the estimates obtained from the detail coefficients at all other levels decreases as the resolution becomes finer.

Therefore, the optimal procedure is to obtain a channel estimate at the coarsest level of resolution using the DWT-based approach.

DWT-Based Channel Equalization

Based on the theory of DWT-based convolution a general procedure for channel equalization within a DWT framework has been developed in Chapter 6. Specifically, the Forward Merge Approach has been used. As a result, MMSE equalization and ZFE have been implemented using DWT convolution. DWT-based equalization, like DWT-based channel estimation, has been developed as a general signal processing strategy that can be used in any application deemed appropriate.

The emphasis in this dissertation, however, is on the application of these signal processing strategies in communication systems. Therefore, the validation of the efficacy of DWT-based channel equalization is carried out with test signals that are transmitted over a channel with a Gaussian PDP as well as AWGN.

The two methods of equalization have been applied using the DWT in a series of Monte Carlo simulations. The results obtained show that the accuracy of DWT-based channel equalization is essentially identical to corresponding standard discrete time-domain equalization.

This observation is significant in the context of the Wavelet Platform. It was previously unknown whether DWT-based equalization was possible, and, if so, with what measure of accuracy. It is now known that this procedure can indeed be used as a component of the Wavelet Platform, and both MMSE equalization and ZFE can both be used with excellent accuracy.

Communications Receivers with Wavelet-Based Sub-Systems

The ultimate intention of developing DWT-based signal processing strategies was so that they can be applied directly in communications systems. This was accomplished in Chapter 8. Three types of systems were selected:

1. A receiver with DWT-based MMSE equalization;
2. A receiver with DWT-based ZFE, but with the channel assumed known *a priori*;
3. A receiver with DWT-based channel estimation and DWT-based ZFE.

Each system was specifically implemented to accommodate the BASK, BFSK and 16-QAM modulation schemes, and all test signals were corrupted by AWGN to model the effects of thermal noise sources in communications systems.

The Monte Carlo simulations conducted to evaluate the performance of each of the nine systems showed that the performance of the receivers with DWT-based sub-systems was essentially identical to the corresponding receivers that used standard discrete time-domain sub-systems.

These results are important because they show that wavelet-based channel estimation and equalization are perfectly viable alternatives to existing standard procedures in terms of performance. These results are more significant, however, when the gestalt that is the Wavelet Platform is considered. In this context the results validate the hypothesis that a Wavelet Platform for communication receivers that consists of several wavelet-based signal processing sub-systems can be invented.

Computational Complexities

In the case of, DWT-based convolution, as shown in Chapter 5, the convolution of two discrete-time signals with lengths N_X and N_Y at M levels of DWT resolution requires approximately MN_XN_Y number of multiplications. This order of complexity, $O(N_XN_Y)$, is essentially the same as the order of complexity of standard discrete time-domain convolution, which requires N_XN_Y number of multiplications.

Next, for DWT-based channel estimation a partial DWT is required, with just one level of resolution being sufficient. In this case the excess computational complexity stems from convolving the signal with one analysis filter. For a signal of length N, and a DWT analysis filter of length L, this excess complexity is $O(NL)$. Of course, if the signal length is much greater than a typically-used wavelets, that are short in length, i.e., $N \gg L$, the excess complexity is $\sim O(N)$. This computational complexity is in excess of the complexity of the algorithm that is used for the deconvolution, which would also be used for the deconvolution of the signal in the time-domain as well.

In DWT-based channel equalization, multiple levels of resolution may be desired. Once again, when $N \gg L$, the computational complexity of DWT-based equalization is comparable to discrete time-domain equalization. This is because the DWT-based equalization procedure is based on the efficient DWT-based convolution.

9.2 Future Work

DWT-Based Adaptive Equalization

The topic of wavelet-based adaptive equalization was briefly discussed in Section 7.3. Being that the foundations for DWT-based equalization have been laid in this dissertation, the natural progression would be to extend these to adaptive schemes. Such schemes are very important in contemporary communication systems, and would greatly enhance the value of the Wavelet Platform.

Choice of Wavelets

Throughout this research study the Haar wavelet and wavelets from the Daubechies family have been used. There are, however, many more wavelets that have been well established in the literature. A systematic study in which the performance of DWT-based deconvolution and DWT-based MMSE equalization and ZFE is evaluated with several different wavelets would be useful.

Integration into the Wavelet Platform

Since the Wavelet Platform for reconfigurable radios is the major motivating factor for this research, the performance of DWT-based estimation and equalization in conjunction with wavelet-based de-noising algorithms should be the subject of a significant research study. After that, these strategies must be integrated with wavelet-based Automatic Modulation Recognition and automatic signal demodulation algorithms for a complete realization of the Wavelet Platform.

References

1. P. H. Young, *Electronic Communication Techniques*. Upper Saddle River, NJ: Pearson Prentice Hall, 5th ed., 2004.
2. I. E. Telatar, "Capacity of Multi-Antenna Gaussian Channels," *European Trans. Telecommun.*, vol. 10, No. 6, pp. 585-595, Nov./Dec. 1999.
3. J. G. Proakis, *Digital Communications*, New York, NY: McGraw-Hill, 4th ed., 2001.
4. J. G. Proakis, M. Salehi and G. Bauch, *Contemporary Communication Systems Using MATLAB and Simulink*, Belmont, CA: Thomson-Brooks/Cole, 2nd ed., 2004.
5. A. Paulraj and T. Kailath, "Increasing Capacity in Wireless Broadcast Systems Using Distributed Transmission/Direction Reception (DTDR)," U.S. Patent 5345599, Sep. 1994.
6. Z. Hong, K. Liu, R. W. Heath, Jr. and A. M. Saeed, "Spatial Multiplexing in Correlated Fading via the Virtual Channel Representation," *IEEE J. Sel. Area Commun.*, vol. 21, no. 5, pp. 856-866, Jun. 2003.
7. Z. Salcic and C. F. Mecklenbrauker, "Software Radio-Architectural Requirements, Research and Developmental Challenges," in *Proc. 8th Int. Conf. Commun. Syst.*, Singapore, Nov. 25-28, 2002, vol. 2, pp. 711-716.
8. J. R. MacLeod, T. Nesimoglu, M. A. Beach and P. A. Warr, "Enabling Technologies for Software Defined Radio Transceivers," in *Proc. MILCOM 2002*, Anaheim, CA, Oct. 7-10, 2002, vol. 1, pp. 354-358.

9. S. Rodriguez-Parera, et al., “Front-End ADC Requirements for Uniform Bandpass Sampling in SDR,” in *Proc. 65th IEEE Vehicular Tech. Conf.*, Dublin, Ireland, Apr. 22-25, 2007, pp. 2170-2174.

10. S. Mallat, *A Wavelet Tour of Signal Processing*, San Diego, CA: Academic Press, 2nd ed., 1999.

11. I. Daubechies, *Ten Lectures on Wavelets*, Philadelphia, PA: Society for Industrial and Applied Mathematics, 8th printing, 2004.

12. R. M. Rao and A. S. Bopardikar, *Wavelet Transforms*, Reading, MA: Addison-Wesley, 1998.

13. D. G. Daut, “Development of adaptive agile transceivers,” Research Pre-Proposal Brief, Rutgers, The State University of New Jersey, Nov. 1, 2009.

14. T. H. Lee, *The Design of CMOS Radio-Frequency Integrated Circuits*, New York, NY: Cambridge University Press, 2002 reprint, 2002.

15. C. Sayre, *Complete Wireless Design*, New York, NY: McGraw-Hill, 2001.

16. S. Haykin, *Communication Systems*, New York, NY: John Wiley & Sons, 4th ed., 2001.

17. R. Chang and R. Gibby, "A theoretical study of performance of an orthogonal multiplexing data transmission scheme," *IEEE Trans. Commun.*, vol. 16, no. 4, pp. 529- 540, Aug. 1968.

18. R. W. Chang, "Synthesis of band-limited orthogonal signals for multi-channel data transmission," *Bell Syst. Tech. J.*, vol. 46, pp. 1775-1796, 1966.

19. J.-J. vim de Beek, et al., "OFDM channel estimation by singular value decomposition", *IEEE Trans. Commun.*, vol. 46, no. 7, pp. 931-939, Jul. 1998.

20. G. J. Foschini and M. J. Gans, “On limits of wireless communications in a fading environment when using multiple antennas,” *Wireless Personal Communications*, vol. 6, no. 3, 1998.

21. G. J. Foschini, "Layered space-time architecture for wireless communication in a fading environment When using multi-element antennas," *Bell Labs Tech. J.*, vol. 1, no. 2, Fall 1996.

22. G. J. Foschini, G. D. Golden, R. A. Valenzuela and P. W. Wolniansky, "Simplified processing for high spectral efficiency wireless communication employing multi-element arrays," *IEEE J. Sel. Area Commun.*, vol. 17, no. 11, Nov. 1999.

23. Y. G. Li, J. H. Winters and N. R. Sollenberger," MIMO-OFDM for wireless communications: Signal detection with enhanced channel estimation," *IEEE Trans. Commun.*, vol. 50, no. 9, pp. 1471-1477, Sep. 2002.

24. M. Jiang and L. Hanzo, "Multiuser MIMO-OFDM for next-generation wireless systems," *Proc. IEEE*, vol. 95, no. 7, pp. 1430-1469, Jul. 2007.

25. H. Bolcskei, "MIMO-OFDM wireless systems: Basics, perspectives, and challenges," *Wireless Commun.*, vol. 13, no. 4, pp. 31-37, Aug. 2006.

26. Y. Ogawa, K. Nishio, T. Nishimura and T. Ohgane, "A MIMO-OFDM system for high-speed transmission," in *Proc. 58th Veh. Technol. Conf.*, Oct. 6-9, 2003, Orlando, FL, vol. 1, pp. 493-497.

27. IEEE 802.11a-1999 Standard. (2007, October). [Online]. Available: http://standards.ieee.org/getieee802/802.11.html

28. ZigBee Specification Document 053474r13. (2007, October). [Online]. Available: http://www.zigbee.org/en/

29. IEEE 802.11b-1999 Standard. (2007, October). [Online]. Available: http://standards.ieee.org/getieee802/802.11.html

30. Bluetooth Specification Version 2.1 + EDR [vol. 0]. (2007, October). [Online]. Available: http://www.bluetooth.com/Bluetooth/Learn/Technology/Specifications/

31. American National Standard ANSI/SCTE 07 2006. Digital Transmission Standard for Cable Television. (2007, October). [Online]. Available: http://www.scte.org/content/index.cfm?pID=102

32. ETSI EN 300 744 V1.5.1 (2004-11). Digital Video Broadcasting (DVB);Framing Structure, Channel Coding and Modulation for Digital Terrestrial Television. (2007, Oct.). [Online]. Available: http://www.etsi.org/WebSite/Standards/Standard.aspx

33. L. Hong and K. C. Ho, "Identification of digital modulation types using the wavelet transform," in *Proc. 1999 Military Commun. Conf.*, Atlantic City, NJ, Oct. 31 - Nov. 3, 1999, vol. 1, pp. 427-431.

34. E. Azzouz and A. K. Nandi, *Automatic Modulation Recognition of Communication Signals*, The Netherlands: Kluwer Academic Publishers, 1996.

35. K. M. Ho, C. Vaz and D. G. Daut, "A wavelet-based method for classification of binary digitally modulated signals," in *Proc. 2009 IEEE Sarnoff Symposium*, Princeton, NJ, Mar. 30 - Apr. 1, 2009.

36. K. M. Ho, “Automatic Recognition and Demodulation of Digitally Modulated Communications Signals Using Wavelet-Domain Templates,” Ph.D. Dissertation, Dept. Elect. and Comput. Engg., Rutgers, The State University of New Jersey, Piscataway, NJ, January 2010.

37. A. V. Oppenheim, R.W. Schaefer and J. R. Buck, *Discrete-Time Signal Processing*, Upper Saddle River, NJ: Prentice Hall, 2nd ed., 1999.

38. C. Vaz and K. M. Ho, "Illustrative Conceptualization of the Wavelet Platform," Technical Report 07/09, Dept. Elect. and Comput. Engg., Rutgers, The State University of New Jersey, Piscataway, NJ, 2009.

39. D. L. Donoho, “De-noising by soft-thresholding,” *IEEE Trans Inform. Theory*, vol. 41, no. 3, pp. 613-627, May 1995.

40. I. M. Johnstone and B. W. Silverman, “Wavelet threshold estimators for data with uncorrelated noise,” *J. Royal Statist. Soc.*, vol. 59, no. 2, pp. 319-351, 1997.

41. M. Jansen, M. Malfait and A. Bultheel, “Generalized cross validation for wavelet thresholding,” *Signal Proc.*, vol. 56, no. 1, pp. 33-44, Jan. 1997.

42. K. M. Ho, C. Vaz and D. G. Daut, “Improved demodulation of phase shift keyed signals using wavelet thresholding,” in *Proc. 2008 IEEE Sarnoff Symposium*, Princeton, NJ, Apr. 28-30, 2008.

43. S. Mallat, “Multiresolution approximation and wavelet orthogonal bases of L2,” *Trans. AMS*, vol. 315, no.1, Sept. 1989.

44. *The Transforms and Applications Handbook*, CRC Press, Inc., Boca Raton, FL, 1996.

45. F. Xiong, *Digital Modulation Techniques*, Boston, MA: 2nd ed., Artech House Publishers, 2006, p. 547.

46. G. Beylkin, R. Coifman and V. Rokhlin, "Fast wavelet transforms and numerical algorithms I," *Commun. Pure Appl. Math.*, vol. XLIV, pp. 141-183, 1991.

47. G. Beylkin, "Wavelets, multiresolution analysis and fast numerical algorithms," A draft of INRIA lectures, May, 1991.

48. G. Beylkin, R. Coifman and V. Rokhlin, "Wavelets in numerical analysis," in *Wavelets and their applications*, Boston, MA: Jones and Bartlett, 1992, pp. 181-210.

49. G. Beylkin, "On the representation of operators in bases of compactly supported wavelets," *SIAM J. Num. Anal.*, vol. 29, no. 6, pp. 1716-1740, Dec. 1992.

50. G. Beylkin, "Wavelets and Fast Numerical Algorithms," in *Proc. Symp. Appl. Math.*, 1993, vol. 47, pp. 89-117.

51. G. Beylkin and N. Saito, "Wavelets, their autocorrelation functions, and multiresolution representation of signals," in *Proc. SPIE*, *Intell. Robot. and Comput. Vis. XI*, 1992, vol. 1826, pp. 39-50.

52. G. Beylkin and B. Torresani, "Implementation of operators via filter banks, hardy wavelets and autocorrelation shell," *Appl. and Comput. Harm. Anal.*, vol. 3, pp.164-185, 1996.

53. S. Barmada and M. Raugi, "Transient numerical solutions of nonuniform MTL equations with nonlinear loads by wavelet expansion in time or space domain," *IEEE Trans. Circuits Syst. I., Fundam. Theory Appl.*, vol. 47, no. 8, pp. 1178-1190, Aug. 2000.

54. S. Barmada, A. Musolino, M. Raugi, "Wavelet-based time-domain solution of multiconductor transmission lines with skin and proximity effect," *IEEE Trans. Electromagn. Compat.*, vol. 47, no. 4, pp. 774-780, Nov. 2005.

55. S. Barmada, "Wavelet expansion methods for the numerical analysis of transmission lines," Ph.D. dissertation, Dipartimento di Sistemi Elettrici e Automazione, Universita degli studi di Pisa, Pisa, Italy, 2000.

56. S. Grivet-Talocia, "Adaptive transient Solution of nonuniform multiconductor transmission lines using wavelets," *IEEE. Trans. Antennas Propag.*, vol. 48, no. 10, pp. 1563-1573, Oct. 2000.

57. Stefano Grivet Talocia, "Wavelet-based numerical methods for the solution of the nonuniform multiconductor transmission lines," Ph.D. dissertation, Politecnico di Torino, Turin, Italy, 1998.

58. P. P. Vaidyanathan, "Multirate digital filters, filter banks, polyphase networks, and applications: A tutorial," *Proc. IEEE*, vol. 78, no. 1, pp. 56-93, Jan. 1990.

59. P. P. Vaidyanathan, "Orthonormal and biorthonormal filter banks as convolvers, and convolutional coding gain," *IEEE Trans. Signal Process.*, vol. 41, no. 6, pp. 2110-2130, Jun. 1993.

60. S.-M. Phoong and P. P. Vaidyanathan, "The biorthonormal filter bank convolver, and application in low sensitivity FIR filter structures," in *Proc. 1993 Int. Conf. Acoustics, Speech, and Signal Process.*, Apr. 27-30, 1993, vol. 3, pp.165-168.

61. T. Chen and P. P. Vaidyanathan, "Vector space framework for unification of one- and multidimensional filter bank theory," *IEEE Trans. Signal Process.*, vol. 42. no. 8, pp. 2003-2021, Aug. 1994.

62. H. Guo and C. S. Burrus, "Convolution using the undecimated discrete wavelet transform," in *Proc. 1996 IEEE Int. Conf. Acoustics, Speech, Signal Process.*, 1996, vol. 3, pp. 1291-1294.

63. A. F. Perez-Rendon and R. Robles, "The convolution theorem for the continuous wavelet transform," *Signal Process.*, vol. 84, pp. 55-67, 2004.

64. M. K. Tsatsanis and G. B. Giannakis, "Time-varying system identification and model validation using wavelets," *IEEE Trans. Signal Process.*, vol. 41, no. 12, Dec. 1993.

65. M. K. Tsatsanis and G. B. Giannakis, "Blind identification of time-varying channels using second-order statistics," *Conf. Record Twenty-Ninth Asilomar Conf. Signal, Syst., Comput.*, Pacific Grove, CA, Oct 30 - Nov 2, 1996, vol. 1, pp. 162-166.

66. M. K. Tsatsanis and G. B. Giannakis, "Subspace methods for blind estimation of time-varying FIR channels," *IEEE Trans. Signal Process.*, vol. 45, no. 12, pp. 3084-3093, Dec. 1997.

67. G. T. Zhou , Y. Kim and G. B. Giannakis, "Estimation and equalization of time-selective fading channels," in *Conf. Record Thirty-Third Asilomar Conf. Signal Syst. Comput.*, Pacific Grove, CA, Oct. 24-27, 1999, vol. 1, pp. 248-252.

68. M. Martone, "Wavelet-based separating kernels for sequence estimation with unknown rapidly time-varying channels," *IEEE Commun. Lett.*, vol. 3, no. 5, Mar. 1999.

69. M. Martone, "Wavelet-based separating kernels for array processing of cellular DS/CDMA signals in fast fading," *IEEE Trans. Commun.*, vol. 48, no. 6, pp. 979-995, Jun. 2000.

70. M. Martone, "Multiresolution sequence detection in rapidly fading channels based on focused wavelet decompositions," *IEEE Trans. Commun.*, vol. 49, no. 8, pp. 1388-1401, Aug. 2001.

71. M. Doroslovacki and L. Stankovic, "Wavelet-based communication channel modeling and identification," *Proc. SPIE*, vol. 4738, pp. 64-78, 2002.

72. H. Harada, M. Hernandez and R. Kohno, "Channel estimation for wavelet packet based UWB transmissions," in *Proc. 9th IEEE Symp. Spread Spectrum Tech. Appl.*, pp.178-182, 2006.

73. S. M. S. Sadough, M. M. Ichir, E. Jaffrot, P. Duhamel, "Multiband OFDM UWB channel estimation via a wavelet based EM-MAP algorithm," in *Proc. 7th IEEE Workshop Signal Process. Adv. Wireless Commun.*, Jul. 2-5, 2006, pp.1-5.

74. H. Luo and Y. Li, "The application of blind channel identification techniques to prestack seismic deconvolution," *Proc. IEEE*, vol. 86, no. 10, pp. 2082-2089, Oct. 1998.

75. A. Quinquis and D. Boulinguez, "Multipath channel identification with wavelet packets," *IEEE J. Ocean. Eng.*, vol. 22, no. 2, pp. 342-346, Apr. 1997.

76. T. Ogunfunmi and L. Dang, "Performance analysis of wavelet transform-based adaptive filtering," in *Conf. Record Twenty-Eighth Asilomar Conf. Signals, Syst., Comput.*, Pacific Grove, CA, Oct. 31-Nov. 2, 1994, vol. 1, pp. 288-292.

77. F. Liu, J. Cheng, J. Xu and X. Wang, "Wavelet based adaptive equalization algorithm," in *Proc. 1997 Global Telecommun. Conf.*, Phoenix, AZ, Nov. 3-8, 1997, vol. 3, pp. 1230-1234.

78. F. Liu, J. Cheng, and X. Wang, "A new kind of equalizer based on orthonormal wavelets," *J. Electron.*, vol. 16, no. 1, pp. 38-43, Jan. 1999.

79. A. M. Jalil, H. Amindavar and F. Almasganj, "Subband blind equalization using wavelet filter banks," in *Proc. 2005 IEEE Int. Symp. Circuits Syst.*, May 23-26, 2005, vol. 6, pp. 5730-5733.

80. X. Niu, "Research of discrete wavelet transform domain adaptive equalization algorithm," in *Proc. 8th Int. Conf. Signal Process.*, Beijing, China, Nov. 16-20, 2006, vol. 1.

81. D. Cariolaro and L. Favalli, "Recovery of ISI channels using multiresolution wavelet equalization," in *Proc. 2002 Int. Conf. Commun.*, New York, NY, Apr. 28-May 2, 2002, pp. 74-78.

82. M. R. Petraglia and J. C. B. Torres, "Performance analysis of adaptive filter structure employing wavelet and sparse subfilters," *IEE Proc. Vis., Image, Signal Process.*, vol. 149, no. 2, pp. 115-119, Apr. 2002.

83. N. G. Prelcic, F. P. Gonzalez and M. E. D. Jimenez, "Wavelet packet-based subband adaptive equalization," *Signal Process.*, vol. 81, pp. 1641-1662, 2001.

84. S. Narayan, A. Peterson and M. Narasimha, "Transform domain LMS algorithm," *IEEE Trans. Acoust., Speech, Signal Process.*, vol. 31, no. 3, pp. 609-615, Jun. 1983.

85. M. K. Tsatsanis and G. B. Giannakis, "Time-varying channel equalization using multiresolution analysis," in *Proc. 1992 IEEE Int. Symp. Time-Freq. Time-Scale Anal.*, Victoria, BC, Canada, Oct. 4-6, 1992, pp. 447-450.

86. M. Doroslovacki and H. Fan, "Wavelet-based adaptive filtering," in *Proc. 1993 IEEE Int. Conf. Acoust., Speech, Signal Process.*, Minneapolis, MN, Spr. 27-30, 1993, vol. 3, pp. 488-491.

87. P.-R. Chang and B.-F. Yeh, "Nonlinear communication channel equalization using wavelet neural networks," in *Proc. 1994 IEEE World Congress Comput. Intell. Neural Netw.*, Orlando, FL, Jun. 27-Jul. 2, 1994, vol. 6, pp. 3605-3610.

88. S. He and Z. He, "Blind equalization of nonlinear communication channels using recurrent wavelet neural networks," in *Proc. 1997 IEEE Int. Conf. Acoust., Speech, Signal Process.*, Munich, Germany, Apr. 21-24, 1997, vol. 4, pp. 3305-3308.

89. M. Jiang, et al., "Wavelet neural networks for adaptive equalization," in *Proc. 6th Intl. Conf. Signal Process.*, Aug. 26-30, 2002, vol. 2, pp. 1251-1254.

90. M. Jiang, D. Yuan and S. Sun, "Varying scales wavelet neural network based on entropy function and its application in channel equalization," in *Advances in Neural Networks*, vol. 3498, Berlin, Germany: Springer-Verlag, 2005, pp. 326-331.

91. A. K. Pradhan, S. K. Meher and A. Routray, "Communication channel equalization using wavelet network," *Digit. Signal Process.*, vol. 16, pp. 445-452, 2006.

92. T. K. Sarkar, et al., "A tutorial on wavelets from an electrical engineering perspective, Part 1: discrete wavelet techniques," *IEEE Antennas Propag. Mag.*, vol. 40, no. 5, pp. 49-68, Oct. 1998.

93 S. G. Mallat, "Multifrequency channel decompositions of images and wavelet models," *IEEE Trans. Acoust., Speech, Signal Process.*, vol. 37, no. 12, pp. 2091-2110, Dec. 1989.

94. R. E. Crochiere and L. R. Rabiner, *Multirate Digital Signal Processing*, Englewood Cliffs, NJ: Prentice-Hall, 1983.

95. G. H. Golub and C. F. van Loan, *Matrix Computations*, The Johns Hopkins University Press, Baltimore, MD: 3rd ed., p. 201, 1996.

96. MATLAB Documentation, Mathematics, pp. 101-110, The MathWorks, Inc., Natick, MA, 2009.

97. J. C.-I. Chuang, "The effects of time delay spread on portable radio communications channels with digital modulation," *IEEE J. Sel. Areas Commun.*, vol. SAC-5, no. 5, Jun. 1987.

98. M. Loeve, *Probability Theory I*, Graduate Texts in Mathematics, Ann Arbor, MI: Springer-Verlag, 1977, 4th ed., vol. 45, p. 12.

99. E. Kreyszig, *Advanced Engineering Mathematics*, John Wiley & Sons (Asia) Pte. Ltd., 2003: 8th ed., p. 1109.

100. S. Orfanidis. (2007). *Optimum Signal Processing: An Introduction* (2nd ed.) [Online]. Available: http://www.ece.rutgers.edu/~orfanidi/osp2e

101. M. L. Honig and D. G. Messerschmitt, *Adaptive Filters: Structures, Algorithms, and Applications*. Hingham, MA: Kluwer Academic Publishers, 1985, pp. 6-7.

102. C. Vaz, "MATLAB code for communications systems," Technical Report TR-DCITL-01, Dept. Elect. and Comput. Engg., Rutgers, The State University of New Jersey, Piscataway, NJ, 2009.

103. C. Vaz, "MATLAB code for equalizers," Technical Report TR-DCITL-02, Dept. Elect. and Comput. Engg., Rutgers, The State University of New Jersey, Piscataway, NJ, 2009.

104. C. Vaz, "MATLAB code for fading channels," Technical Report TR-DCITL-03, Dept. Elect. and Comput. Engg., Rutgers, The State University of New Jersey, Piscataway, NJ, 2009.

105. C. Vaz, "MATLAB code for miscellaneous functions," Technical Report TR-DCITL-04, Dept. Elect. and Comput. Engg., Rutgers, The State University of New Jersey, Piscataway, NJ, 2009.

106. C. Vaz, "MATLAB code for wavelet-based convolution," Technical Report TR-DCITL-05, Dept. Elect. and Comput. Engg., Rutgers, The State University of New Jersey, Piscataway, NJ, 2009.

107. C. Vaz, "MATLAB code for wavelet-based equalization," Technical Report TR-DCITL-06, Dept. Elect. and Comput. Engg., Rutgers, The State University of New Jersey, Piscataway, NJ, 2009.

Appendix A

The Levinson-Durbin Recursion Algorithm for Non-Hermitian Toeplitz Matrix Equations

Consider the case where the scalars $r_1, r_2, \ldots, r_{n-1}$, $p_1, p_2, \ldots, p_{n-1}$ and $b_1, b_2, \ldots, b_{n-1}$ are known, and they form a system of linear equations, $\mathbf{Tx} = \mathbf{b}$, which is of the form

$$\underbrace{\begin{bmatrix} 1 & r_1 & r_2 & \cdots & r_{n-1} \\ p_1 & 1 & r_1 & \cdots & r_{n-2} \\ p_2 & p_1 & 1 & \cdots & r_{n-3} \\ \vdots & \vdots & \vdots & \ddots & \vdots \\ p_{n-1} & p_{n-2} & p_{n-3} & \cdots & 1 \end{bmatrix}}_{\mathbf{T}} \underbrace{\begin{bmatrix} x_1 \\ x_2 \\ x_3 \\ \vdots \\ x_{n-1} \end{bmatrix}}_{\mathbf{x}} = \underbrace{\begin{bmatrix} b_1 \\ b_2 \\ b_3 \\ \vdots \\ b_{n-1} \end{bmatrix}}_{\mathbf{b}}. \tag{A1}$$

The matrix **T** is a non-Hermitian Toeplitz matrix, the elements of which are known, x is vector, the elements of which are unknown and are to be solved for, and b is a vector, the elements of which are known.

In order to find the unknown vector **x**, the leading principle sub-matrices $\mathbf{T}_k = \mathbf{T}(1:k, 1:k)$, $k = 1:n-1$, must be non-singular.

From the matrix **T**, three systems of equations, which need to be solved, can be described according to

$$\mathbf{T}_k^{\mathrm{T}}\mathbf{y} = -\mathbf{r} = -\left[r_1\, r_2 \ldots r_k\right]^{\mathrm{T}}, \tag{A2}$$

$$\mathbf{T}_k\mathbf{w} = -\mathbf{p} = -\left[p_1\, p_2 \ldots p_k\right]^{\mathrm{T}}, \tag{A3}$$

and

$$\mathbf{T}_k\mathbf{x} = \mathbf{b} = \left[b_1\, b_2 \ldots b_k\right]^{\mathrm{T}}. \tag{A4}$$

It is worthy to note that (A2) and (A3) are the Yule-Walker equations.

An $n \times n$ exchange matrix, $\mathbf{E}$, in which the elements on the counterdiagonal are 1s whereas all other elements are 0s, is defined as

$$E_{i,j} = \begin{cases} 1, & j = n - i \\ 0, & j \neq n - i \end{cases}. \tag{A5}$$

An example of a 4×4 exchange matrix is

$$\mathbf{E} = \begin{bmatrix} 0 & 0 & 0 & 1 \\ 0 & 0 & 1 & 0 \\ 0 & 1 & 0 & 0 \\ 1 & 0 & 0 & 0 \end{bmatrix}. \tag{A6}$$

Now, (A2), (A3) and (A4) can be expressed, respectively, as

$$\mathbf{y} = -\left(\mathbf{T}_k^{\mathrm{T}}\right)^{-1}\mathbf{r}, \tag{A7}$$

$$\mathbf{w} = -\mathbf{T}_k^{-1}\mathbf{p}, \tag{A8}$$

and

$$\mathbf{x} = \mathbf{T}_k^{-1}\mathbf{b}. \tag{A9}$$

In order to solve (A2), (A3) and (A4) an assumption is made that the solution to the kth equation is known.

Now, (A2) can be expressed as

$$\begin{bmatrix} \mathbf{T}_k & \mathbf{E}_k\mathbf{r} \\ \mathbf{p}^{\mathrm{T}}\mathbf{E}_k & 1 \end{bmatrix}^{\mathrm{T}} \begin{bmatrix} \mathbf{z} \\ \alpha \end{bmatrix} = -\begin{bmatrix} \mathbf{r} \\ \mathbf{r}_{k+1} \end{bmatrix}$$

$$\Rightarrow \begin{bmatrix} \mathbf{T}_k & \mathbf{E}_k^{\mathrm{T}}\mathbf{p} \\ \mathbf{r}^{\mathrm{T}}\mathbf{E}_k^{\mathrm{T}} & 1 \end{bmatrix} \begin{bmatrix} \mathbf{z} \\ \alpha \end{bmatrix} = -\begin{bmatrix} \mathbf{r} \\ \mathbf{r}_{k+1} \end{bmatrix}. \tag{A10}$$

The first equation from (A10) is

$$\mathbf{T}_k^{\mathrm{T}}\mathbf{z} + \mathbf{E}_k\mathbf{p}\alpha = -\mathbf{r}$$

$$\Rightarrow \mathbf{z} = -\left(\mathbf{T}_k^{\mathrm{T}}\right)^{-1}\mathbf{r} - \left(\mathbf{T}_k^{\mathrm{T}}\right)^{-1}\mathbf{E}_k\mathbf{p}\alpha. \tag{A11}$$

Substituting y from (A9) into (A11) gives

$$\mathbf{z} = \mathbf{y} - \left(\mathbf{T}_k^{\mathrm{T}}\right)^{-1}\mathbf{E}_k\mathbf{p}\alpha$$

$$\Rightarrow \mathbf{z} = \mathbf{y} - \left(\mathbf{T}_k^{-1}\right)^{\mathrm{T}}\mathbf{E}_k\mathbf{p}\alpha. \tag{A12}$$

Since $\mathbf{T}_k$ is persymmetric, i.e.,

$$\mathbf{T}_k = \mathbf{E}\mathbf{T}_k^{\mathrm{T}}\mathbf{E}, \tag{A13}$$

it follows that

$$\left(\mathbf{T}_k^{-1}\right)^{\mathrm{T}}\mathbf{E}_k = \mathbf{E}_k\mathbf{T}_k^{-1}. \tag{A14}$$

Substituting (A14) into (A12) gives

$$\mathbf{z} = \mathbf{y} - \mathbf{E}_k \mathbf{T}_k^{-1} \mathbf{p} \alpha \,, \tag{A15}$$

and introducing w from (A8) into (A15) results in

$$\boxed{\mathbf{z} = \mathbf{y} + \alpha \mathbf{E}_k \mathbf{w}}. \tag{A16}$$

Now, the second equation from (A10) is

$$\mathbf{r}^{\mathrm{T}} \mathbf{E}_k \mathbf{z} + \alpha = -\mathbf{r}_{k+1}$$

$$\Rightarrow \alpha = -\mathbf{r}_{k+1} - \mathbf{r}^{\mathrm{T}} \mathbf{E}_k \mathbf{z} \,. \tag{A17}$$

Substituting the previously-obtained expression for **z**, from (A16), into (A17) gives

$$\alpha = -\mathbf{r}_{k+1} - \mathbf{r}^{\mathrm{T}} \mathbf{E}_k \left(\mathbf{y} + \alpha \mathbf{E}_k \mathbf{w} \right)$$

$$\Rightarrow \alpha = -\mathbf{r}_{k+1} - \mathbf{r}^{\mathrm{T}} \mathbf{E}_k \mathbf{y} - \mathbf{r}^{\mathrm{T}} \mathbf{E}_k \alpha \mathbf{E}_k \mathbf{w} \,. \tag{A18}$$

Applying the property that the product of an exchange matrix with itself results in an identity matrix, i.e.,

$$\mathbf{E}_k \mathbf{E}_k = \mathbf{I}_k \,, \tag{A19}$$

to (A18) results in the simplified expression

$$\alpha = -\mathbf{r}_{k+1} - \mathbf{r}^{\mathrm{T}} \mathbf{E}_k \mathbf{y} - \alpha \mathbf{r}^{\mathrm{T}} \mathbf{w}$$

$$\Rightarrow \alpha + \alpha \mathbf{r}^{\mathrm{T}} \mathbf{w} = -\left(\mathbf{r}_{k+1} + \mathbf{r}^{\mathrm{T}} \mathbf{E}_k \mathbf{y} \right)$$

$$\Rightarrow \boxed{\alpha = -\frac{\mathbf{r}_{k+1} + \mathbf{r}^{\mathrm{T}} \mathbf{E}_k \mathbf{y}}{1 + \mathbf{r}^{\mathrm{T}} \mathbf{w}}}. \tag{A20}$$

Next, the second Yule-Walker equation, (A3), i.e.,

$$\mathbf{T}_k \mathbf{w} = -\mathbf{p} \,,$$

can be expressed as

$$\begin{bmatrix} \mathbf{T}_k & \mathbf{E}_k\mathbf{r} \\ \mathbf{p}^T\mathbf{E}_k & 1 \end{bmatrix}\begin{bmatrix} \mathbf{u} \\ \nu \end{bmatrix} = -\begin{bmatrix} \mathbf{p} \\ \mathbf{p}_{k+1} \end{bmatrix}. \tag{A21}$$

The first linear equation from this expression is

$$\mathbf{T}_k\mathbf{u} + \mathbf{E}_k\mathbf{r}\nu = -\mathbf{p}$$

$$\Rightarrow \mathbf{u} = -\mathbf{T}_k^{-1}\mathbf{p} - \mathbf{T}_k^{-1}\mathbf{E}_k\mathbf{r}\nu\,. \tag{A22}$$

Introducing **w** from (A8) into (A22) results in the expression

$$\mathbf{u} = \mathbf{w} - \mathbf{T}_k^{-1}\mathbf{E}_k\mathbf{r}\nu\,. \tag{A23}$$

Since $\mathbf{T}_k$ is persymmetric,

$$\mathbf{T}_k^{-1}\mathbf{E}_k = \mathbf{E}_k\left(\mathbf{T}_k^{-1}\right)^{\mathrm{T}}, \tag{A24}$$

(A23) can be written as

$$\mathbf{u} = \mathbf{w} - \mathbf{E}_k\left(\mathbf{T}_k^{-1}\right)^{\mathrm{T}}\mathbf{r}\nu\,. \tag{A25}$$

Furthermore, since

$$\left(\mathbf{T}_k^{\mathrm{T}}\right)^{-1} = \left(\mathbf{T}_k^{-1}\right)^{\mathrm{T}} \tag{A26}$$

and, from (A7), i.e.,

$$\mathbf{y} = -\left(\mathbf{T}_k^{\mathrm{T}}\right)^{-1}\mathbf{r}\,,$$

(A25) can be described in terms of **y** as

$$\boxed{\mathbf{u} = \mathbf{w} + \mathbf{E}_k \mathbf{y} \nu}. \tag{A27}$$

Next, the second equation from (A21) is

$$\mathbf{p}^{\mathrm{T}} \mathbf{E}_k \mathbf{u} + \nu = -\mathbf{p}_{k+1}$$

$$\Rightarrow \nu = -\mathbf{p}_{k+1} - \mathbf{p}^{\mathrm{T}} \mathbf{E}_k \mathbf{u}. \tag{A28}$$

Substituting u from (A27) into (A28) results in the expression

$$\nu = -\mathbf{p}_{k+1} - \mathbf{p}^{\mathrm{T}} \mathbf{E}_k \left(\mathbf{w} + \mathbf{E}_k \mathbf{y} \nu \right)$$

$$\Rightarrow \nu = -\mathbf{p}_{k+1} - \mathbf{p}^{\mathrm{T}} \mathbf{E}_k \mathbf{w} - \mathbf{p}^{\mathrm{T}} \mathbf{E}_k \mathbf{E}_k \mathbf{y} \nu$$

$$\Rightarrow \nu = -\mathbf{p}_{k+1} - \mathbf{p}^{\mathrm{T}} \mathbf{E}_k \mathbf{w} - \mathbf{p}^{\mathrm{T}} \mathbf{y} \nu$$

$$\Rightarrow \nu + \mathbf{p}^{\mathrm{T}} \mathbf{y} \nu = -\mathbf{p}_{k+1} - \mathbf{p}^{\mathrm{T}} \mathbf{E}_k \mathbf{w}$$

$$\Rightarrow \boxed{\nu = -\frac{\mathbf{p}_{k+1} + \mathbf{p}^{\mathrm{T}} \mathbf{E}_k \mathbf{w}}{1 + \mathbf{p}^{\mathrm{T}} \mathbf{y}}}. \tag{A29}$$

Now that recursive solutions for the two Yule-Walker equations have been obtained, the non-Hermitian Toeplitz matrix equation, $\mathbf{T}_k \mathbf{x} = \mathbf{b}$, (A4), can be solved. Similar to the previous two equations, (A4) too can be expanded and expressed in terms of a known reduced-order solution as

$$\begin{bmatrix} \mathbf{T}_k & \mathbf{E}_k \mathbf{r} \\ \mathbf{p}^T \mathbf{E}_k & 1 \end{bmatrix} \begin{bmatrix} \mathbf{v} \\ \mu \end{bmatrix} = \begin{bmatrix} \mathbf{b} \\ \mathbf{b}_{k+1} \end{bmatrix}. \tag{A30}$$

The first equation from (A30) is

$$\mathbf{T}_k \mathbf{v} + \mathbf{E}_k \mathbf{r}\mu = \mathbf{b}$$

$$\Rightarrow \mathbf{v} = \mathbf{T}_k^{-1}\mathbf{b} - \mathbf{T}_k^{-1}\mathbf{E}_k \mathbf{r}\mu \,. \tag{A31}$$

Introducing **x** from (A9) into the expression in (A31) yields

$$\mathbf{v} = \mathbf{x} - \mathbf{T}_k^{-1}\mathbf{E}_k \mathbf{r}\mu \,. \tag{A32}$$

Again, due to the persymmetry of $\mathbf{T}_k$,

$$\mathbf{T}_k^{-1}\mathbf{E}_k = \mathbf{E}_k \left(\mathbf{T}_k^{-1}\right)^{\mathrm{T}}, \tag{A33}$$

which, when substituted in (A32) gives

$$\mathbf{v} = \mathbf{x} - \mathbf{E}_k \left(\mathbf{T}_k^{-1}\right)^{\mathrm{T}} \mathbf{r}\mu \,. \tag{A34}$$

Now, recalling (A7),

$$\mathbf{y} = -\left(\mathbf{T}_k^{\mathrm{T}}\right)^{-1} \mathbf{r} \,,$$

and the property,

$$\left(\mathbf{T}_k^{\mathrm{T}}\right)^{-1} = \left(\mathbf{T}_k^{-1}\right)^{\mathrm{T}}, \tag{A35}$$

which is due to the persymmetry of $\mathbf{T}_k$, (A34) can be rewritten as

$$\mathbf{v} = \mathbf{x} + \mathbf{E}_k \left(\mathbf{T}_k^{\mathrm{T}}\right)^{-1} \mathbf{r}\mu$$

$$\Rightarrow \boxed{\mathbf{v} = \mathbf{x} + \mathbf{E}_k \mathbf{y}\mu}. \tag{A36}$$

Next, the second equation from (A30) is

$$\mathbf{p}^{\mathrm{T}}\mathbf{E}_k\mathbf{v}+\mu=\mathbf{b}_{k+1}$$

$$\Rightarrow \mu=\mathbf{b}_{k+1}-\mathbf{p}^{\mathrm{T}}\mathbf{E}_k\mathbf{v}\,. \tag{A37}$$

Introducing the expression for **v**, from (A36), into (A37) gives

$$\mu=\mathbf{b}_{k+1}-\mathbf{p}^{\mathrm{T}}\mathbf{E}_k\left(\mathbf{x}+\mathbf{E}_k\mathbf{y}\mu\right)$$

$$\Rightarrow \mu=\mathbf{b}_{k+1}-\mathbf{p}^{\mathrm{T}}\mathbf{E}_k\mathbf{x}-\mathbf{p}^{\mathrm{T}}\mathbf{E}_k\mathbf{E}_k\mathbf{y}\mu$$

$$\Rightarrow \mu=\mathbf{b}_{k+1}-\mathbf{p}^{\mathrm{T}}\mathbf{E}_k\mathbf{x}-\mathbf{p}^{\mathrm{T}}\mathbf{y}\mu$$

$$\Rightarrow \mu+\mathbf{p}^{\mathrm{T}}\mathbf{y}\mu=\mathbf{b}_{k+1}-\mathbf{p}^{\mathrm{T}}\mathbf{E}_k\mathbf{x}$$

$$\Rightarrow \boxed{\mu=\frac{\mathbf{b}_{k+1}-\mathbf{p}^{\mathrm{T}}\mathbf{E}_k\mathbf{x}}{1+\mathbf{p}^{\mathrm{T}}\mathbf{y}}}\,. \tag{A38}$$

A recapitulation of the main results of this derivation thus far is composed of the following results:

$$\mathbf{z}=\mathbf{y}+\alpha\mathbf{E}_k\mathbf{w}$$

$$\alpha=-\frac{\mathbf{r}_{k+1}+\mathbf{r}^{\mathrm{T}}\mathbf{E}_k\mathbf{y}}{1+\mathbf{r}^{\mathrm{T}}\mathbf{w}}$$

$$\mathbf{u}=\mathbf{w}+\mathbf{E}_k\mathbf{y}\nu$$

$$\nu=-\frac{\mathbf{p}_{k+1}+\mathbf{p}^{\mathrm{T}}\mathbf{E}_k\mathbf{w}}{1+\mathbf{p}^{\mathrm{T}}\mathbf{y}}$$

$$\mathbf{v}=\mathbf{x}+\mathbf{E}_k\mathbf{y}\mu$$

$$\mu=\frac{\mathbf{b}_{k+1}-\mathbf{p}^{\mathrm{T}}\mathbf{E}_k\mathbf{x}}{1+\mathbf{p}^{\mathrm{T}}\mathbf{y}}\,.$$

Now consider the denominator of the expression for the scalar coefficient α in (A20). Let the denominator be denoted by β, and more specifically by β_k for the kth recursive evaluation of the expression, i.e.,

$$\beta_k = 1 + \left[\mathbf{r}^{(k)}\right]^{\mathrm{T}} \mathbf{w}^{(k)}. \tag{A39}$$

Now, $\mathbf{w}^{(k+1)}$ has been expressed in terms of **u** and ν in (A21) as

$$\mathbf{w}^{(k+1)} = \begin{bmatrix} \mathbf{u}^{(k)} \\ \nu \end{bmatrix} \tag{A40}$$

$$\Rightarrow \mathbf{w}^{(k+1)} = \begin{bmatrix} \mathbf{w}^{(k)} + \mathbf{E}_k \mathbf{y}^{(k)} \nu_k \\ \nu_k \end{bmatrix}, \tag{A41}$$

having substituted the expression for u from (A27) into (A41). Hence, the expression for β_k, in (A39) can be updated as

$$\beta_k = 1 + \begin{bmatrix} \mathbf{r}^{(k-1)^{\mathrm{T}}} & r_k \end{bmatrix} \begin{bmatrix} \mathbf{w}^{(k-1)} + \nu_{k-1} \mathbf{E}_{k-1} \mathbf{y}^{(k-1)} \\ \nu_{k-1} \end{bmatrix}$$

$$\Rightarrow \beta_k = \left(1 + \left[\mathbf{r}^{(k-1)}\right]^{\mathrm{T}} \mathbf{w}^{(k-1)}\right) + \nu_{k-1} \left(\left[\mathbf{r}^{(k-1)}\right]^{\mathrm{T}} \mathbf{E}_{k-1} \mathbf{y}^{(k-1)} + r\right). \tag{A42}$$

Simplifying (A42) with the use of (A39) and (A20) results in the expression

$$\beta_k = \beta_{k-1} + \nu_{k-1} \left(-\alpha_{k-1} \beta_{k-1}\right)$$

$$\Rightarrow \boxed{\beta_k = \beta_{k-1} \left(1 - \alpha_{k-1} \nu_{k-1}\right)}. \tag{A43}$$

In a similar fashion, let γ denote the denominator of the expression for ν in (A29), therefore let γ_k denote the value of the denominator of the k^{th} recursion of ν, i.e.,

$$\gamma_k = 1 + \left[\mathbf{p}^{(k)}\right]^{\mathrm{T}} \mathbf{y}^{(k)}. \tag{A44}$$

Again, since $\mathbf{y}^{(k+1)}$ has been expressed in (A10) as

$$\mathbf{y}^{(k+1)} = \begin{bmatrix} \mathbf{z}^{(k)} \\ \alpha \end{bmatrix}, \tag{A45}$$

and since it has been shown in (A29) that

$$\mathbf{z}^{(k)} = \mathbf{y}^{(k)} + \alpha \mathbf{E}_k \mathbf{w}^{(k)},$$

(A44) can be recast as

$$\gamma_k = 1 + \left[\mathbf{p}^{(k-1)^{\mathrm{T}}} p_k\right] \begin{bmatrix} \mathbf{y}^{(k-1)} + \alpha_{k-1} \mathbf{E}_{k-1} \mathbf{w}^{(k-1)} \\ \alpha_{k-1} \end{bmatrix}$$

$$\Rightarrow \gamma_k = \left(1 + \left[\mathbf{p}^{(k-1)}\right]^{\mathrm{T}} \mathbf{y}^{(k-1)}\right) + \alpha_{k-1} \left(\left[\mathbf{p}^{(k-1)}\right]^{\mathrm{T}} \mathbf{E}_{k-1} \mathbf{w}^{(k-1)} + p_k\right). \tag{A46}$$

Simplifying (A46) with the use of (A44) and (A29) gives

$$\gamma_k = \gamma_{k-1} + \alpha_{k-1}\left(-\nu_{k-1}\gamma_{k-1}\right)$$

$$\Rightarrow \boxed{\gamma_k = \gamma_{k-1}\left(1 - \alpha_{k-1}\nu_{k-1}\right)}. \tag{A47}$$

Finally, let δ denote the denominator of the expression for μ in (A39), let δ_k denote the value of the denominator during the k^{th} recursion of the expression, i.e.,

$$\delta_k = 1 + \left[\mathbf{p}^{(k)}\right]^{\mathrm{T}} \mathbf{y}^{(k)}. \tag{A48}$$

Once again using the expression for $\mathbf{y}^{(k+1)}$ from (A10), i.e.,

$$\mathbf{y}^{(k+1)} = \begin{bmatrix} \mathbf{z}^{(k)} \\ \alpha \end{bmatrix},$$

and the expression for z in (A29), i.e.,

$$\mathbf{z}^{(k)} = \mathbf{y}^{(k)} + \alpha \mathbf{E}_k \mathbf{w}^{(k)},$$

(A48) becomes

$$\delta_k = 1 + \left[\mathbf{p}^{(k-1)^{\mathrm{T}}} p_k \right]^{\mathrm{T}} \begin{bmatrix} \mathbf{y}^{(k-1)} + \alpha_{k-1} \mathbf{E}_{k-1} \mathbf{w}^{(k-1)} \\ \alpha_{k-1} \end{bmatrix}$$

$$\Rightarrow \delta_k = \left(1 + \left[\mathbf{p}^{(k-1)} \right]^{\mathrm{T}} \mathbf{y}^{(k-1)} \right) + \alpha_{k-1} \left(\left[\mathbf{p}^{(k-1)} \right]^{\mathrm{T}} \mathbf{E}_{k-1} \mathbf{w}^{(k-1)} + p_k \right). \tag{A49}$$

Simplifying (A49) using (A48) and (A29) therefore gives

$$\delta_k = \delta_{k-1} + \alpha_{k-1} \left(-\nu_{k-1} \delta_{k-1} \right)$$

$$\Rightarrow \boxed{\delta_k = \delta_{k-1} - \alpha_{k-1} \nu_{k-1} \delta_{k-1}}. \tag{A50}$$

Hence, the denominators of the scalar variables α, ν, and μ, in (A20), (A29), and (A38), respectively, can be updated by using the expressions found in (A43), (A47), and (A50), respectively:

$$\alpha = -\frac{\mathbf{r}_{k+1} + \mathbf{r}^{\mathrm{T}} \mathbf{E}_k \mathbf{y}}{\beta_k}, \tag{A51}$$

$$\nu = -\frac{\mathbf{p}_{k+1} + \mathbf{p}^{\mathrm{T}} \mathbf{E}_k \mathbf{w}}{\gamma_k}, \tag{A52}$$

and

$$\mu = \frac{\mathbf{b}_{k+1} - \mathbf{p}^{\mathrm{T}}\mathbf{E}_k\mathbf{x}}{\delta_k}. \tag{A53}$$

The final set of equations needed to solve the original equation $\mathbf{T}\mathbf{x} = \mathbf{b}$ for $\mathbf{x}$ is:

$$\mathbf{z} = \mathbf{y} + \alpha\mathbf{E}_k\mathbf{w}$$

$$\alpha = -\frac{\mathbf{r}_{k+1} + \mathbf{r}^{\mathrm{T}}\mathbf{E}_k\mathbf{y}}{\beta_k}$$

$$\beta_k = \beta_{k-1}\left(1 - \alpha_{k-1}\nu_{k-1}\right)$$

$$\mathbf{u} = \mathbf{w} + \mathbf{E}_k\mathbf{y}\,\nu$$

$$\nu = -\frac{\mathbf{p}_{k+1} + \mathbf{p}^{\mathrm{T}}\mathbf{E}_k\mathbf{w}}{\gamma_k}$$

$$\gamma_k = \gamma_{k-1}\left(1 - \alpha_{k-1}\nu_{k-1}\right)$$

$$\mathbf{v} = \mathbf{x} + \mathbf{E}_k\mathbf{y}\mu$$

$$\mu = \frac{\mathbf{b}_{k+1} - \mathbf{p}^{\mathrm{T}}\mathbf{E}_k\mathbf{x}}{\delta_k}$$

$$\delta_k = \delta_{k-1} - \alpha_{k-1}\nu_{k-1}\delta_{k-1}.$$

The algorithm is described in pseudocode below.

$y(1) = -r(1);$ $\quad w(1) = -p(1);$ $\quad x(1) = b(1);$

$\beta = 1;$ $\quad \gamma = 1;$

$\alpha = -r(1);$ $\quad \nu = -p(1);$

for $k = 1 : n-1$

$\delta = \delta - \alpha\nu\gamma$;

$\mu = \left(b(k+1) - p(1:k)^{\mathrm{T}}\, x(k:-1:1)\right) \big/ \beta$;

$v(1:k) = x(1:k) + \mu y(k:-1:1)$;

$x(1:k+1) = \begin{bmatrix} v(1:k) & \mu \end{bmatrix}$;

if $k < n-1$

$\gamma = (1 - \alpha\nu)\gamma$;

$\nu = -\left(p(k+1) + p(1:k)^{\mathrm{T}}\, w(k:-1:1)\right) \big/ \gamma$;

$u(1:k) = w(1:k) + \nu y(k:-1:1)$;

$w(1:k+1) = \begin{bmatrix} u(1:k) & \nu \end{bmatrix}$;

$\beta = \beta(1 - \alpha\nu)$;

$\alpha = -\left(r(k+1) + r(1:k)^{\mathrm{T}}\, y(k:-1:1)\right) \big/ \beta$;

$z(1:k) = y(1:k) + \alpha w(k:-1:1)$

$y(1:k+1) = \begin{bmatrix} z(1:k) & \alpha \end{bmatrix}$

end

end

Curriculum Vitae

CANUTE VAZ

Education

May 2002	**Bachelor of Science**, Electrical and Computer Engineering Rutgers, The State University of New Jersey
May 2004	**Master of Science**, Electrical and Computer Engineering Rutgers, The State University of New Jersey
January 2010	**Doctor of Philosophy**, Electrical and Computer Engineering Rutgers, The State University of New Jersey

Employment

2004 - 2008	**Teaching Assistant** Department of Electrical and Computer Engineering Rutgers, The State University of New Jersey
2004 - 2008 (Summers)	**Part-Time Lecturer** Department of Electrical and Computer Engineering Rutgers, The State University of New Jersey
2003	**Part-Time Lecturer** Department of Physics and Astronomy Rutgers, The State University of New Jersey

Publications

1. K. M. Ho, C. Vaz and D. G. Daut, "Automatic classification of amplitude, frequency, and phase shift keyed signals in the wavelet-domain," *2010 IEEE Sarnoff Symp.*, submitted for publication.

2. K. M. Ho, C. Vaz and D. G. Daut, "A wavelet-based method for classification of binary digitally modulated signals," in *Proc. 2009 IEEE Sarnoff Symp.*, Princeton, New Jersey, March 30-April 1, 2009.

3. K. M. Ho, C. Vaz and D. G. Daut, "Improved demodulation of phase shift keyed signals using wavelet thresholding," in *Proc. 2008 IEEE Sarnoff Symp.*, Princeton, New Jersey, April 28-30, 2008.

4. K. Vaz, K. M. Ho and M. Caggiano, "Error reducing techniques for the scattering parameter characterization of differential networks using a two-port network analyzer," in *Proc. 28th IEEE Intl. Spring Seminar Electron. Technol.*, Austria, May 2005, pp. 342-347.

5. K. Vaz, K. M. Ho and M. Caggiano, "Scattering parameter characterization of differential four-port networks using two-port network analyzers," in *Proc. 55th IEEE Electron. Componen. Technol. Conf.*, Orlando, FL, May 2005, vol. 2, pp. 1846-1853.

6. K. Vaz and M. Caggiano, "Measurement technique for the extraction of differential s-parameters from single-ended s-parameters," in *Proc. 27th IEEE Intl. Spring Seminar Electron. Technol.*, Bulgaria, May 2004, vol. 2, pp. 313-317.

7. W. Zhang, K. M. Ho, Y.-T. Yeh, K. Vaz and M. Caggiano, "Circuit modeling inductances and resistances at radio frequencies," in *Proc. 9th Intl. Symp. Design Technol. Electron. Packag.*, Romania, September 2003.